«ELECTRICAL ENGINEERING & ELECTROMECHANICS»

SCIENTIFIC & PRACTICAL JOURNAL

Journal was founded in 2002 by

National Technical University «Kharkiv Polytechnic Institute»

Co-Founder – State Institution «Institute of Technical Problems of Magnetism of the NAS of Ukraine»

ISSUE 2/2017

TABLE OF CONTENTS

Editorial office address: Dept. of Electrical Apparatus, NTU «KhPI», Kyrpychova Str., 2, Kharkiv, 61002, Ukraine
phones: +380 57 7076281, +380 67 3594696, **e-mail:** a.m.grechko@gmail.com (**Grechko O.M.)**

ISSN (print) 2074-272X
ISSN (online) 2309-3404

Printed 28.04.2017. Format 60 x 90 ⅛. Paper – offset. Laser printing. Edition 200 copies. Order no.66/172-02-2017.

Printed by Printing house «Madrid Ltd» (11, Maksymilianivska Str., Kharkiv, 61024, Ukraine)

UDC 621.3: 537.8: 910.4 **doi: 10.20998/2074-272X.2017.2.01**

M.I. Baranov

AN ANTHOLOGY OF THE DISTINGUISHED ACHIEVEMENTS IN SCIENCE AND TECHNIQUE. PART 37: NOBEL PRIZE LAUREATES IN PHYSICS FOR 2000-2004

Purpose. Implementation of brief analytical review of the distinguished scientific achievements of the world scientists-physicists, awarded the Nobel bonus on physics for period 2000-2004. Methodology. Scientific methods of collection, analysis and analytical treatment of scientific and technical information of world level in area of modern theoretical and experimental physics. Results. The brief analytical review of the scientific openings and distinguished achievements of scientists-physicists is resulted in area of modern physical and technical problems which were marked the Nobel Prizes on physics for period 2000-2004. Originality. Systematization is executed with exposition in the short concentrated form of the known scientific and technical materials, devoted creation of semiconductor geterostructures scientists-physicists, integral microcircuit, to the receipt of condensation of Boze-Einstein in rarefied gases of alkaline metals, finding out a space neutrino, opening of space sources of X-rays, development of theory of superconductors and superfluid liquids and opening of asymptotic freedom in the theory of strong interactions of elementary particles. Practical value. Popularization and deepening of scientific and technical knowledges for students, engineers and technical specialists and research workers in area of modern theoretical and experimental physics, extending their scientific range of interests and cooperant of further development of scientific and technical progress in human society. References 36, figures 16.

Key words: **modern physics, achievements, semiconductor geterostructure, integrated circuit, condensation of Boze-Einstein in rarefied gases of alkaline metals, space neutrino, space sources of X-rays, theory of superconductors and superfluid liquids, asymptotic freedom in the theory of strong interactions of elementary particles**.

Приведен краткий аналитический обзор выдающихся научных достижений ученых мира, отмеченных Нобелевской премией по физике за период 2000-2004 гг. В число таких достижений вошли разработка полупроводниковых гетероструктур для высокочастотной техники и оптоэлектроники, изобретение интегральной микросхемы, получение конденсации Бозе-Эйнштейна в разреженных газах щелочных металлов, обнаружение космических нейтрино, открытие космических источников рентгеновского излучения, разработка теории сверхпроводников и сверхтекучих жидкостей и открытие асимптотической свободы в теории сильных взаимодействий элементарных частиц. Библ. 36, рис. 16.

Ключевые слова: **современная физика, достижения, полупроводниковая гетероструктура, интегральная микросхема, конденсация Бозе-Эйнштейна в разреженных газах щелочных металлов, космические нейтрино, космические источники рентгеновского излучения, теория сверхпроводников и сверхтекучих жидкостей, асимптотическая свобода в теории сильных взаимодействий элементарных частиц.**

Introduction. Nobel Prizes are unique international awards, whose prestige in the world is extremely high. Nobel Laureate in a solemn atmosphere in the presence of the King of Sweden on December 10 every year, beginning in 1901, is awarded a diploma, a gold medal (Fig. 1) and a large cash award, the amount of which has changed over the years. On the front side of the medal is a profile of the famous Swedish engineer-businessman Alfred Nobel (1833-1896), and on the back – along its perimeter the inscription «*Promotes the ennobling of life with discoveries in the field of arts*» [1]. This inscription was taken from the verse of the «Aeneid» by the Roman poet Maron Virgil (70-19 BC). There is also depicted nature in the image of a goddess descending from the clouds and holding in her hand a «cornucopia». Its veil is raised by a woman who embodies the «genius of science».

For the first Nobel Laureate in physics for 1901, Wilhelm Conrad Roentgen (1845-1923), the monetary compensation was 150 thousand SEK. In 2005 this amount was already 10 million SEK or about 1.3 million USD [1].

Fig. 1. External view of the gold medal of the Nobel Prize in physics (on the left – the front side of the coin, and on the right – the reverse, the diameter of the medal is 65 mm and the weight is 205 g) [1]

1. Creation of semiconductor heterostructures for high-frequency engineering and optoelectronics. In 2000, the Nobel Prize in Physics was awarded the results of important studies by the Russian Jaurès Alferov (Fig. 2), the German Herbert Krömer (Fig. 3) and the American Jack Kilby (Fig. 4).

Fig. 2. Prominent Russian physicist, Academician of the Academy of Sciences of the USSR and Russian Academy of Sciences Jaurès Ivanovich Alferov, born in 1930, Nobel Prize Laureate in physics for 2000

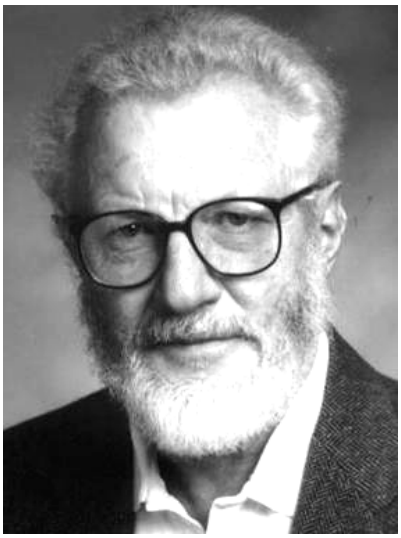

Fig. 3. Prominent German theoretical and experimental physicist Herbert Krömer, born in 1928, Nobel Prize Laureate in physics for 2000

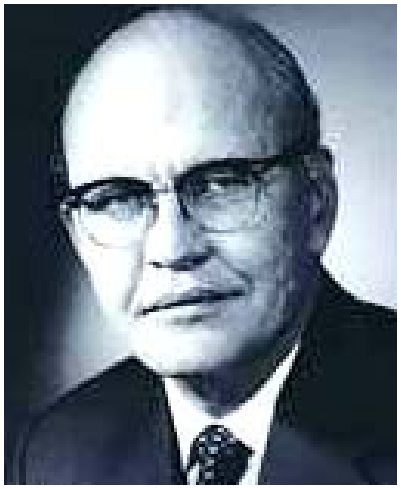

Fig. 4. American physicist and engineer-inventor Jack Kleyr Kilby, born in 1923, Nobel Prize Laureate in physics for 2000

The first two experimental physicists (the Russian J.I. Alferov and the German H. Krömer) of this high premium were awarded «*for the development of physics of semiconductor heterostructures for high-frequency engineering and optoelectronics*», and the third physicist (American engineer-inventor J.K. Kilby) – «*for the contribution to the discovery of the integrated circuit*» [1-4].

Nobel Laureates in physics J.I. Alferov and H. Krömer became one of the founders of modern information-based high-speed technology capable of transmitting a large amount of information in a short period of time. It was for this technique that they discovered and created fast-acting opto- and microelectronic devices based on semiconductor *heterostructures* [2-4]. These devices include high-speed transistors, laser diodes for information transmission systems in fiber-optic networks and powerful efficient light-emitting diodes. It is common knowledge that most semiconductor devices are based on the use of a *p-n*-junction formed between the surfaces (parts) of the same semiconductor with different types of its conductivity («electronic» or «hole»), created by introduction (introduction) into them (these surface or part) of the corresponding impurities (for example, phosphorus atoms P or Boron B) [5, 6]. Recall that the transistor effect was discovered in 1947 by American physicists John Bardin (1908-1991), Walter Brattein (1902-1987) and William Bradford Shockley (1910-1989), and the world's first semiconductor devices-transistors with *p-n-p* junction (crystalline germanium triodes-amplifiers with point contact) were created in 1949 [4]. In 1956, the noted US scientist-physicist «*for researching semiconductors and discovering the transistor effect*» was awarded the Nobel Prize in physics [1]. In addition, W.B. Shockley in 1949 predicted the possibility of implementing a semiconductor diode with a *p-n*- junction and developed his theory, and in 1951 he proposed using *heterojunctions* in transistors [1]. The *heterojunction* in the semiconductor structure is essentially a contact zone between two semiconductors of different chemical composition with different widths of their forbidden energy bands [4, 7]. The practical realization of *heterojunctions* made it possible to create electronic and optoelectronic devices of extremely small sizes up to atomic scales. Attempts to create such highly effective *heterojunctions* in the physics and technology of semiconductors for many years remained unsuccessful. To create an ideal *heterojunction*, physicists had to pick up two different semiconductors with practically the same atomic size as the elementary cells of their crystal lattices. The first in the world to solve this problematic physico-technical problem in the late 1960s was succeeded by our native scientist – then Candidate of Physical and Mathematical Sciences J.I. Alferov (his PhD. Thesis, devoted to the acquisition of ultrapure germanium and silicon crystals, he defended in 1961), who worked in the

world-famous Leningrad Physicotechnical Institute (LPhTI) named after A.F. Ioffe [4, 8]. Note that later from 1987 to 2003 Doctor of Physical and Mathematical Sciences (he defended his Doctoral Thesis in 1970 in LPhTI on the results of studies of *heterojunctions* in semiconductors) J.I. Alferov, becoming in 1979 Academician of the Russian Academy of Sciences (in the period 1990-2013 he was also Vice-President of the Academy of Sciences of the USSR and the Russian Academy of Sciences), was the Director of this Institute [8, 9]. He and his colleagues at the LPhTI named after A.F. Ioffe by 1970, based on gallium Ga and arsenic As, created an effective *heterojunction* from semiconductors with close periods of the crystal lattice – the GaAs type and then, using aluminum Al, a triple semiconducting compound with a *heterojunction* of the AlGaAs type [4]. The development of technology for obtaining *heterojunctions* by epitaxial growth in vacuum of a crystalline film of one semiconductor on the surface of another has led to a further miniaturization of radio electronic devices up to nanometric dimensions [4, 8]. It was found that in a semiconductor active medium with linear dimensions (thickness) from 50 μm to 1 mm, it was possible to achieve very high optical light amplification indices necessary for the creation of high-power laser radiation in the field of quantum electronics. It should be noted that quantum transitions between the energy levels of a *heterostructural* semiconductor are used in semiconductor lasers [8]. However, physicists for a long time could not solve the very important problem connected with the fact that semiconductor lasers worked steadily only at low temperatures. Thus, the first semiconductor lasers created on Ga gallium and arsenic compounds As worked in the low-temperature range from 4 to 20 K [8]. Thanks to the development of J.I. Alferov semiconductor lasers have reliably earned (since 1969) and at room temperatures. Soviet scientists, physicists, actively worked alongside J.I. Alferov understood that under conditions of intense competition with Western firms, the relevant domestic developments in the field of semiconductor physics and technology had to be carried out in extremely short terms. On the example of the selfless labor of the outstanding modern scientist and physicist J.I. Alferov is convinced that success in life and science comes not just to a talented person, but to a talented and hard-working person [2, 4, 9]. Unseen prospects are now being opened to people thanks to new ways of processing and transmitting information, including optoelectronics. Microelectronics is replaced by nanoelectronics. The above-mentioned Nobel Laureates for 2000 [1] made their significant contribution to these most important fields of physics.

We note out that in 1952 H. Krömer defended his doctoral dissertation at the University of Göttingen on the subject of studying the effect of «hot» electrons in transistors [3]. In the 1950s he developed the theory of a bipolar transistor made on the basis of *heterostructures* and which could operate in a gigahertz frequency range. In 1963 he was independent of the Soviet scientist-physicist J.I. Alferov developed the physical foundations for the construction of semiconductor lasers using double *heterostructures*. These developments for many years were ahead of the development of radio and quantum electronics [3]. They found their practical application only in the period of the 1970-1980s with the development of atomic (molecular) *epitaxy* – oriented growth in a vacuum of one crystal on the surface of another (substrate) in the world [3, 10]. In the mid-1970s, H. Krömer, working as a Professor at the University of California, Santa Barbara, USA, studied molecular combinations of semiconductor *heterostructures* on a silicon substrate, including Ga gallium and phosphorus P, a compound of the form GaP, using molecular *epitaxy* as weel as proposed by J.I. Alferov at the LPhTI named after A.F. Ioffe compound of the form GaAs. Since 1985 H. Krömer has directed his research interests to the study of other semiconductor *heterostructures*, including indium In combinations with arsenic As is a compound of the type InAs, Ga gallium with antimony Sb, a compound of the form GaSb and aluminum Al with antimony. Sb is a compound of the AlSb type [3, 8].

2. Creating an integrated circuit. First of all, it should be noted that under the *integrated circuit* in low-current electronics is meant a microminiature electronic device whose elements are inseparably linked together constructively, technologically and electrically [10]. Microelectronics, grown on integrated circuits, has become the basis of many modern technologies. Therefore, it is not without reason that 1/2 of the Nobel Prize in physics for 2000 in the field of fundamental works on information and communication technologies was awarded by the Royal Swedish Academy of Sciences to American physicist and inventor J. K. Kilby (Texas Instruments, Dallas, USA) an integrated microcircuit. And all this work began in 1958, when J.K. Kilby created the first elementary integrated circuit on a germanium crystal. In February 1959, he filed an application for an integrated circuit to the United States Patent Office (a patent was issued to him in 1964), in which the transistor was manufactured with layer-by-layer *p-n-p* or *n-p-n* junctions [1, 8]. The fundamental development of the talented physicist and engineer-inventor J.K. Kilby proved to be truly priceless for the rapid development of modern information technologies in our entire world. At present, microchips (microcircuits) produce a wide range of electronic devices, ranging from watches to computers, managing complex ground and space objects. According to the apt statement of the member of the above-mentioned Academy of Sciences G. Grimmais [8]: «*…Without the development of J.K. Kilby on integrated circuits, it would be impossible to create personal computers, and without the development of J.I. Alferov*

and H. Krömer on semiconductor heterostructures would be impossible to quickly transmit huge information flows through communication satellites.»

3. The discovery of Bose-Einstein condensation. The discovery of a new state of matter in extreme temperature conditions – the *Bose-Einstein condensate* [11] – in 1995 by American and German experimental physicists was another penetration of the inquisitive human mind into the secrets of the microscopic world of matter surrounding us. These pioneering scientists were talented physicists – Americans Eric Allin Cornell (Fig. 5), Carl Wieman (Fig. 6) and German Wolfgang Ketterle (Fig. 7) [1].

Fig. 5. Prominent American experimental physicist Eric Allin Cornell, born in 1961, Nobel Prize Laureate in physics for 2001

Fig. 6. Prominent American experimental physicist Carl Wieman, born in 1951, Nobel Prize Laureate in physics for 2001

The material substance, first obtained experimentally by working at various American research institutions (E.A. Cornell at the National Institute of Standards, K. Wieman at the University of Colorado, W. Ketterle at the Massachusetts Institute of Technology), these physicists as a result of the so-called condensation Bose-Einstein at ultralow temperatures (about $20 \cdot 10^{-9}$ K), in nature itself does not exist [12-15]. The possibility of the existence of matter in such a new physical state was predicted in the 1920s by the outstanding theoretical physicists from India Shatendranat Bose (1894-1974) and Germany Albert Einstein (1879-1955) [1, 16]. In June 1995 E.A. Cornell and C. Wieman experimentally obtained a small «speck» of Bose-Einstein substance, consisting of 2000 supercooled atoms of the alkaline rubidium element Rb.

Fig. 7. Prominent German experimental physicist Wolfgang Ketterle, born in 1957, Nobel Prize Laureate in physics for 2001

To obtain the Bose-Einstein condensation in the gas of this metal, for which it is characteristic that at practically low final temperature practically all the atoms (molecules) entering it make up one energy level corresponding to their zero momentum (the amount of motion) The experimenters «captured» the atoms of the alkaline chemical element rubidium Rb with «magnetic traps,» and then by their (atoms) super-deep cooling (to temperatures of the order of 10^{-5} K) the «web» of laser beams slowed down their motion [15]. We note that in the «magnetic traps» they used, the interaction of these atoms with the walls of a low-temperature vessel was excluded (the magnetic field of a parabolic configuration played the role of the wall of such a vessel). Using further the technique of physical experiment, similar to the usual evaporation («evaporative cooling method»), these physicists got rid of the most «hot» (fast) atoms and worked with these atoms in a state close to absolute zero temperature (at temperatures of the order of 10^{-8} K) [11, 15]. As a result of such hyperfine optical manipulations (nothing else could be introduced into the working volume of the condensed gas – otherwise, a unique condensed medium «died» [17]) at an atomic level at a fantastically low temperature (about $2 \cdot 10^{-8}$ K) succeeded to obtain a Bose-Einstein condensation of a rarefied gas with rubidium atoms Rb [15, 17]. In 1995, several months later, W. Ketterle succeeded not only in replicating the scientific results of E.A. Cornell and C. Wieman, but also obtained by using in such low-temperature experiments another alkaline element from the periodic system of chemical elements by D.I. Mendeleev sodium Na significantly larger amount of Bose-Einstein condensate (up to 10^5 supercooled atoms

of this element) [17]. In addition, in 1997 W. Ketterle, in studying this unique Bose-Einstein condensate of a rarefied gas of alkali metal (with a density of the order of 10^{21} m^{-3}), showed that the behavior of sodium Na atoms in such a condensate is completely consistent and in it a cluster of these atoms Fluctuates in unison and coherently. He managed to form a kind of laser «atomic ray» consisting of light particles (photons) rather than light quasiparticles (photons) from the new aggregate state of matter [15]. Professor of Physics Daniel Kleppner on the discovery of Bose-Einstein condensation said the following noteworthy words [15]: *«... Demonstration of the fact that atoms can exist in a kind of quantum-mechanical unison state will have a significant impact on many sections of physical knowledge. The picture of the fusion of atomic waves and the realization, so to speak, of an atomic laser, amazed the scientific imagination of many physicists*». Scientists-physicists actually took 70 years to experimentally confirm the Bose-Einstein condensate theory proposed in 1924-1925 [14]. Where can this applied new discovery of outstanding physicists find application? First of all, when creating super-precision atomic clocks, ultraminiature electronic circuits and quantum computers with unimaginable speed [15, 17]. In 2001 E.A. Cornell, C. Wieman and W. Ketterle «*for the experimental observation of Bose-Einstein condensation in rarefied gases of alkali metal atoms and for the first fundamental studies of the properties of such condensates*» were awarded the Nobel Prize in physics [1]. About this important event in the world of science Academician of the Russian Academy of Sciences Yu.M. Kagan (Research Center «Kurchatov Institute», RF) said [17]: *«... the Nobel Prize in physics for 2001 marked outstanding work, which is destined to play a significant role in modern science*».

4. Detection of cosmic neutrinos. In 2002, the American physicist-chemist Raymond Davis Jr. (Fig. 8) and the Japanese experimental physicist Masatosi Kosiba (Fig. 9) «*for the creation of neutrino astronomy*» and the Italian experimental physicist Riccardo Giacconi (Fig. 10) «*for the discovery of cosmic X-ray sources*» became the next Nobel Prize Laureates [18]. After defending in 1942 at the Yale University of the USA a doctoral dissertation on the subject from the field of physical chemistry and service in the US Army associated with the testing of chemical weapons, R. Davis Jr. was at the Brookhaven National Laboratory dealing with the peaceful use of atomic energy [19]. Here he decided to take up the physics of neutrinos, one of the nine absolutely stable particles [1, 20].

Fig. 8. Prominent American physicist-chemist Raymond Davis Jr. (1914-2006), Nobel Prize Laureate in physics for 2002

Fig. 9. Prominent Japanese experimental physicist Masatosi Kosiba, born in 1926, Nobel Prize Laureate in physics for 2002

Fig. 10. Prominent Italian hysicist-astronomer Riccardo Giacconi, born in 1931, Nobel Prize Laureate in physics for 2002

Note that in the late 1940s neutrinos existed only in the form of a theoretical postulate. Experimental results in the physics of elementary particles on this subject in the world were not yet. In his first nuclear experiments,

R. Davis Jr. decided to implement the idea of 1946 by the Italian theoretical physicist Bruno Pontecorvo (1913-1993) who later became a famous Soviet physicist in the field of nuclear physics (Academician of the Academy of Sciences of the USSR since 1964 and the Russian Academy of Sciences since 1991) [1]. This idea consisted in recording neutrinos emerging in the core of nuclear reactors using a nuclear reaction of the following form [1, 19]: ${}_{17}{}^{37}\mathrm{Cl} + \nu_e \rightarrow {}_{18}{}^{37}\mathrm{Ar} + e^-$. This reaction, involving the capture of the electron *neutrino* ν_e by the chlorine isotope, should lead to the formation of an isotope of argon and an electron e^-. In 1955, as a chlorine-containing medium trapping the *neutrino* ν_e, he used a container with a volume much more than 3.78 m^3 filled with carbon tetrachloride and located near the nuclear power reactor at the US object in the Savannah River Site area [19]. However, in these *neutrino* ν_e detection schemes, the final result for scientists turned out to be negative for the reason that *antineutrinos* $\nu_e^{\sim}$ appeared in the nuclear reactors used, and experimental setup of R. Davis Jr. was sensitive only to the *neutrino* ν_e. However, the purposeful R. Davis-Jr. in the 1960s decided to use his experimental method for detecting and measuring solar (cosmic) *neutrinos* ν_e in the radiation flux from the Sun. To this end, an installation with a chlorine-containing liquid (perchlorethylene) was already installed at a depth of 1400 m in the deep mine of Homestake, located near the city of Lid (South Dakota, South Dakota, USA) with a volume of 378 m^3 [19]. In 1970, using this unique experimental setup and the chlorine-argon method of detecting elementary particles, R. Davis-Jr. was able for the first time in the world register solar *neutrinos* ν_e. Moreover, he experimentally showed that the velocity of a nuclear reaction of the form ${}_{17}{}^{37}\mathrm{Cl} + \nu_e \rightarrow {}_{18}{}^{37}\mathrm{Ar} + e^-$ is 2.1 ± 0.3 of solar neutrino units (this was equivalent to the flow in a chlorine-containing capacity of the specified volume of one nuclear interaction in 1 s per 10^{36} atoms of the nuclear target) [1]. The probability of such a nuclear act of interaction was negligible. R. Davis Jr. was able to convince the world scientific community of the real existence in the microcosm of the matter of events occurring at a frequency of several tens of times a month. Therefore R. Davis Jr. is rightfully considered one of the founders of neutrino astrophysics.

In 1955, M. Kosiba, who graduated from the University of Tokyo in 1951, defended his doctoral dissertation at the University of Rochester, on a topic devoted to ultrahigh-energy phenomena in cosmic rays [21]. In the 1970s, these scientific studies and interests in the field of high-energy physics led M. Kosiba to an attempt to deepen our knowledge of such representatives of the microworld of matter as *muons* and *neutrinos* [20]. He designed the «Kamiokande» elementary particle detector, originally designed to register in the frame of the German-Japanese project JADE decay products on the nuclear target of accelerated protons, was used to detect cosmic *neutrinos* ν_e [21] in the DESY proton accelerator (Hamburg, Germany). In the process of an explosion in the space of the supernova 1987A, he succeeded in registering 12 pieces on the indicated detector. Cosmic *neutrinos* ν_e, and nine of which he recorded in the first two seconds of this grand cosmic phenomenon. These experimental results were the first direct experimental data confirming the theories of processes developed earlier by astrophysicists that occur during the collapse of the stars of our Universe. In particular, the theory of «neutrino cooling» of these «living» billions of years and sometime «dying» unique cosmic objects unique in size and internal processes [22] regularly observed by us on the night sky.

5. Discovery of cosmic X-ray sources. To begin with, we point out that in 1960 astronomers learned to obtain the image of the Sun in the X-ray range for the first time. In 1962, a group of US scientists, including the future Nobel Laureate R. Giacconi, with the help of installed on a neglected and existed in the near-Earth space about 6 minutes rocket the Geiger counter [1, 20], it was possible to open the first X-ray source outside the solar system (star X-1 in the constellation of Scorpio) [23].

Inspired by this success, R. Giacconi initiated the development and creation of the satellite «UHURU» (this name in translation from the African language «swahili» means «FREEDOM» [10, 23]) for X-ray astronomy launched into near-earth orbit in 1970. This US satellite Turned out to be the most technically advanced astronomical device in the world in the 1970s [23]. It was with his help that astronomical scientists succeeded in discovering in space more than 400 new astronomical objects, including the first «X-ray pulsars» and «black holes» [24]. A new success of R. Giacconi was the launch in 1978 of the orbital X-ray observatory «EINSTEIN» created under his scientific guidance in the USA (it was named after the outstanding German-American theoretical physicist Albert Einstein [1, 16]). The sensitivity of the X-ray equipment of this observatory was so high that it made it possible to detect objects in outer space with luminosity millions of times weaker than from the above-mentioned X-1 star. In 1990, under the scientific leadership of R. Giacconi, the world's largest space telescope «HUBBLE» named after the famous American astronomer Edwin Powell Hubble (1889-1953), was created and put into orbit around Earth [24]. After the elimination in 1993 by American astronauts of mistakes made during its assembly in the terrestrial conditions and the defects caused by them in its work on the unique images received with its help and transmitted to Earth, humanity was faced with a completely new, magnificent in clarity and resolution majestic picture of ours Universe [23]. In 1999, again under the inspirational creative start of R. Giacconi, a new space X-ray observatory, «CHANDRA», was built in the USA, which was named

after the famous American astrophysicist and Nobel Prize Laureate in physics for 1983 («*for studying the structure and evolution of stars*») S. Chandrasekhar (1910-1995) [1, 23]. For several years of work in the near-earth orbit, its unique equipment has made it possible to detect supermassive «black holes» in the nuclei of a number of galaxies and x-ray «pulsars» as well as to obtain unique images of many stars, nebulae and other heavenly objects In X-rays that are invisible to the human eye [23]. The scientific contribution of astronomer R. Giacconi to astrophysics and the invention of original X-ray telescopes that led to the discovery of sources of intense cosmic X-rays and the creation of a new section in astronomical science – X-ray astronomy, and was appreciated in 2002 by members of the Nobel Committee of the Swedish Royal Academy of Sciences [25].

6. Creation of the theory of superconductors and superfluid liquids. In 2003, the Nobel Prize in physics was awarded to three outstanding theoretical physicists «*for the pioneer contribution to the theory of superconductors and superfluid liquids*» [25, 26]. The laureates of this prestigious award were [1]: Russian-American Alexej Alexeevich Abrikosov (Fig. 11), Russian Vitaly Lazarevich Ginzburg (Fig. 12) and British-American Anthony James Leggett (Fig. 13). A.A. Abrikosov, working at the Institute of Physical Problems of the Academy of Sciences of the USSR (Moscow), in 1955 defended his Doctoral dissertation in the field of high-energy quantum electrodynamics [26]. Further, he directed his creative efforts to unravel the secrets of the superconductivity of matter. By that time, the three outstanding American theoretical physicists John Bardin (1908-1991), Leon Cooper (born in 1930), and John Schrieffer (born in 1931) had already created a microscopic theory of material superconductivity (the BCS theory) awarded in 1972 with the Nobel Prize in physics [1, 27]. This theory for the superconductivity of pure metals (superconductors of the first kind [26], based on the idea of «Cooper electronic pairs») was not able to substantiate the physical mechanisms of the appearance of this phenomenon in alloys (superconductors of the second type [26]) having practical application and preserving superconducting properties under the action of strong magnetic fields on them with magnetic flux density of 1 T and more (for a magnetic field strength of 10 kOe and higher) [26-29]. A.A. Abrikosov was able to explain the properties of superconductors of the second kind [26].

Developing the theoretical approaches presented in 1950 by well-known Soviet physicists in the phenomenological theory of Ginzburg-Landau superconductivity, in 1952 he used the regular lattice of magnetic lines to explain this phenomenon in superconductors of the second kind («the Abrikosov vortex lattice») surrounded by circular microcurrents [30]. He put forward a new idea of the existence in hyperconductors of hyperfine regions of the normal phase [1, 26, 27].

Fig 11. Prominent Russian-Americal theoretical physicist, Academician of the Academy of Sciences of the USSR and Russian Academy of Sciences Alexej Alexeevich Abrikosov, born in 1928, Nobel Prize Laureate in physics for 2003

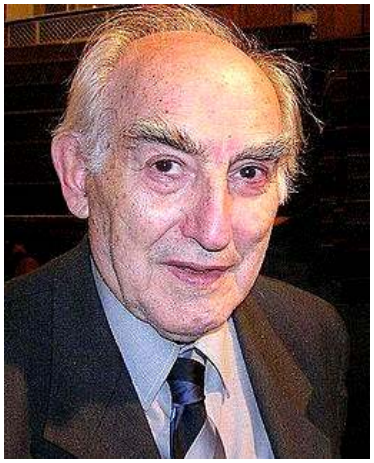

Fig. 12. Prominent Russian theoretical physicist, Academician of the Academy of Sciences of the USSR and Russian Academy of Sciences Vitaly Lazarevich Ginzburg (1916-2009), Nobel Prize Laureate in physics for 2003

Fig 13. Prominent British-American theoretical physicist Anthony James Leggett, born in 1938 г, Nobel Prize Laureate in physics for 2003

In 1957, A.A. Abrikosov, refining his scientific constructs in the field under consideration, developed a theory according to which in normal type II superconductors there are simultaneously normal and superconducting phases [1, 27]. He carried out a detailed calculation of the structure of such a «mixed» state in superconductors of the second kind, which showed that the normal phase in them arises in the form of thin filaments («Abrikosov vortices»). These filaments, having a thickness comparable to the penetration depth Δ_M of the magnetic field in a superconductor of this kind (as a rule, $\Delta_M \approx 10$ nm [27]) permeate the entire volume of the material of the superconductor. Moreover, as the strength of the external magnetic field increases, the concentration of these filaments increases in it [31]. The zone of normal regions also grows accordingly. At a critical level of magnetic field strength, a material of type II superconductor loses its superconducting properties. In 1960, A.A. Abrikosov together with the future Academician of the Academy of Sciences of the USSR (since 1987) and Russian Academy of Sciences (since 1991) L.P. Gorkov created a theory with respect to superconductors containing magnetic impurities in their composition, and also predicted a new phenomenon of gapless superconductivity [1, 27].

V.L. Ginzburg, working since 1940 at the theoretical Department of the Institute of Physics named after P.N. Lebedev of the Academy of Sciences of the USSR (PhIAN), in 1942 (in difficult years for citizens and scientists of the Soviet state and the military evacuation period of the PhIAN in Kazan) defended his Doctoral dissertation on the theory of microparticles with higher spins [32]. He repeatedly asked the relevant military authorities to go to the front as a volunteer, but his requests were not satisfied (apparently, he was destined to fulfill in life something different and no less important). Since 1943, he switched at the PhIAN on topics related to the nature of the phenomenon of superconductivity of matter, which at that time had no physical explanation. In 1950, V.L. Ginzburg, together with the future Nobel Prize winner in physics in 1962 («*for pioneering research in the theory of the condensed state of matter, especially liquid helium*» [1]), Academician of the Academy of Sciences of the USSR Lev Davidovich Landau, developed a theory of superconductivity («Ginzburg-Landau theory») [32]. This theoretical development is considered the most significant scientific contribution of V.L. Ginzburg in the physical nature of the phenomenon of superconductivity. In 1958, V.L. Ginzburg, together with the future Academician of the Academy of Sciences of the USSR (since 1990) and Russian Academy of Sciences (since 1991) L.P. Pitaevsky developed a phenomenological theory of superfluidity of matter (the «Ginzburg-Pitaevsky theory») [1, 32]. Investigations in the physics of superfluid liquids allow humanity to penetrate deeper into the complex and often unknown processes occurring in matter at ultralow temperatures in the lowest and orderly energy state of its atoms.

In 1964, A.J. Leggett defended his doctoral dissertation in the field of condensed matter physics related to high-temperature superconductivity and superfluidity of matter at the University of Oxford (Oxford, England) and from 1983 worked as a professor of theoretical physics at the University of Illinois, Illinois, USA. We point out that A.J. Leggett developed a theory of superfluidity of the light helium isotope ${}_2^3\mathrm{He}$ at ultralow temperatures [1]. He carried out deep theoretical studies of macroscopic quantum coherence and processes of scattering of matter waves in a number of quantum systems important for practice. He initiated theoretical studies of macroscopic dissipative systems and the application of special condensed systems to test the basic assumptions of quantum mechanics (in particular, the possibility of extending the quantum formalism to the macroscopic level) [1].

7. Discovery of asymptotic freedom in the theory of strong interactions of elementary particles. The Nobel Prize in hysics for 2004 was awarded to three American theoretical physicists «*for the discovery of asymptotic freedom in the theory of strong interactions*» [33]: David Jonathan Gross (Fig. 14), Hugh David Politzer (Fig. 15) and Frank Antony Wilczek (Fig. 16). In 1966, D.J. Gross defended his Doctoral Thesis in physics at the University of California (Berkeley, USA) [33, 34].

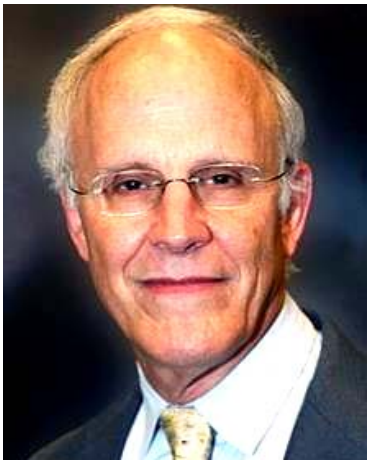

Fig. 14. Prominent American theoretical physicist David Jonathan Gross, born in 1941, Nobel Prize Laureate in physics for 2004

D.J. Gross in 1973 together with his PhD student F.A. Wilczek discovered «asymptotic freedom», according to which a strong interaction between *quarks* weakens with a decrease in the distance between them [34, 35]. Note that under «*quarks*» in the physics of elementary particles we mean hypothetical particles (they are not directly fixed in the world by a direct experimental method) with a fractional electric charge (1/3 and 2/3 of the elementary negative electron charge $e^- = 1.602 \cdot 10^{-19}$ C [20]) [10]. According to one of the proposed hypotheses,

it is believed that, probably, from *quarks* elementary particles (*hadrons*) consist which participate in the microworld in strong interactions.

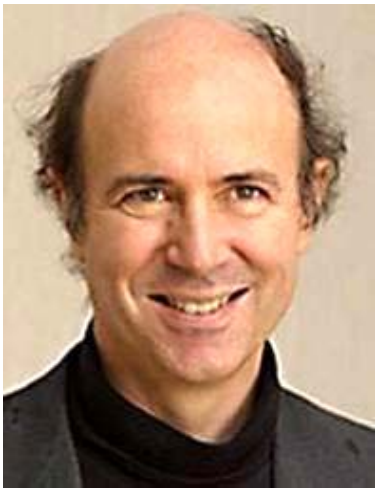

Fig. 15. Prominent American theoretical physicist Hugh David Politzer, born in 1949, Nobel Prize Laureate in physics for 2004

Fig. 16. Prominent American theoretical physicist Frank Anthony Wilczek, born in 1951, Nobel Prize Laureate in physics for 2004

According to theoretical data by D.J. Gross and F.A. Wilczek obtained by them at Princeton University (Princeton, USA), in the case of a very close arrangement of *quarks*, they should behave like free particles. This is precisely the phenomenon of «asymptotic freedom» discovered by theoretical physicists for the considered elementary particles of a new type [1]. Similar results were obtained in 1973 in theoretical studies of the interaction of *quarks*, and by H.D. Politzer who worked at Harvard University in the USA [36].

Further developments in the physics of elementary particles and high-energy physics have shown that the phenomenon of «asymptotic freedom», discovered by American theoretical physicists, played a key role in the development of quantum chromodynamics, which deals with the theoretical aspects of strong interactions of representatives of the microworld [36].

REFERENCES

1. Khramov Yu.A. *Istoriia fiziki* [History of Physics]. Kiev, Feniks Publ., 2006. 1176 p. (Rus).

2. Available at: https://en.wikipedia.org/wiki/Zhores_Alferov (accessed 15 August 2012).

3. Available at: https://en.wikipedia.org/wiki/Herbert_Kroemer (accessed 25 September 2013).

4. Available at: http://www.phys.msu.ru/rus/about/sovphys/ISSUES-2000/5(19)-2000/19-4 (accessed 11 April 2012). (Rus).

5. Alferov Z.I., Andreev V.M., Rumyantsev V.D. Solar photovoltaics: Trends and prospects. *Semiconductors*, 2004, vol.38, no.8, pp. 899-908. **doi: 10.1134/1.1787110**.

6. Baranov M.I. An anthology of the distinguished achievements in science and technique. Part 32: Alternative energy: state and prospects of development. *Electrical engineering & electromechanics*, 2016, no.3, pp. 3-16. (Rus). **doi: 10.20998/2074-272X.2016.3.01**.

7. Kuhling H. *Spravochnik po fizike. Per. s nem*. [Dictonary on Physics. Translated from German]. Moscow, Mir Publ., 1982. 520 p. (Rus).

8. Available at: http://allrefs.net/c24/22vfk (accessed 10 July 2011).

9. Khramov Yu.A. *Alpherov Gores Ivanovich. Fiziki: Biograficheskij spravochnik* [Alferov Zores Ivanovich. Physics: Biographical Directory]. Moscow, Nauka Publ., 1983. 400 p. (Rus).

10. *Bol'shoj illjustrirovannyj slovar' inostrannyh slov* [Large illustrated dictionary of foreign words]. Moscow, Russkie slovari Publ., 2004. 957 p. (Rus).

11. Available at: http://nature.web.ru/db/msg.html?mid=1171898 (accessed 18 September 2013). (Rus).

12. Available at: https://en.wikipedia.org/wiki/Eric_Allin_Cornell (accessed 21 February 2012).

13. Available at: https://en.wikipedia.org/wiki/Carl_Wieman (accessed 22 May 2012).

14. Available at: https://en.wikipedia.org/wiki/Eric_Allin_Cornell (accessed 15 August 2012).

15. Available at: http://www.sbras.ru/HBC/hbc.phtml?8+71+1 (accessed 03 May 2012). (Rus).

16. Baranov M.I. An anthology of the distinguished achievements in science and technique. Part 34: Discovery and study of quantum-wave nature of microscopic world of matter. *Electrical engineering & electromechanics*, 2016, no.5, pp. 3-15. (Rus). **doi: 10.20998/2074-272X.2016.5.01.**

17. Available at: http://vivovoco.astronet.ru/VV/JOURNAL/NATURE/01_02/NOBEL2001.HTM (accessed 10 April 2014). (Rus).

18. Available at: http://www.afportal.ru/physics/prize/2002 (accessed 23 July 2013). (Rus).

19. Available at: https://en.wikipedia.org/wiki/Raymond_Davis_Jr. (accessed 06 December 2013).

20. Kuz'michev V.E. *Zakony i formuly fiziki* [Laws and formulas of physics]. Kiev, Naukova Dumka Publ., 1989. 864 p. (Rus).

21. Available at: https://en.wikipedia.org/wiki/Masatoshi_Koshiba (accessed 20 May 2012).

22. Available at: http://velchel.ru/index.php?cnt=9 (accessed 09 October 2012). (Rus).

23. Available at: https://en.wikipedia.org/wiki/Riccardo_Giacconi (accessed 11 October 2013).
24. Baranov M.I. *Antologiia vydaiushchikhsia dostizhenii v nauke i tekhnike: Monografiia v 2-kh tomakh. Tom 2.* [An anthology of outstanding achievements in science and technology: Monographs in 2 vols. Vol.2]. Kharkov, NTMT Publ., 2013. 333 p. (Rus).
25. Available at: http://nobelprize.org/nobel_prizes/physics (accessed 02 June 2015).
26. Available at: http://n-t.ru/nl/2003.htm (accessed 12 July 2014).
27. Baranov M.I. *Antologiia vydaiushchikhsia dostizhenii v nauke i tekhnike: Monografiia v 2-kh tomakh. Tom 1.* [An anthology of outstanding achievements in science and technology: Monographs in 2 vols. Vol.1]. Kharkov, NTMT Publ., 2011. 311 p. (Rus).
28. Knopfel' G. *Sverkhsil'nye impul'snye magnitnye polia* [Ultra strong pulsed magnetic fields]. Moscow, Mir Publ., 1972. 391 p. (Rus).
29. Baranov M.I. *Izbrannye voprosy elektrofiziki: Monografija v 2-h tomah. Tom 1: Elektrofizika i vydajushhiesja fiziki mira* [Selected topics electrophysics: Monographs in 2 vols. Vol.1: Electrophysics and outstanding physics of the world]. Kharkov, NTU «KhPI» Publ., 2008. 252 p. (Rus).
30. Available at: https://en.wikipedia.org/wiki/Alexei_Alexeyevich_Abrikosov (accessed 15 December 2014).
31. Available at: http://elementy.ru./lib/430825/430827 (accessed 22 May 2012). (Rus).
32. Available at: https://en.wikipedia.org/wiki/Vitaly_Ginzburg (accessed 30 July 2014).
33. Available at: http://www.afportal.ru/physics/prize/2004 (accessed 14 April 2013). (Rus).
34. Available at: https://en.wikipedia.org/wiki/David_Gross (accessed 02 September 2012).
35. Available at: https://en.wikipedia.org/wiki/Frank_Wilczek (accessed 14 June 2013).
36. Available at: https://en.wikipedia.org/wiki/Hugh_David_Politzer (accessed 22 August 2014).

Received 14.01.2016

M.I. Baranov, Doctor of Technical Science, Chief Researcher,
Scientific-&-Research Planning-&-Design Institute «Molniya»
National Technical University «Kharkiv Polytechnic Institute»,
47, Shevchenko Str., Kharkiv, 61013, Ukraine,
phone +38 057 7076841, e-mail: eft@kpi.kharkov.ua

How to cite this article:
Baranov M.I. An anthology of the distinguished achievements in science and technique. Part 37: Nobel Prize Laureates in Physics for 2000-2004. *Electrical engineering & electromechanics*, 2017, no.2, pp. 3-12. **doi: 10.20998/2074-272X.2017.2.01.**

UDC 621.318 **doi: 10.20998/2074-272X.2017.2.02**

J. Gerlici, I.A. Shvedchikova, I.V. Nikitchenko, J.A. Romanchenko

INVESTIGATION OF INFLUENCE OF SEPARATOR MAGNETIC SYSTEM CONFIGURATION WITH PERMANENT MAGNETS ON MAGNETIC FIELD DISTRIBUTION IN WORKING AREA

Purpose. *To carry out research the influence of magnetic system configuration (shape and size of the permanent magnets) on magnetic field spatial distribution in working area of new structure design magnetic separator with active front surface by numerical methods.* ***Methodology.*** *We have applied the magnetic field numerical simulation for permanent magnets system in absence of electrical current in magnetostatic approximation. We have solved the problem by using finite element method. Research of permanent magnets cross-sectional shape influence made in the two-dimensional formulation using software package Elcut. Research of magnetic field induction spatial (three-dimensional) distribution in new construction magnetic separator working area is conducted using software package COMSOL Multiphysics 3.5a.* ***Results.*** *Magnetic flux density maximum in the immediate vicinity of permanent magnet surface provide magnets with spherical and trapezoidal cross-sectional shape. At a distance from pole surface, where the separation process working, magnetic field density produced by trapezoidal and spherical cross section magnets, substantially lower in comparison with rectangular magnets. Rectangular and rectangular with beveled corners cross-section shape magnets create approximately same magnetic field intensity not significantly different in weight. Analysis of the spatial distribution of magnetic field induction in the working area of a new construction magnetic separator has shown that a strong magnetic field with high magnetic flux density gradient value is formed in the interpolar working volume.* ***Originality.*** *For the first time research of magnetic flux density distribution in working area of new construction magnetic separator is conducted. Developed device feature is complex spatial distribution of magnetic field.* ***Practical value.*** *Results of research can be used for selection of rational parameters of separator magnetic system. Received results also can be used for determination of separator force characteristics.* References 11, figures 8.

Key words: **magnetic separator, permanent magnet, magnetic field, finite element method.**

В работе проведено исследование влияния конфигурации магнитной системы (формы и размеров постоянных магнитов) на пространственное распределение индукции магнитного поля в рабочей зоне магнитного сепаратора нового конструктивного исполнения. Поставленные задачи решены с использованием численного метода конечных элементов. Показано, что кольцевые постоянные магниты с прямоугольной формой поперечного сечения обеспечивают наиболее высокие показатели магнитной индукции в рабочих воздушных зазорах на требуемых расстояниях от поверхности магнитов. В результате анализа пространственного распределения индукции магнитного поля установлено, что в межполюсном рабочем объеме сепаратора образуется достаточно интенсивное магнитное поле с высоким значением градиента индукции. Отмечена целесообразность использования результатов исследования для выбора рациональных конструктивных параметров магнитной системы и определения силовых характеристик сепаратора. Библ. 11, рис. 8.

Ключевые слова: **магнитный сепаратор, постоянный магнит, магнитное поле, метод конечных элементов.**

Introduction. In recent years, high-coercive rare-earth permanent magnets (PM) based on NdFeB (neodymium-iron-boron) are widely used in electromechanical devices for technological purposes (separators, feeders). At a relatively low cost, they have a high residual magnetic flux density B_r (up to B_r = 1.44 T); Characterized by temperature stability at temperatures up to 150 °C; have a small volume per unit of energy; are resistant to the influence of demagnetizing fields [1, 2].

The variety of shapes, structural layouts and directions of PM magnetization allows creating new magnetic systems of electromechanical devices with the necessary topology of the magnetic field in working gaps. Electromechanical devices with PM can not only successfully compete with their electromagnetic counterparts, but also have extended functionality.

Analysis of literary data and problem definition. Analysis of the distribution of the magnetic field is an important stage in the design of separation devices based on PM. The nature of the distribution of the magnetic field in the working gaps of such devices depends essentially on the configuration of the magnetic system, which should be optimized for the mass of the PM.

In high-performance magnetic separators, as shown in [3, 4], mainly magnets of cylindrical or annular shape are used. In [3], a mathematical model is proposed for the distribution of the scalar magnetic potential created in the surrounding space by a cylindrical or circular PM. This model is based on the representation of a PM in the form of an equivalent solenoid, contains in explicit form PM parameters and can be used to analyze the external field of magnets in a homogeneous medium.

In [5] experimental studies of the magnetic field induction distribution in the simplest case – for single and paired magnetic elements in various modules of magnetic separators were performed. The possibility and practical expediency of using the superposition principle to establish the resulting induction characteristic of the field between opposing magnetic elements is shown to replace the actual simulation with the calculated one.

The results of experimental studies of the distribution of magnetic forces in the working zones of cylindrical magnetic systems of drum separators are presented in [6]. The influence of the main operating parameters on the performance of a high-gradient separator with a PM was investigated in [7].

Much of the publication is devoted to the use of computer simulation to study magnetic fields created by PM in the working gaps of magnetic separators.

In [8] the results of calculation and introduction of the drum separator on the PM are presented. To solve the problem of choosing the optimal parameters of the magnetic system, a finite element modeling package for partial differential equations FEMLAB was used. In this case, a plane-parallel analogy was considered, which, taking into account the length of the separator, sufficiently well reflects the real spatial picture of the field distribution.

A new design of a magnetic separator with transversely magnetized disk permanent magnets was proposed in [9]. Calculation of the magnetic field is performed using the finite element method. It is shown that the largest values of the force factor (about T^2/m) are reached in regions with the highest magnetic field density.

As the analysis of publications [3-9] has shown, the calculation of the magnetic field in the working interpolar gaps of magnetic separators is a rather complex task, which for most configurations of magnetic systems has not been solved analytically until now, and the experimental methods are rather laborious. When developing new designs of magnetic separators to obtain information on the distribution of magnetic field induction in working gaps, it is expedient to use numerical calculations with the use of appropriate computer programs.

The goal of the work is to investigate the influence of the configuration of the magnetic system (shape and dimensions of the PM) on the spatial distribution of the magnetic flux density in the working area of the magnetic separator of a new design.

Material and results of investigations. Investigation of the influence of the configuration of the magnetic system on the topology of the magnetic field was carried out for a new design of a disk separator [10, 11] proposed by the authors of the paper. The disk separator is designed to extract ferromagnetic inclusions from granular media conveyed by belt conveyors. In the operating mode, the device is installed above the surface of the bulk material. The magnetic system of the separator includes annular magnets arranged along the Archimedes spiral at equal distances from each other with alternating polarity of the poles in the radial direction and in the direction of the spiral deployment. In this case, the same distance is also maintained between adjacent coils of the spiral forming its pitch. With this configuration of the magnetic system, conditions are created for self-cleaning of the working surface of the disk from the extracted ferromagnetic inclusions, which greatly simplifies the process of unloading them without stopping the separation process.

Fig. 1 shows a fragment of a spiral magnetic disk separator system containing four annular magnets, indicating the main design parameters: δ – air gap; a – transverse dimension (width) of the magnet; b – distance between adjacent coils of the spiral; t – thickness of the magnets (assumed to be unchanged, equal to t = 12.5 mm).

The magnetic field in the system with PM in the absence of an electric current is described by a system of Maxwell equations, which in the magnetostatic approach has the form [10]:

$$\begin{aligned} \nabla \times \boldsymbol{H} &= 0, \\ \nabla \cdot \boldsymbol{B} &= 0, \end{aligned} \tag{1}$$

where $\boldsymbol{H}$ is the vector of the magnetic field strength; $\boldsymbol{B}$ – is the vector of the magnetic flux density.

Equation of state for permanent magnets:

$$\boldsymbol{B} = \mu_0 \mu_r \boldsymbol{H} + B_r, \tag{2}$$

where μ_r, B_r are the relative value of the magnetic permeability and the residual magnetic flux density of the PM, respectively; $\mu_0 = 4\pi \cdot 10^{-7}$ H/m is the magnetic constant.

Equation of state for ferromagnetic materials and surrounding medium (air):

$$\boldsymbol{B} = \mu_0 \mu_r \boldsymbol{H}, \tag{3}$$

where μ_r is the relative value of the magnetic permeability for the ferromagnetic material and air (μ_r = 1), respectively.

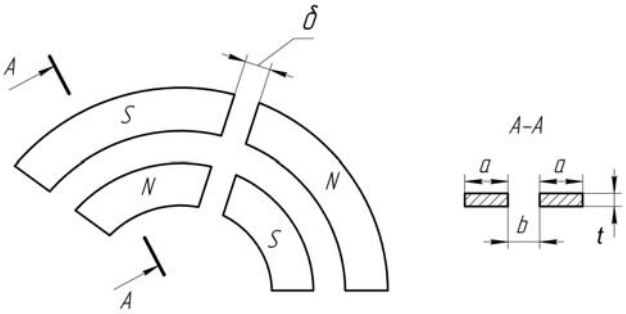

Fig. 1. A fragment of the separator magnetic system indicating main dimensions

At the first stage, the effect of the shape of the cross section of the PM on the distribution of the induction of the magnetic field in the air gap was investigated. The task was to determine the shape of the PM cross section, at which the mass of the magnetic system is minimal, and the induction created in the air gap is maximum. Four shapes of the cross section of the poles were considered (the width of the magnets a was assumed to be a = 67.5 mm): rectangular (Fig. 2,*a*); rectangular with oblique angles (Fig. 2,*b*); trapezoidal (Fig. 2,*c*); spherical (Fig. 2,*d*).

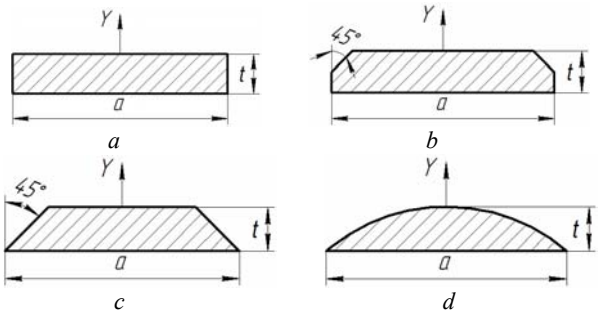

Fig. 2. The investigated shapes of the cross-section of poles: *a* – rectangular; *b* – rectangular with oblique angles; *c* – trapezoidal; *d* – spherical

The solution of the problem defined for investigating the effect of the shape of the cross section of a PM is performed by the numerical finite element method in two-dimensional formulation using the Elcut software package. The following characteristics of the high-

coercive magneto-hard material of the NdFeB type were set: the relative magnetic permeability μ_r = 1.06; residual magnetic flux density of magnets B_r = 1.2 T (vertical component directed along the Y axis, see Fig. 2), coercive force $H_c \geq 995$ kA/m. As the boundary conditions at the outer boundaries of the computational domain, the condition of magnetic isolation was used. In Fig. 3, as an example, a geometric model is shown (Fig. 3,*a*) with a mesh of finite elements applied to it and a simulation result in the form of a field pattern (Fig. 3,*b*) for a PM with a rectangular cross-sectional shape.

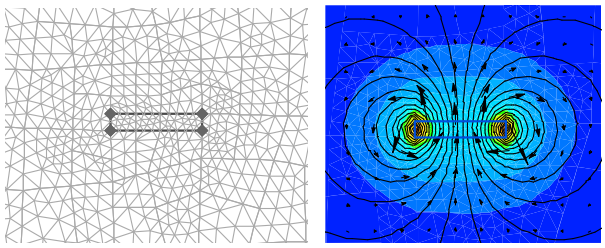

a *b*

Fig. 3. Modeling of PM with rectangular cross-sectional shape: *a* – geometrical model; *b* – results of modeling

Determination of the magnetic flux density module B_i (i = 1, ..., 4, where 1 corresponds to a rectangular, 2 – rectangular with oblique angles, 3 – trapezoidal and 4 – spherical shape of the cross section PM, respectively) was carried out along the Y axis (see Fig. 2) at distances from the surface of the magnets from 0 to 100 mm in increments of 5 mm. Fig. 4 shows the data of the ratio of the values of the magnetic flux density modules B_i at selected points for all four forms of the cross sections of the poles to the corresponding values of the magnetic flux density module B_1 for PM with a rectangular cross-sectional shape.

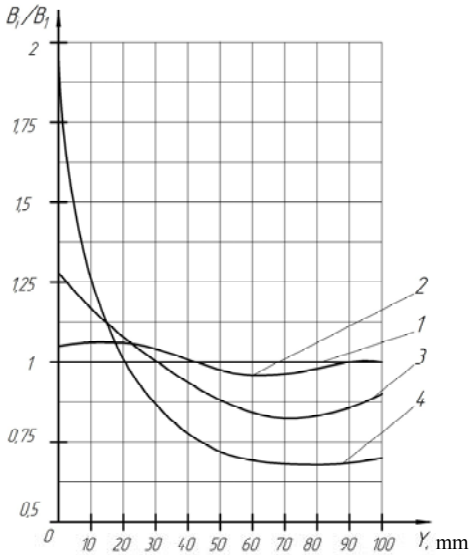

Fig. 4. Comparison of the ratios of the magnetic flux density modules B_i/B_1 for PM with different cross-sectional shapes: 1 – rectangular; 2 – rectangular with oblique angles; 3 – trapezoidal; 4 – spherical

As can be seen from Fig. 4, at small distances from the surface of the PM ($0 \leq Y \leq 15$ mm), the maximum values of the magnetic induction are provided by spherical (curve 4 in Fig. 4) and trapezoidal (curve 3 in Fig. 4) PM. They also gain considerably in weight in comparison with magnets of rectangular cross section (for the same length of magnets): the calculated mass of a spherical magnet is 32%, and the trapezoidal magnet is 19% less than the calculated mass of a PM with a rectangular cross-sectional shape.

However, at large distances ($Y \geq 20$ mm), where the separation process usually occurs, the intensity of the magnetic field, produced by the magnets of the spherical and trapezoidal sections, decreases significantly. In this case, the magnets with a rectangular (curve 1 in Fig. 4) and rectangular with oblique angles (curve 2 in Fig. 4) form nearly uniform magnetic field intensity, not significantly different in mass (no more than 5%).

In view of the foregoing, further studies should recommend the use of circular PM with a rectangular cross-sectional shape. They provide the highest indices of magnetic induction in working air gaps at the required distances. In addition, magnets of this form are widely represented in the catalogs of companies engaged in the sale of PM.

At the second stage, in order to substantiate the basic geometric dimensions of the magnetic system of a given configuration, the magnetic field distribution for two three-dimensional models of the magnetic system was calculated (Fig. 5) with the same calculated PM masses (16.28 kg): model 1 (Fig. 5,*a*) : δ = 25 mm, a = 67.5 mm, b = 51.7 mm; model 2 (Fig. 5, *b*): δ = 50 mm, a = 25.5 mm, b = 19.0 mm. Fig. 5 also shows the characteristic points at which measurements were taken (model 1 has 39, and model 2 has 119 characteristic points, respectively).

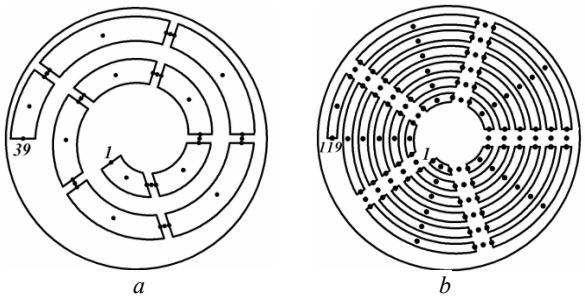

a *b*

Fig. 5. Magnetic systems with indication of characteristic points: *a* – model 1; *b* – model 2

The study of the regularities of the spatial distribution of the magnetic flux density in the working area of a new-design magnetic separator is performed by the finite element method using the COMSOL Multiphysics 3.5a application package.

A three-dimensional geometric model 1 of a magnetic system with a mesh of finite elements applied to it is shown in Fig. 6,*a*. For a ferromagnetic disk on which a PM is installed, it is assumed that the relative magnetic permeability μ_r of the disk material is constant (μ_r = 1000). The geometric dimensions of the disk (diameter – 700 mm, thickness – 15 mm) are selected, based on the dimensions of the conveyor systems most often used in practice. Fig. 6,*b* is a fragment of the pattern of the distribution of magnetic flux density lines in the

gap between the annular poles of the PM. Fig. 6,*b* shows that the lines of force thicken in the vicinity of the gaps and somewhat rarefy within the magnets.

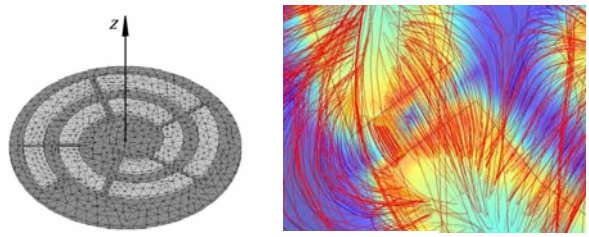

a *b*

Fig. 6. 3D modeling of the magnetic system:
a – geometrical model; *b* – results of modeling

Some results of modeling, in particular change of the magnetic flux density module B along lines $a - a'$ and $b - b'$ (shown in Fig. 7) for the model 1 at $Z = 0$ mm are shown in Fig. 8.

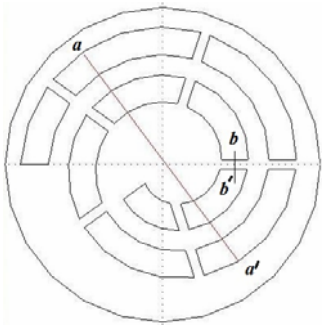

Fig. 7. Lines along which measurement of the magnetic flux density module B is carried out

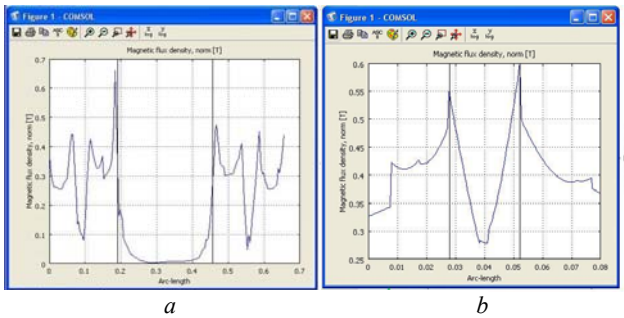

a *b*

Fig. 8. Distribution of the magnetic flux density on the interface between media «PM – air gap»:
a – in radial direction (along line $a - a'$);
b – in the direction of unfolding the spiral (along line $b - b'$)

As can be seen from Fig. 8,*a* very large difference is observed between the maximum (B_{max}) and minimum (B_{min}) values of the magnetic flux density at the surface of the magnets at $Z = 0$ mm, both in the radial direction (Fig. 8,*a*) and in the direction of the spiral (Fig. 8,*b*). The maximum value of the magnetic flux density B is at the points lying on the interface between media «PM – air gap», and the minimum – at points located in the middle of the magnet and air gap, respectively. On the magnet surfaces (at $Z = 0$ mm), there is a sufficiently strong magnetic field: $B_{max} = 0.76$ T (for model 1) and $B_{max} = 0.80$ T (for model 2) – at the boundary PM – air gap; $B_{max} = 0.31$ T (for model 1) and $B_{max} = 0.55$ T (for model 2) – in the middle of the magnet pole. The greatest difference ΔB between the maximum B_{max} and the minimum B_{min} values of the magnetic flux density is also observed at $Z = 0$ mm at the boundary PM – air gap and is: 0.34 T for model 1 and 0.47 T for model 2.

Thus, using computer modeling, the influence of the configuration of the magnetic system (cross-sectional shape and PM dimensions) on the spatial distribution of the magnetic flux density in the working area of the magnetic separator on the PM has been carried out.

Conclusions.

Investigation of the influence of the shape of the cross-section of the PM on the distribution of the magnetic flux density in the air gap of the device made it possible to establish the following regularities:

– at small distances from the surface of the PM ($0 \le Y \le 15$ mm), the maximum values of magnetic flux density are provided by a PM with a spherical and trapezoidal cross-sectional shape with a much lower calculated mass of the PM in comparison with the PM of a rectangular section;

– at relatively large distances from the surface of the poles of the PM ($Y \ge 20$ mm), where the separation process takes place, the intensity of the magnetic field produced by the magnets of the spherical and trapezoidal sections is significantly lower than for magnets with a rectangular and rectangular cross-sectional shape. In this case, magnets with rectangular and rectangular cross-sectional shapes with cross-sectional shapes create approximately equal intensity fields, differing in mass by no more than 5%.

An analysis of the spatial distribution of the magnetic flux density in the working area of the magnetic separator of the new design showed that a strong magnetic field ($B_{max} = 0.76$ ... 0.8 T) with a high gradient of magnetic flux density is formed in the interpolar working volume. The highest degree of field inhomogeneity takes place at the media interface «PM – air gap».

The obtained results can be used to select rational design parameters of the magnetic system and determine the power characteristics of the separator.

REFERENCES

1. Furlani E. Permanent Magnet and Electromechanical Devices: Materials, Analyses and Application. *New York Academic Press*, 2001, p. 518. **doi:10.1016/B978-012269951-1/50005-X.**

2. Strnat K.J. Modern Permanent Magnets for Application in Electro-Technology. *Proceedings of the IEEE*, 1990, vol. 78, no. 6, pp.923. **doi: 10.1109/5.56908**.

3. Bulyzhev E.M., Menshov E.N., Dzhavahija G.A. Modeling of the field permanent magnet. *Proceedings of the Samara Scientific Center of the Russian Academy of Sciences*, 2011, vol.13, no.4, pp.106-110. (Rus).

4. Bulyzhev E.M., Menshov E.N. Mathematical modeling of the field a permanent magnet. *Electricity*, 2010, no. 9. pp. 65-69. (Rus).

5. Sandulyak A.A., Ershov D.V., Oreshkin D.V., Sandulyak A.V. Characteristics of Magnetic Field Induction inside a Module of a Magnetic Separator. *Vestnik MGSU*, 2013, no.5, pp. 103-111. (Rus).

6. Kilin V.I. Kilin S.V. By choosing the pole pitch of the magnetic separator systems for dry processing. *Obogashchenie Rud*, 2008, no.6, pp. 14-18. (Rus).

7. S. Zeng, W. Zeng, L. Ren, D. An, H. Li. Development of a high gradient permanent magnetic separator (HGPMS). *Minerals Engineering*, Feb. 2015, vol.71, pp. 21-26. **doi: 10.1016/j.mineng.2014.10.009**.

8. Lozin A.A., Arsenjuk V.M., Petrivskij Ya.B. Information and analytical technologies at calculation and modeling stationary magnetic systems in the construction of separators based on permanent magnets. *Gornyi Zhurnal*, 2004, no.5. (Rus). Available at: http://www.prodecolog.com.ua/pdf/gorec.pdf.

9. S. Nedelcu, J. H. P. Watson. Magnetic separator with transversally magnetised disk permanent magnets. *Minerals Engineering*, May 2002, vol.15, no.5, pp. 355-359. **doi: 10.1016/s0892-6875(02)00043-2**.

10. Shvedchikova I.A., Zemziulin M.A. Research of the magnetic field distribution in the magnetic disk separator with spiral-type system. *Electromechanical and energy saving systems*, 2013, no.2(22), part 2, pp. 18-24. (Rus).

11. Shvedchikova I.O., Romanchenko J.A. *Diskoviy magnitniy separator* [Disc magnetic separator]. Patent UA, no. 110206, 2016. (Ukr).

Received 21.01.2017

Juraj Gerlici[1]*, Professor, Dr. Ing.,*
I.A. Shvedchikova[2]*, Doctor of Technical Science, Professor,*
I.V. Nikitchenko[2]*, Postgraduate Student,*
J.A. Romanchenko[2]*, Postgraduate Student,*
[1] University of Žilina , Žilina, Slovak Republic,
1, Univerzitná, SK 01026 Žilina, Slovak Republic,
phone 421(41)513 2550,
e-mail: juraj.gerlici@fstroj.uniza.sk
[2] Volodymyr Dahl East Ukrainian National University,
59-a, pr. Central, Severodonetsk, 93400, Ukraine,
phone +380 99 0448571,
e-mail: ishved@i.ua, inna.mia.lg@gmail.com

How to cite this article:

Gerlici J., Shvedchikova I.A., Nikitchenko I.V., Romanchenko J.A. Investigation of influence of separator magnetic system configuration with permanent magnets on magnetic field distribution in working area. *Electrical engineering & electromechanics*, 2017, no.2, pp. 13-17. **doi: 10.20998/2074-272X.2017.2.02.**

UDC 621.313:536.2.24:539.2 **doi: 10.20998/2074-272X.2017.2.03**

V.F. Bolyukh, A.I. Kocherga, S.V. Oleksenko, I.S. Schukin

A TECHNIQUE OF EXPERIMENTAL INVESTIGATIONS OF LINEAR IMPULSE ELECTROMECHANICAL CONVERTERS

Purpose. *Development of a technique of experimental studies linear pulse electromechanical converters parameters, which are used as shock-power devices and electromechanical accelerators, and comparing the experimental results with the calculated indices obtained using the mathematical model.* ***Methodology.*** *Method of experimental investigations of linear electromechanical converter is that the electrical parameters are recorded simultaneously (inductor winding current) and mechanical parameters characterizing the power and speed indicators of the joke with actuator. Power indicators are primarily important for shock-power devices, and high velocity – for electromechanical accelerators. Power indices were investigated using piezoelectric sensors, a system of strain sensors, pressure pulsation sensor and high-speed videorecording. Velocity indicators were investigated using a resistive movement sensor which allows to record character of the armature movement with actuating element in each moment.* ***Results.*** *The technique of experimental research, which is the simultaneous recording of electrical and mechanical power and velocity parameters of the linear electromechanical converter pulse, is developed. In the converter as a shock-power device power indicators are recorded using a piezoelectric transducer, strain sensors system, pressure pulsation sensor and high-speed video. The parameters of the inductor winding current pulse, the time lag of mechanical processes in relation to the time of occurrence of the inductor winding current, the average speed of the joke, the magnitude and momentum of electrodynamics forces acting on the plate strikes are experimentally determined. In the converter as an electromechanical accelerator velocity performance recorded using resistive displacement sensors. It is shown that electromechanical converter processes have complex spatial-temporal character. The experimental results are in good agreement with the calculated figures obtained by means of a mathematical model that describes the ultrafast electromagnetic, thermal and mechanical processes that occur when the yoke moves relative to the inductor.* ***Originality.*** *For the first time offered during experimental studies of impulse linear electromechanical converter to both to measure the electrical parameters, namely the inductor winding current, and mechanical parameters characterizing the power and velocity performance with yoke actuator.* ***Practical value.*** *The technique of experimental investigations the parameters of the linear pulse electromechanical converter that can be used to investigate the shock-power devices and electromechanical accelerators is proposed.* References 13, figures 18.

Key words: **linear impulse electromechanical converter, shock-power device, electromechanical accelerator, experimental investigations technique, mathematical model.**

Разработана методика экспериментальных исследований, которая состоит в одновременной регистрации электрических и механических силовых и скоростных параметров линейного импульсного электромеханического преобразователя. При работе преобразователя в качестве ударно-силового устройства силовые показатели регистрируются с использованием пьезодатчика, системы тензодатчиков, датчика пульсации давления и скоростной видеосъемки. При работе преобразователя в качестве электромеханического ускорителя скоростные показатели регистрируются с использованием резистивного датчика перемещений. Показано, что электромеханические процессы в преобразователе носят сложный пространственно-временной характер. Результаты экспериментальных исследований удовлетворительно согласуются с расчетными показателями, полученными при помощи математической модели, которая описывает быстропротекающие электромагнитные, тепловые и механические процессы, возникающие при перемещении якоря относительно индуктора. Библ. 13, рис. 18.

Ключевые слова: **линейный импульсный электромеханический преобразователь, ударно-силовой устройство, электромеханический ускоритель, методика экспериментальных исследований, математическая модель.**

Introduction. Linear impulse electromechanical converters (LIEC) are designed to create shock-mechanical pulses to the object of action with little movement of the actuating element (AE) or to accelerate it on a short active site [1]. These converters are used in many branches of science and technology as shock-power devices and electromechanical accelerators.

Electromagnetic hammers and pile driving devices are used in the construction industry, ratchel beaters and vibrators in the mining industry, vibration seismic sources in geological exploration, presses and hammers with a large range of impact energy in the engineering industry, vibration mixers and dispensers in the chemical and medical-biological industry.

LIEC are also used in high-speed valve and switching equipment, in test complexes for testing critical equipment for impact loads, in magnetic-pulse devices for pressing ceramics powders, cleaning containers from sticking loose materials, destroying information on digital media, etc. [2-4].

The inductive-type LIEC provide a non-contact movement of the electrically conductive armature with respect to a stationary inductor driven from a pulsed source, for example, capacitive energy storage (CES) with an electronic current pulse generation system [5]. In it, there are rapid electromagnetic, thermal and mechanical processes that occur when the yoke is moved rapidly in an environment.

Mathematical models of LIEC are realized, as a rule, using either chain or field representations [6, 7]. This raises the question of the correspondence between the parameters of the LIEC obtained by calculation methods using mathematical models, and parameters obtained experimentally.

Since the working cycle of the transducers under consideration lasts 1 ... 2 ms with a rapid movement of the armature, this imposes special features on carrying out experimental investigations [8].

The goal of the paper is a substantiation of a technique of experimental investigations of LIEC which are used as shock-power devices and electromechanical accelerators, and comparison of experimental results with the calculated parameters obtained by means of mathematical model.

Mathematical model. In the induction-type LIEC, excitation from the CES generates fast electromagnetic, thermal and mechanical processes that occur when the armature moves rapidly relative to the inductor winding (IW). The implementation of the mathematical model of LIEC using a chain approach based on the theory of electrical circuits does not allow us to fully describe the totality of spatial and temporal processes [7]. Proceeding from this, a mathematical model of the LIEC was developed, which is based on the field approach using the finite element method [9]. To determine the electromagnetic parameters of the LIEC in the cylindrical coordinate system $\{r, z\}$ the vector magnetic potential A is calculated

$$\frac{\partial}{\partial r}\left(\frac{1}{r\mu(B)}\frac{\partial(rA)}{\partial r}\right)+\frac{\partial}{\partial z}\left(\frac{1}{\mu(B)}\frac{\partial A}{\partial z}\right)-\sigma\frac{\partial A}{\partial t}=0. \quad (1)$$

where $\mu(B)$ is the magnetic permeability depending on the magnetic flux density B of ferromagnetic material; σ is the yoke electrical conductivity.

Components of the magnetic flux density vector are calculated by known relations:

$$B_z=\frac{1}{r}\frac{\partial(rA)}{\partial r};\ B_r=-\frac{\partial A}{\partial z}. \quad (2)$$

The boundary conditions of the system is equation $n\times A = 0$, where n is the unit vector of the outer normal to the surface. For ferromagnetic materials nonlinear magnetization curve $B = f(H)$ is used.

Current in the inductor is determined by using the equation:

$$(R_e+R_1)i_1+L_e\frac{di_1}{dt}+\frac{1}{C}\int i_1dt+\frac{N_1}{s}\int_V\frac{dA_l}{dt}dv=U_0, \quad (3)$$

where R_e is the active resistance of the external circuit; R_1 is the IW active resistance; i_1 is the IW current; L_e is the inductance of the external circuit; U_0 is the CES charging voltage; C is the CES capacitance; N_1 is the number of turns of the inductor; s is the cross-sectional area of the IW penetrated by the magnetic flux; A_l is the projection of the magnetic vector potential on the direction of traversal of the contour; V is the volume of the inductor.

Electrodynamical forces (EDF) acting on the yoke are determined by using the Maxwell tension tensor:

$$f_z=0{,}5\oint_S\left[H(B\cdot n)+B(H\cdot n)-n(H\cdot B)\right]ds, \quad (4)$$

where S is the area bounding the yoke cross-section; n is the unit vector of the normal to the surface of the yoke.

EDF impulse determining integral force action on the yoke is described by the expression:

$$F_z=\int_0^t f_z dt. \quad (5)$$

Mechanical processes in the LIEC at the axial yoke displacement are described by the equation

$$(m_e+m_2)\frac{dv_z}{dt}=f_z', \quad (6)$$

where $f_z'=f_z-k_\mu v_z-0.125\pi\gamma_a\beta_a D_m^2 v_z^2$; m_e is the AE mass; m_2 is the yoke mass; v_z is the yoke velocity; k_μ is the dynamic friction coefficient; γ_a is the air density; β_a is the aerodynamic resistance coefficient; D_m is the AE external diameter.

Axial displacement Δz and yoke velocity v_z on each calculation step Δt can be represented as recurrent relations [5]

$$\Delta z(t_{k+1})=\Delta z(t_k)+v_z(t_k)\Delta t+f_z'\Delta t^2(m_e+m_2)^{-1}; \quad (7)$$

$$v_z(t_{k+1})=v_z(t_k)+f_z'\Delta t(m_e+m_2)^{-1}. \quad (8)$$

Equations (1) – (8) describe electromechanical processes in LIEC at initial conditions: $u_c(0)=U_0$; $i_1(0)=0$; $\Delta z(0)=0$; $v_z(0)=0$, where u_c is the CES voltage. In the calculation, we assume the absence of mechanical movements (recoil) of the inductor, the deformation of the elements, and the strictly axial disposition and movement of the yoke relative to the inductor.

To determine the heating temperature of the IW and the joke of the LIEC, we use the field model, which allows to take into account at each time step the spatial distribution of the temperatures in the active (IW and yoke) and passive elements (inductor frame, armature yoke disk) of the LIEC elements [10].

The solution of the system of equations (1) – (8) was obtained using the finite element method in integration with respect to spatial variables and the improved Gear method in time integration. When moving the joke, a «deformable» grid is used. To solve this goal, the mathematical model of LIEC was developed in the software package *Comsol Multiphysics* which allows to adaptively change the grid and to monitor errors when working with various numerical solvers [11].

The simulation of electrical processes was carried out by physical modules «Electrical circuit», which calculated the transient processes, and «Magnetic fields», which calculated the parameters on the basis of the magnetic field taking into account the displacement of the electrically conductive armature. Modeling of magnetic processes was carried out by the physical module «Magnetic fields», in which the electromagnetic process is described by a system of differential equations for each node of the grid partition. Modeling of thermal processes was carried out by the physical module «Heat transfer in solid».

The mathematical model of LIEC is realized in the following sequence:

– Physical modules («*Magnetic fields*», «*Electrical circuit*», «*Heat transfer in solid*», «*Fluid structure interaction*»), problem dimension (*2D*), model type (*time-dependent*) and calculation method are selected;

– the geometry of the LIEC is formed and the calculated areas of physical problems are determined;

– initial data are given in the form of quantities and functions describing the relationships between the parameters, for example, the dependence of the resistivity of the material on temperature;

– initial and boundary conditions for the physical problems under consideration;

– the calculated areas are discretized taking into account the geometric model of the LIEC;

– methods of solution are chosen, usually *MUMPS*, *PARDISO* and numerical calculations are performed.

The solution of the LIEC multiphysical mathematical model is produced by the *BDF* (*backward differentiation formula*) method or the *Generalized alpha* method with floating step and time constraints. This is due to a change in the value of the calculation error, depending on the selected step. The solution of the problem begins with a step in time by 6 orders of magnitude less than the maximum set step. This step automatically varies depending on convergence conditions and the relative error of the solutions obtained.

Electromechanical processes in LIEP. Let us consider the LIEC of an induction type of a coaxial disk configuration [12]. This LIEC consists of a fixed IW with an outside diameter D_{ex1} = 100 mm, internal diameter D_{in1} = 10 mm, height H_1 = 10 mm and the number of turns N_1 = 46. Copper bus section $a \times b$ = 1.8×4.8 mm^2. The joke is made in the form of a copper disk with the following parameters: outer diameter D_{ex2} = 100 mm, inner diameter D_{in2} = 10 mm, height H_2 = 3 mm. An impact AE with a mass m_e = 0.275 kg is attached to the joke. The CES has a capacitance C = 2850 μF and a charging voltage U_0 = 400 V. The electronic system provides the formation of a polar aperiodic current in the IW, for which the latter is shunted by a reverse diode.

Electromechanical processes in LIEC have a complex space-time character. Fig. 1 shows the current density in the inductor j_1, the current density in the joke j_2 averaged over the cross section, the EDF value f_z and the EDF impulse F_z which act on the armature, moved by a distance z with respect to the inductor with the velocity v_z. After t = 1.2 ms after the start of the working process, the current in the armature changes polarity, which causes the following character of the force action: the initial repulsion is replaced by the subsequent attraction.

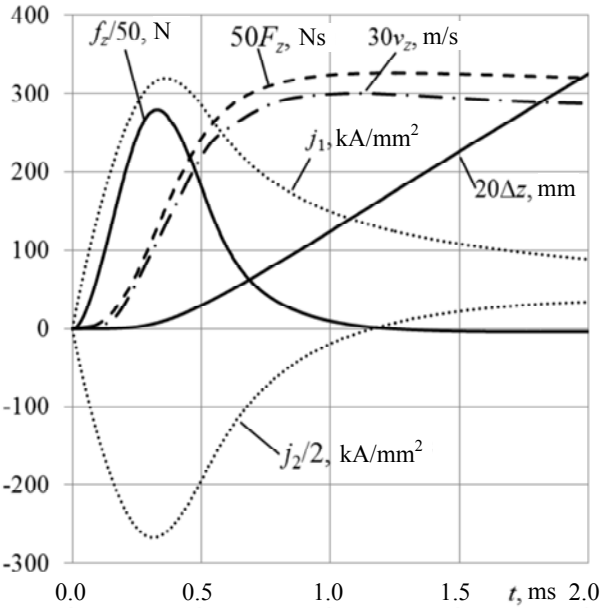

Fig. 1. Electromechanical characteristics of LIEC

The process of moving the joke begins after a certain time after the start of the work process. At each time step, an appreciable uneven distribution of the flux density of the magnetic field B in the active elements of the LIEC is observed (Fig. 2,*a*). The greatest concentration of the field is observed in the region between the IW and the joke. However, this occurs only at certain points in time, for example, at the time of the maximum EDF. In the following, the maximum induction of the magnetic field decreases and moves to the central part of the inductor.

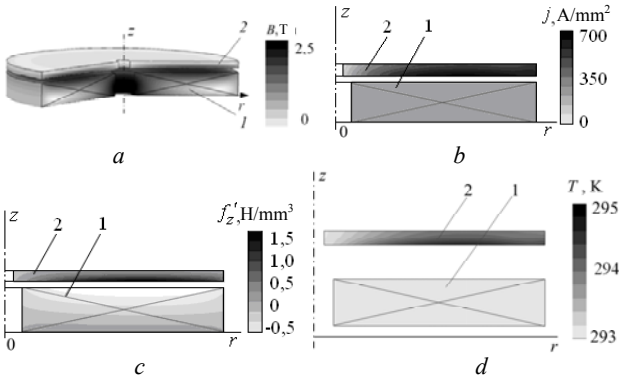

Fig. 2. Distribution of the magnetic fields (*a*) and current densities (*b*) and specific axial forces (*c*) at the instant of the maximum of the EDF and the distribution of the thermal field at the end of the working cycle (*d*): 1 – IW; 2 – joke

When the LIEC is operating at each instant of time, there is a significant spatial unevenness in the density of the induced current in the armature (Fig. 2,*b*). Specific EDF f_z' unevenly affect both the joke and the IW (Fig. 2,*c*). In this case, the temperature gradients T in the joke are insignificant, and in the IW practically absent in 1 ms after the start of work with one working cycle (Fig. 2,*d*).

When the LIEC works as an accelerator, it is first of all necessary to control the movement of the armature, and when operating as a shock-power device, it is necessary to force the relevant object.

In the experimental investigations, electrolytic capacitors HJ with a nominal voltage U_0 = 450 V and capacitances C = 150 μF and C = 330 μF were used.

The method of carrying out the experimental research of the LIEP is that simultaneously the electric parameters (current in the IW) and the mechanical parameters characterizing the power and velocity parameters of the joke with IE are registered. Power indicators, first of all, are important for shock-power devices, and high-speed ones for electromechanical accelerators.

Power indicators were studied using piezoelectric sensors, a strain gage system, a pressure pulsation sensor, and high-speed video recording. Velocity indicators were investigated with the help of a resistive displacement sensor, which allows recording the character of the armature movement with AE at each moment of time.

Investigations of LIEC as a shock-power device.

Investigations using piezoelectric sensors. For experimental investigations of the LIEC operating as a shock-power device, a device was developed that includes

an inductor 1 containing IW, which, with the help of an epoxy resin, is padlocked in a glass-textolite frame (Fig. 3).

The inductor is attached to the support plate 2. A steel impact wheel 4 is connected to the armature 3, which acts on a vertically mounted striker 5 made of steel 70, striking the upper steel plate 6. The support plate 2 is fixed to the lower steel plate 7. The plates 6 and 7 are connected to each other by means of adjustable supports 8, which makes it possible to vary the working stroke of the striker Z_e. Springs 9 provide the given force of counteraction to movement. On the plate 6, limiting the working stroke of the striker 5, a piezo-sensor 10 is installed on top, which converts the mechanical vibrations that occur when the striker strikes the electric signals, transmitting them to the noise and vibration meter ВШВ-003. The meter converts the electric signals of the piezoelectric sensor into the values of vibration acceleration a_f and the vibration velocity v_f. In the LIEC study, the current in the IW and the vibration of the plate 6 are measured simultaneously using a two-channel electronic oscilloscope *RIGOL DS 522M*.

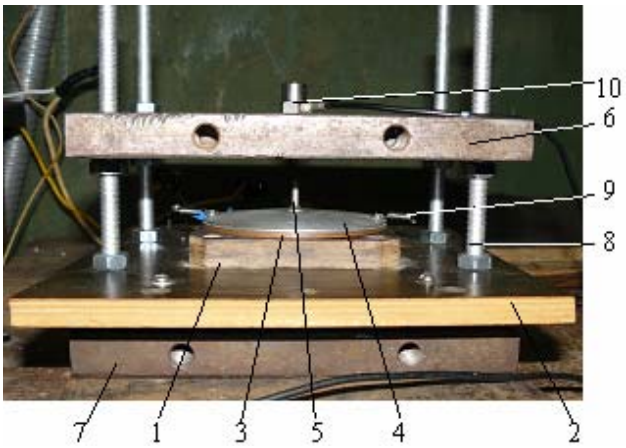

Fig. 3. Experimental installation for the investigation of LIEP using a piezoelectric sensor

In Fig. 4 shows the oscillograms of the currents of IW i_1 and vibration acceleration a_f for different values of the working stroke of the joke Z_e.

In the absence of the joke travel, the vibration of the upper plate, detected by the sensor, occurs with a certain delay t_0 with respect to the instant of the current in the IW. As the value of the working stroke Z_e increases, the delay time of the vibrational processes of the upper plate increases with respect to the instant of the current in the IW t_z.

On the basis of experimental investigations, it is determined:

– form i_1 and amplitude value I_{1m} of the current of the IW;

– duration of the edge of the current pulse of the IW t_{fr};

– duration of the current pulse of the IW t_{pul};

– delay time of vibration of the upper plate in relation to the moment of occurrence of the current of the IW t_z;

– average joke velocity with AE $V_0 = Z_e(t_z - t_0)^{-1}$;

– the value of vibration acceleration $a_f(t)$ proportional to the instantaneous force $f_z(z, t)$ acting on the upper plate;

– the value of the vibration velocity $v_f(t)$ proportional to the momentum F_z acting on the upper plate.

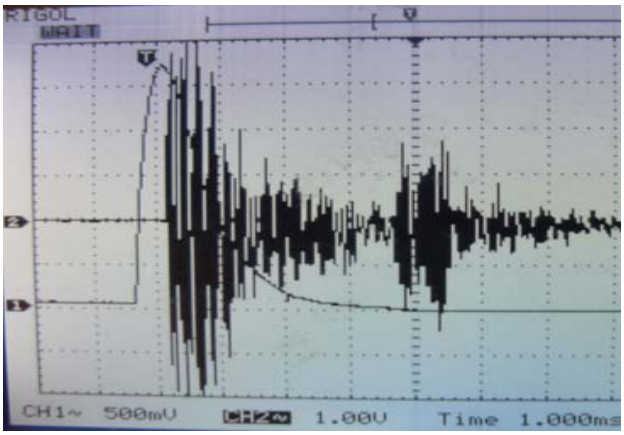

a

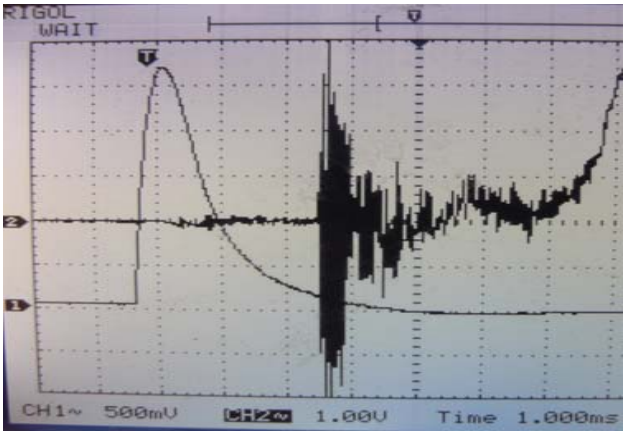

b

Fig. 4. Oscillograms of current in the IW (channel CH1) and vibration acceleration (channel CH2) with the value of the working stroke Z_e: 0 mm (*a*); 10 mm (*b*)

The measured values of the average speed of the joke with the AE V_0 for different values of the working stroke of the joke Z_e are 8 to 15% less than the calculated ones, which can be explained not by complete consideration of all opposing and braking forces. Analogous dependencies appear between the calculated and experimental values of the EDF pulse F_z (Fig. 5).

Thus, the largest values of the EDF pulse F_z arise when the joke is locked, then they decrease practically linearly with the increase in the working stroke of the joke Z_e. Both experimental and calculated dependences practically linearly increase with increasing voltage U_0, and the current amplitude of the IW I_{1m} in the presence of the joke increases.

The influence of the shape of the joke, the parameters of the CES, the working stroke Z_e, the initial gap ΔZ_0 between the joke and the inductor, and the accelerated mass on the LIEC indicators were studied experimentally. It is established that when the round armature is used in comparison with the rectangular joke, the processes change as follows: the maximum value of the EDF f_z increases by 25%, the amplitude of the current

of the IW I_{1m} increases by 5%, and the duration of the IW current pulse t_{pul} and the time delay t_z decrease by 10%. This indicates a greater efficiency of the round joke than the rectangular one.

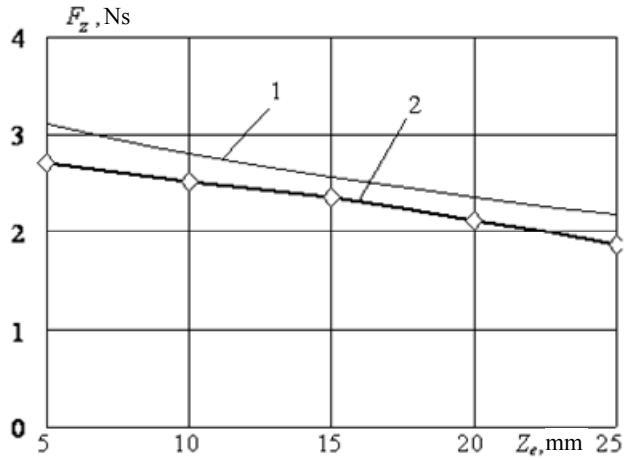

Fig. 5. Dependences of the calculated (1) and measured (2) values of the EDF pulse on the joke stroke

With an increase in the voltage of the CES, the amplitude of the current of the IW increases by more than 2 times, the amplitude of the vibrative acceleration a_{vib}, and therefore the instantaneous value of the EDF f_z acting on the upper plate, increases almost 5 times. The delay time t_z decreases from 0.7 to 0.5 ms.

As the working stroke Z_e increases, the delay time t_z of the vibration of the upper plate increases with respect to the beginning of the current pulse of the IW which leads to a decrease in the EDF amplitude f_z. On oscillograms, an insignificant vibration of the upper plate, which occurs before the impact of the striker, is caused by the return of the inductor transmitted through the adjustable supports (Fig. 4,*b*).

Fig. 6 shows the effect of capacitance C at different voltages U_0 of the CES on the amplitude of the current of the IW I_{1m} of the LIEC. The experimental and calculated values of the current amplitude increase with increasing capacitance C: with an increase in capacitance by a factor of 2 (from 2000 to 4000 μF), the current increases by 17%. Moreover, the amplitude of the current of the IW I_{1m} is higher, the higher the voltage U_0. The growth of I_{1m} values is more significant in the range of capacitances C = 2000 ... 3000 μF.

The magnitude of the voltage U_0 of the CES slightly affects the duration of the edge of the current pulse of the IW t_{fr}. The front duration remains practically unchanged for different U_0 and fixed values of the capacitance C of the CES. Fig. 6,*b* shows the effects of the CES capacitance on the duration of the edge of the current pulse of the IW t_{fr} in the presence and absence of the joke in the LIEC. Both the experimental and calculated values of the duration of the front of the current of the IW increase with an increase in the capacity of the CES C, having practically the same regularity. And the duration of the current front of the IW t_{fr} is higher in the LIEC without joke.

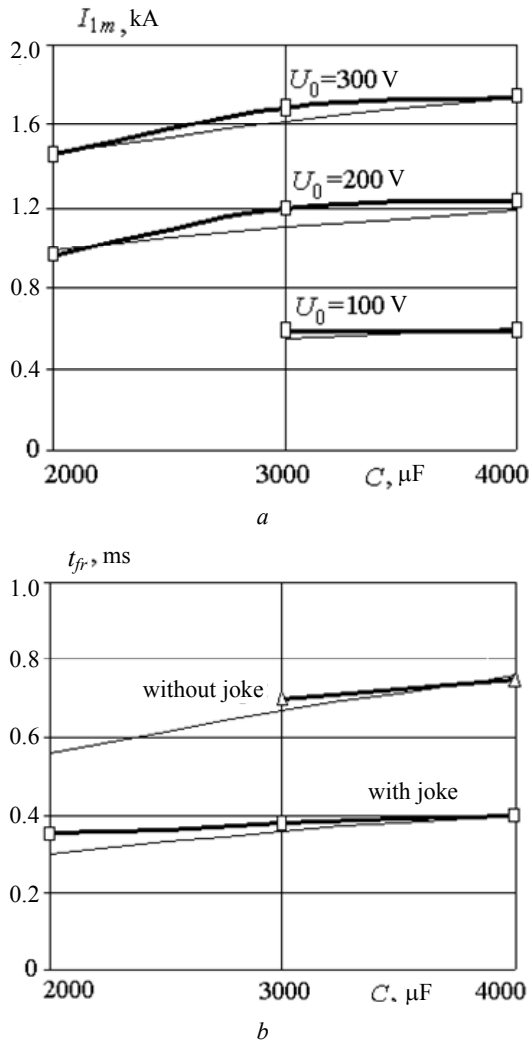

Fig. 6. Dependence of experimental (fat lines) and calculated (fine lines) values of the amplitude (*a*) and the duration of the front (*b*) of the IW LIEC current from the CES capacitance

The efficiency of the LIEC is significantly influenced by the initial gap between the joke and the inductor ΔZ_0 (Fig. 7). With increasing clearance ΔZ_0, the magnetic coupling between the joke and the IW decreases, and hence the influence of the armature on the current of the IW i_1 decreases, which leads to a decrease in the amplitude of the current I_{1m}.

The larger the initial clearance, the greater the IW current curve becomes similar to the IW current curve in the absence of the joke (the magnetic coupling of the inductor to the joke is zero). An increase in the initial gap ΔZ_0 leads to a significant decrease in the EDF pulse. Fig. 7,*b* shows the dependence of the experimental and calculated values of the EDF pulse on the initial gap when using the CES with parameters C = 3000 V, U_0 = 200 V.

With an increase in the initial gap ΔZ_0 between the armature and the inductor by a factor of 2 from 2.5 to 5 mm, the amplitude of the current in the IW I_m decreases by 8%, the duration of the current pulse in the IW t_{pul} increases by 6%, and the edge of the current pulse in the IW t_{fr} by 8%. At the same time, the magnitude of the vibration acceleration a_{vib}, and hence the EDF f_z decreases by 25%, the time delay t_z increases almost 2 times. As the ΔZ_0 increases from 0 to 5 mm, the value of the force pulse

decreases by 54%. This indicates that the initial gap between the inductor and the joke must be chosen as small as possible.

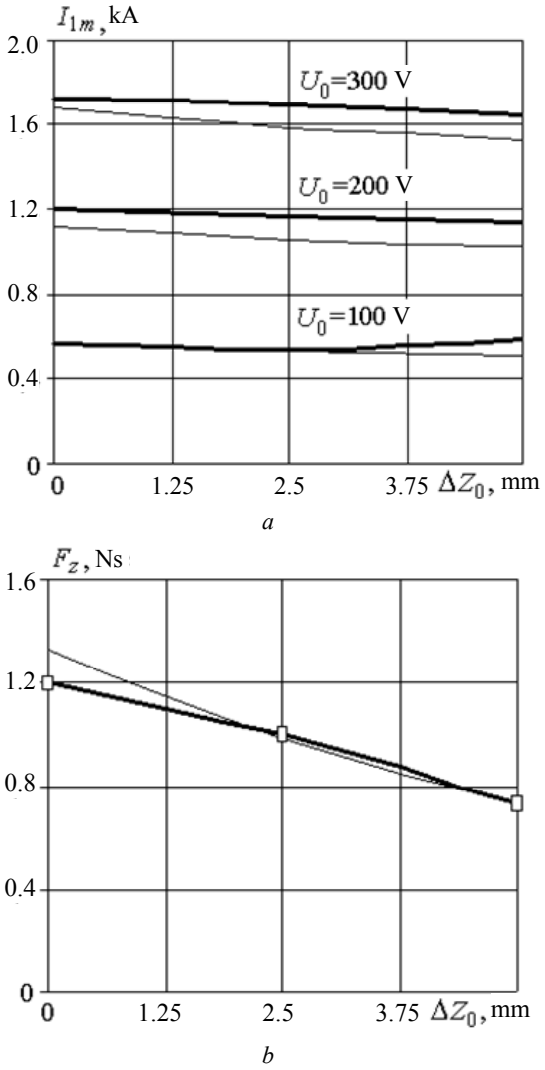

Fig. 7. Dependence of the experimental (thick lines) and calculated (fine lines) values of the current amplitude in the IW (*a*) and the EDF pulse (*b*) on the initial gap between the inductor and the joke

Fig. 8 shows the experimental and calculated values of the average velocity of the joke V_0 in the section of the working path Z_e at C = 7000 uF, but different voltages U_0 of the CES. The calculated velocity is somewhat higher than the experimental one, which can be explained by the more complex nature of the real aerodynamic resistance, compared with the mathematical model, not fully taking into account all the opposing forces and the presence of the inductor yield.

As the capacity of the CES C decreases 2.2 times (from 6270 to 2859 μF), the electrical processes change as follows: the amplitude of the current in the IW I_m decreases by 28%, the duration of the current pulse in the IW t_{pul} by 71%, the edge of the current pulse in the IW t_{fr} by 43%. As a result, the delay time t_z decreases by 14%, and the magnitude of the EDF pulse F_z by 3.12 times.

In general, the conducted experimental investigations using piezoelectric sensors are in satisfactory agreement with the theoretical results. They showed that it is possible to effectively record the indicators of the force impact of the LIEC on the object, which is important for shock-power devices.

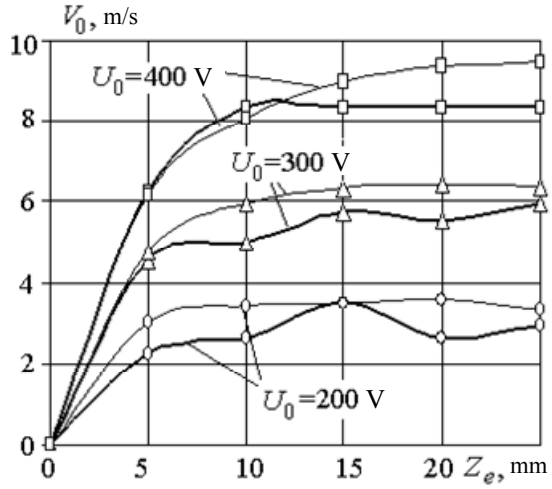

Fig. 8. Experimental (fat lines) and calculated (thin lines) dependence of the average velocity on the displacement of the LIEC joke

Study using strain sensors. Consider the effectiveness of the use of strain sensors for recording force effects on an object. An experimental stand for the investigation of the LIEC, operating as a shock-power device, is shown in Fig. 9,*a*. LIEC is attached to an insulating base plate, which is mounted on vertical adjustable supports. With these supports, it is possible to change the height of the support plate, thus setting the joke travel with firing Z_e.

LIEC provides for the movement of the joke with the striker vertically downwards before colliding with the object of impact-a shock steel plate with dimensions of 0.18×0.18×0.006 m^3 (Fig. 9,*b*). The shock plate on the reverse side is covered with a network of strain gauges, united in rosettes. The wires from the sensors are led out through the holes in the plate, which is fixed to the support frame. These sensors form five groups symmetrically located relative to the point of impact, with each group containing three sensors, one side of which forms a node, and the other sides – rays at an angle of 45º to each other (Fig. 9,*c*). The stand contains a replaceable shock plate holder, which allows to realize different types of fastening: articulated, rigid and free support.

A bridge circuit was used to measure the resistance of strain gauges. A differential signal receiver is used to measure the voltage drop.

During the experiments, information and measuring complex was used to record deformation processes in the target [13]. The complex contains a strain gage sensor, a stabilized power supply, a conjugation and protection unit, an ADA-1406 ADC and a personal computer. The digital data received from the ADC board is delivered to the computer, where it is processed using special software. It allows you to record a signal, determine the values of the measured parameters, the signal spectra and the decay

time of the oscillations. As a receiver in the sensor signal generation unit, a precision instrument amplifier AD623 is used, which allows to suppress the common-mode interference coming to the input along with the useful signal. The start-up of the test facility takes place remotely simultaneously with the commencement of the tests.

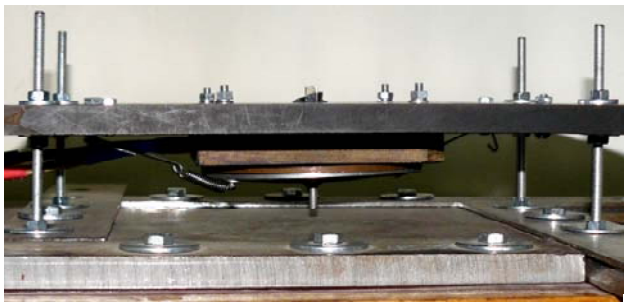

a

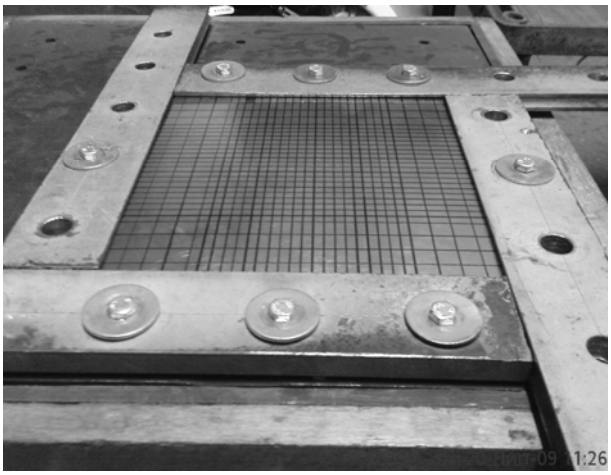

b

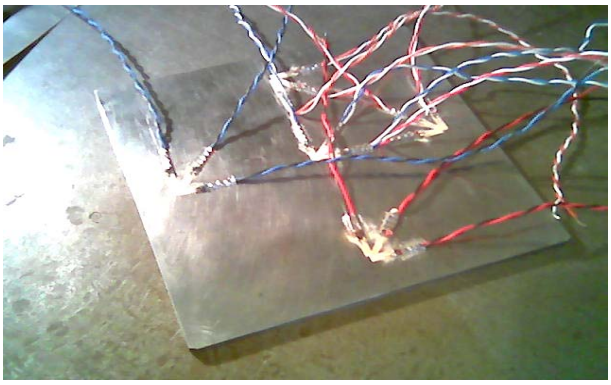

c

Fig. 9. Experimental installation for the investigation of LIEC using strain sensors (*a*) and object of effects – steel plate with strain sensors: top view (*b*) and bottom view (*c*)

During the operation of the LIEC, intensive magnetic fields are excited which generate load cell signals proportional to the axial component of the field at their location. Thus, in the absence of deformation processes in the shock plate, the magnetic field of the LIEC generates the background signals of the strain sensors, whose amplitudes increase with increasing voltage U_0 (Fig. 10).

It has been experimentally established that the impact of the striker along the center of the shock plate does not cause plastic deformations in it. A series of shock effects was performed, on the basis of which the average value of the amplitude of the signal, taken from the central «socket» of the shock absorber strain sensors, was determined. Subtracting the background level from the signal values, we get the value of the deformation of the shock plate. In Fig. 11 circles show outbursts of strain sensor signals on oscillograms that correspond to the deformation processes caused by impact forces of the LIEC striker on the plate.

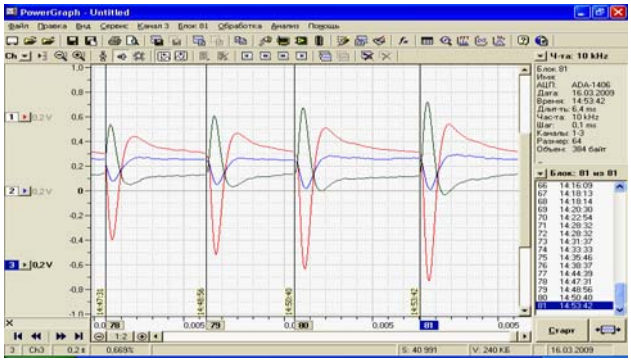

Fig. 10. Background signals of strain sensors induced by magnetic field at voltages U_0: 250; 300; 350; 400 V (from left to right)

The averaged value of the maximum values of these bursts corresponds to the maximum EDF value f_z acting on the shock plate (1 mV signal is equivalent to the power load of 8.936 N). The duration of the shock pulse t_{pul} is determined by the duration of the first burst of the signal.

As the voltage U_0 of the CES is increased in these experiments, as in the case of a piezoelectric sensor, the amplitudes of the IW and joke currents (background signals of the magnetic field), the size of the shock plate deformation, and the delay time between the electric and deformation processes t_z are increased.

It has been experimentally established that the EDF pulse F_z decreases with increasing work path Z_e at U_0 = const and increases with an increase in the voltage of the CES U_0 at Z_e = const. At the LIEC, from the beginning of the current pulse of the IW (electromagnetic processes) to the interaction of the striker accelerated by the joke, with the shock plate (mechanical processes), there is a lag of t_0 = 0.5 ms at C = 2850 μF and U_0 = 300…350 V and Z_e = 0.

Experimental studies were carried out to determine the average velocities of the joke V_0 in the section of the working stroke Z_e at different voltages U_0. The resulting average velocity of the joke at voltage of 200 V was 5.1 m/s which is in satisfactory agreement with the results of the calculation.

Thus, strain sensors allow recording not only the beginning and value of the force action, but also its duration. In general, the experimental results obtained using piezoelectric and strain sensors are in good agreement with each other.

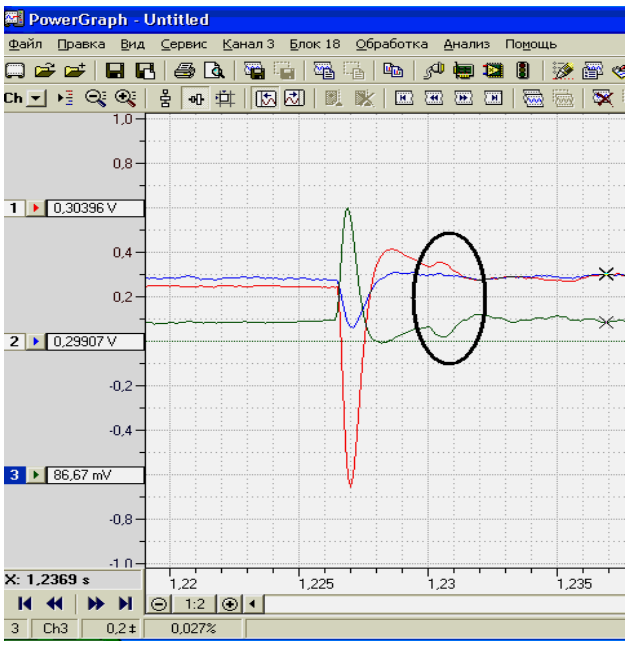

a

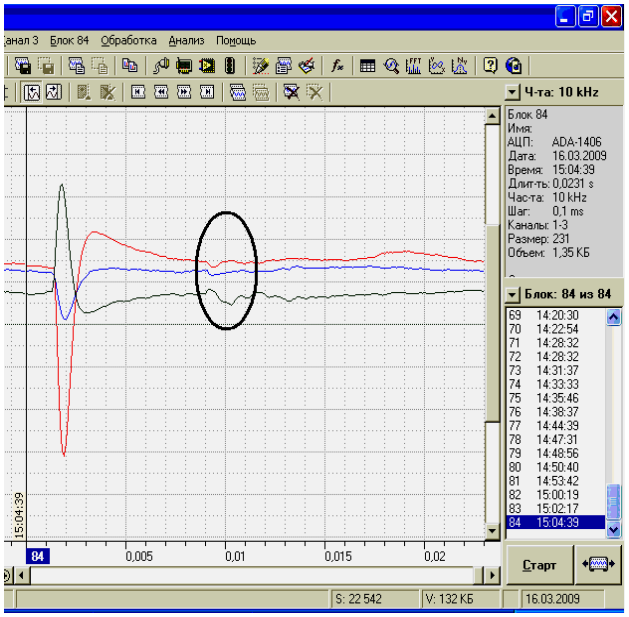

b

Fig. 11. Strain sensors signals at U_0 = 350 V, C = 2850 μF, Z_e = 10 mm (*a*), Z_e = 25 mm (*b*)

Investigation of the cyclic shock impact of LIEC on a thin steel plate.

Experiments were conducted to penetrate thin (1.5 mm) stainless steel plates. With a voltage of the CES of U_0 = 200 V in this plate, the value of mechanical stresses is 93.4 MPa, and when U_0 = 400 V – 186.8 MPa. For a thin sheet of 12X18H10T steel, the yield strength is σ_T = 205 MPa. Thus, at a voltage of the CES U_0 = 400 V, the mechanical stresses in the plate are at the boundary of the yield point. To study the impact of the LIEC on this plate, a low-cycle shock loading was used and the average value of the number of cycles N was determined before the plate was pierced by the striker.

For the first group of experiments in which a load with stress value of 400 MPa was realized, N = 146 cycles, and for the second group, at a voltage of 457 MPa, N = 39 cycles. When punching, a bulge (cork) with a diameter of 4 mm and a thickness of 1.1 mm was formed with even edges.

Fig. 12,*a* shows the experimental curve of the low-cycle impact strength and photographs of a thin steel plate deformed at the corresponding values of the mechanical stresses. Fig. 12,*b* shows a photo of a plate pierced by a striker. As a result of several experiments during the cyclic operation of the LIEC, it was found that the average number of cycles before punching the plate was N = 79.

Investigations using videorecording. At the test bench for the LIEC investigations using strain sensors, measurements were made of the instantaneous velocity of the joke with a striker using a video camera with a digital camera. After the shooting, the recording was processed and its decomposition into separate frames (Fig. 13). In this case, the time was determined for which the joke with the striker passes the distance to the shock plate. On average, the time from the detachment of the joke to the contact of the striker with the shock plate was 9.65 ms. The distance from the end of the striker to the shock plate in this experiment is 5 mm. Consequently, the average speed in the section of the working stroke was 5.18 m/s which is in satisfactory agreement with the results of the experiments described above.

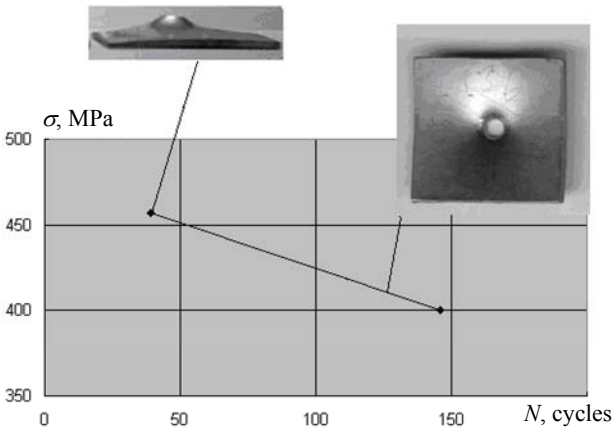

a

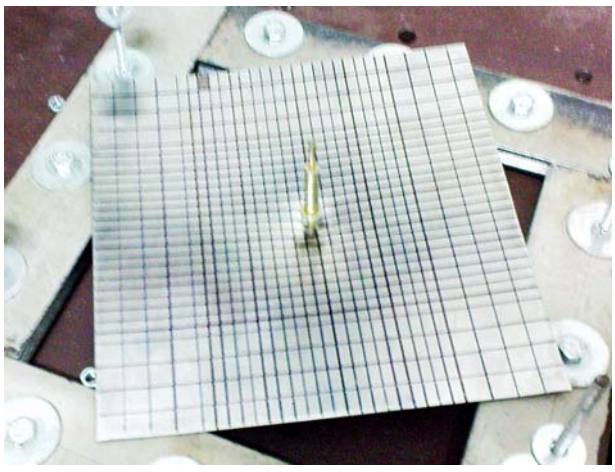

b

Fig. 12. The low-cycle impact strength curve (*a*) and a thin steel plate pierced by the LIEC striker (*b*)

a

b

Fig. 13. Outcomes of videorecording at the beginning (*a*) and at the end (*b*) of the operation process

Investigations using a pressure pulsation sensor. A piezoelectric pressure pulsation sensor M101A06 by the PCB Company (USA) was used to measure the dynamic pressure exerted by the striker on the shock plate (Fig. 14).

Fig. 14. External view of the piezoelectric sensor of pressure pulsations M101A06 by the PCB Company

The sensor is equipped with an integrated amplifier, has dynamic range of 0.68-3450 kPa, sensitivity of 1.45 mV / kPa and frequency range of 0.01-130000 Hz. The sensor withstanding maximum pressure of 34.5 MPa contains a built-in ICP amplifier (ICP – *Integrated Circuit Piezoelectric*). The sensor readings were recorded using an electronic oscilloscope *RIGOL* (Fig. 15).

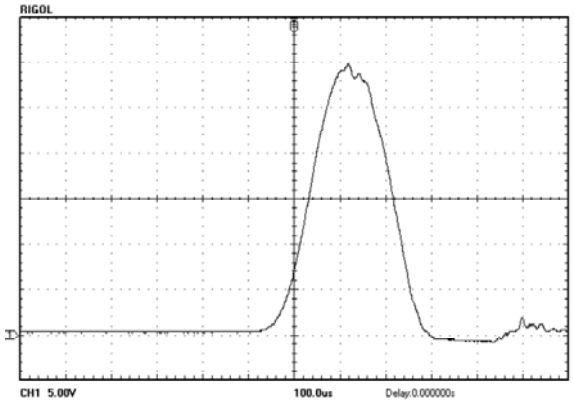

a

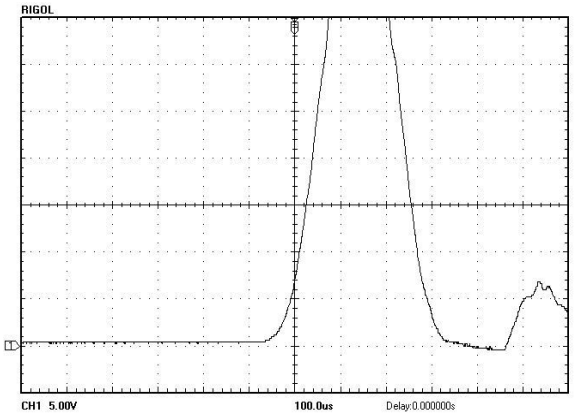

b

Fig. 15. Oscillograms of dynamic pressure on the shock plate with voltage of the CES 300 V (*a*) and 400 V (*b*)

In these experiments, the shape, size, and duration of the force pulse in the shock plate were determined upon the action of the LIEC striker on it. The results of these studies are in satisfactory agreement with both the calculated EDF values (Fig. 1) and the results of the experiments described above.

Investigations of LIEC as an electromechanical accelerator. To investigate the LIEC operating as an electromechanical accelerator, it is necessary to measure the movements of the armature at each instant of time in the working area. For this purpose, the installation shown in Fig. 16 was developed. LIEC inductor 1 consists of a multi-turn winding wound from a copper bus in two layers and hardened with an epoxy resin. A steel shock wheel 3 is attached to the joke 2. The inductor is connected to the CES by way of the current leads 4. To measure vertical movements, a resistive sensor 5 fixed to the C-shaped frame 6 is used.

Between the horizontal walls of the frame 6 is movably installed a guide rod 7 passing through the central holes of the inductor and the armature. The inductor is mounted on a nonmetallic base 8 on the bottom wall of the frame, and a resistive displacement sensor is mounted on the top wall of the frame 5. A damper spring is attached to the top wall of the frame (not shown in the photo). The guide rod is connected to the shock disk and the movable contact of the displacement sensor, the signal from which is fed to the electronic oscilloscope. In this way, the current in the

inductor i_1 and the displacement Δz of the armature with the steel shock disk and the guide rod are measured simultaneously (Fig. 17).

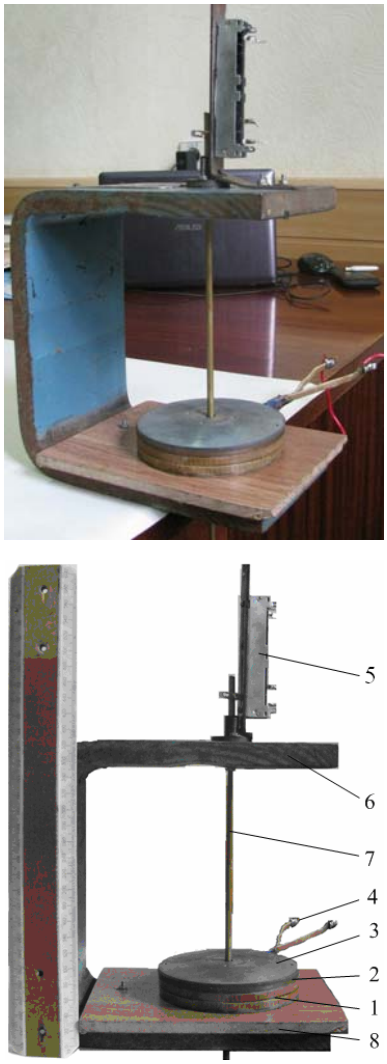

Fig. 16. General view of the experimental setup for investigations of LIEC working as an accelerator with steel power disk

It has been experimentally established that the movement of the armature begins with a delay in relation to the moment of occurrence of the current pulse and is practically linear in the initial part of the acceleration. At an increased voltage of the CES U_0 = 400 V, the movement of the armature after the passage of the initial segment slows down, which is due to its interaction with the damper spring.

The impact of the impact disk material on the performance of the electromechanical accelerator was studied. In the experiments we used steel (Fig. 16) and ceramic (Fig. 18) impact discs.

As investigations have shown with the use of a ceramic power disk, the pulse duration of the current of the IW increases by 11%, and its magnitude by 15 %. At the same time, the joke velocity increases by 3% after 1.5 ms, and after 5 ms – by 7%. Thus, a ceramic power disk is more efficient than a steel disk, although its manufacturing technology and operating conditions are more complex.

In general, the results of the LIEC investigations as an electromechanical accelerator are in satisfactory agreement with the calculated parameters: electrical parameters (current in the IW) – to 4%, and mechanical indicators (joke velocity) – with accuracy of 9%.

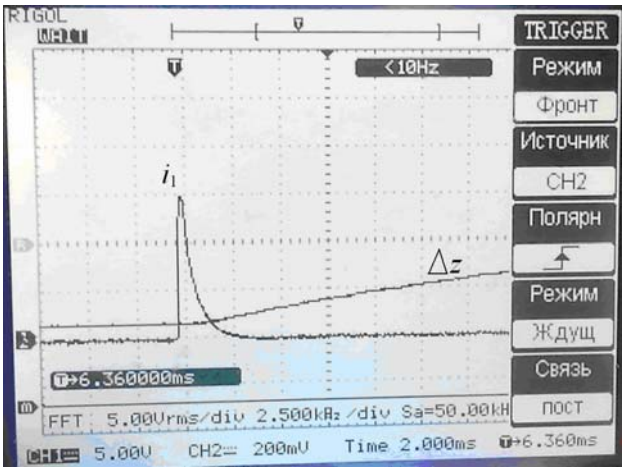

a

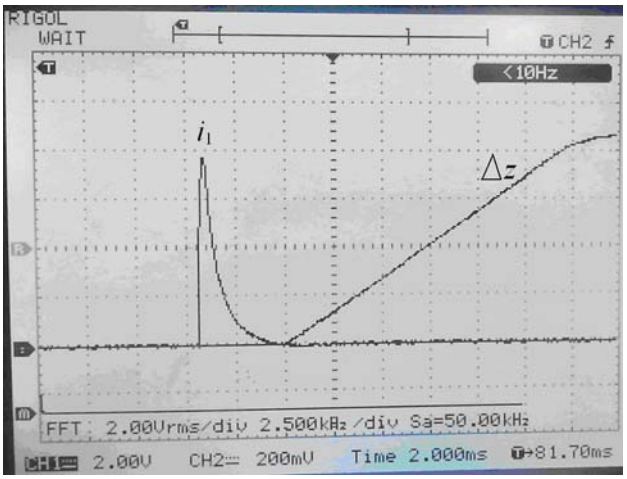

b

Fig. 17. Oscillograms of the current of the inductor i_1 and the displacement of the yoke Δz at the voltage of the CES 300 V (*a*) and 400 V (*b*) using a steel power disk

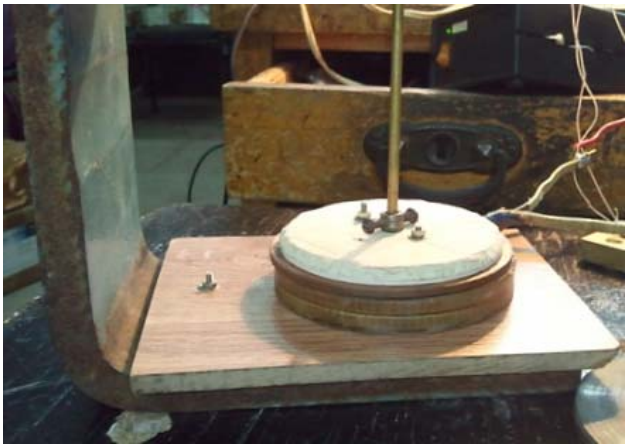

Fig. 18. General view of the experimental setup for investigations of LIEC working as an accelerator with ceramic power disk

Conclusions.

A technique for experimental research has been developed, which consists in the simultaneous recording of electrical and mechanical parameters characterizing the power and velocity indicators of the LIEC.

A mathematical model of the LIEC of induction type is developed, which describes fast electromagnetic, thermal and mechanical processes that appear when the joke moves relative to the inductor.

It is shown that the electromechanical processes in the LIEC have a complex spatial and temporal character, and at each instant of time, an appreciable spatial unevenness of the current density induced in the joke is observed.

Power indicators are recorded using a piezoelectric sensor, a system of strain sensors, a pressure pulsation sensor and high-speed videorecording, and velocity indicators using a resistive displacement sensor.

The results of experimental investigations are in satisfactory agreement with the results of calculations obtained with the help of a mathematical model.

REFERENCES

1. Bissal A. *Licentiate thesis on the design of ultra-fast electro-mechanical*. Stockholm, Sweden. 2013. 120 p.

2. D.-K. Lim, D.-K. Woo, I.-W. Kim, D.-K. Shin, J.-S. Ro, T.-K. Chung, H.-K. Jung. Characteristic Analysis and Design of a Thomson Coil Actuator Using an Analytic Method and a Numerical Method. *IEEE Transactions on Magnetics*, 2013, vol.49, no.12, pp. 5749-5755. **doi: 10.1109/tmag.2013.2272561**.

3. Bolyukh V.F., Vinnichenko A.I. Concept of an induction-dynamic catapult for a ballistic laser gravimeter. *Measurement Techniques*, 2014, vol.56, iss.10, pp. 1098-1104. **doi: 10.1007/s11018-014-0337-z**.

4. Bolyukh V.F., Luchuk V.F., Rassokha M.A., Shchukin I.S. High-efficiency impact electromechanical converter. *Russian electrical engineering*, 2011, vol.82, no.2, pp. 104-110. **doi: 10.3103/s1068371211020027**.

5. Bolyukh V.F., Shchukin I.S. *Lineinye induktsionno-dinamicheskie preobrazovateli* [Linear induction-dynamic converters]. Saarbrucken, Germany, LAP Lambert Academic Publ., 2014. 496 p. (Rus).

6. Podoltsev A.D., Kucheriava I.N. *Mul'tifizicheskoe modelirovanie v elektrotekhnike* [Multiphysical modeling in electrical engineering]. Kyiv: Institute of Electrodynamics of NAS of Ukraine, 2015. 305 p. (Rus).

7. L. Shoubao, R. Jiangjun, P. Ying, Z. Yujiao, Z. Yadong. Improvement of Current Filament Method and Its Application in Performance Analysis of Induction Coil Gun. *IEEE Transactions on Plasma Science*, 2011, vol.39, no.1, pp. 382-389. **doi: 10.1109/tps.2010.2047276**.

8. Bolyukh V.F., Oleksenko S.V., Schukin I.S. Experimental study of ferromagnetic core parameters influence on electromechanical characteristics of a linear induction-dynamic converter. *Electrical engineering and electromechanics*, 2014, no.5, pp. 13-18. (Rus). **doi: 10.20998/2074-272X.2014.5.02**.

9. Bolyukh V.F., Oleksenko S.V. The influence of the parameters of a ferromagnetic shield on the efficiency of a linear induction-dynamic converter. *Russian Electrical Engineering*, 2015, vol.86, no.7, pp. 425-431. **doi: 10.3103/s1068371215070044**.

10. Bolyukh V.F., Shchukin I.S. The thermal state of an electromechanical induction converter with impact action in the cyclic operation mode. *Russian electrical engineering*, 2012, vol.83, no.10, pp. 571-576. **doi: 10.3103/s1068371212100045**.

11. Comsol Multiphysics modeling and simulation software. Available at: http://www.comsol.com (accessed 05 May 2015).

12. Bolyukh V.F., Luchuk V.F., Rassokha M.A., Shchukin I.S. High-efficiency impact electromechanical converter. *Russian electrical engineering*, 2011, vol.82, no.2, pp. 104-110. **doi: 10.3103/s1068371211020027**.

13. Naumov I.V, Bolyukh V.F., Breslavskiy D.V. Deformation and fracture of the plates during loading cylindrical drummer. *Mechanics and engineer*, 2010, no.1, pp. 207-216. (Rus).

Received 30.11.2016

V.F. Bolyukh[1], *Doctor of Technical Science, Professor,*
A.I. Kocherga[1], *Postgraduate Student,*
S.V. Oleksenko[2], *Candidate of Technical Science,*
I.S. Schukin[3], *Candidate of Technical Science, Associate Professor,*
[1] National Technical University «Kharkiv Polytechnic Institute»,
2, Kyrpychova Str., Kharkiv, 61002, Ukraine,
phone +38 057 7076427, e-mail: bolukh@kpi.kharkov.ua
[2] Joint-stock company «Kharkivoblenergo»,
149, Plekhanovskaia Str., Kharkiv, 61037, Ukraine,
phone +38 057 7312486, e-mail: oleksenko_sergii@mail.ru
[3] Firm Tetra, LTD,
2, Kyrpychova Str., Kharkiv, 61002, Ukraine,
phone +38 057 7076427, e-mail: tech@tetra.kharkiv.com.ua

How to cite this article:
Bolyukh V.F., Kocherga A.I., Oleksenko S.V., Schukin I.S. A technique of experimental investigations of linear impulse electromechanical converters. *Electrical engineering & electromechanics*, 2017, no.2, pp. 18-28. **doi: 10.20998/2074-272X.2017.2.03.**

UDC 621.3.01 **doi: 10.20998/2074-272X.2017.2.04**

B.I. Kuznetsov, T.B. Nikitina, A.V. Voloshko, I.V. Bovdyj, E.V. Vinichenko, B.B. Kobilyanskiy

SYNTHESIS OF ACTIVE SCREENING SYSTEM OF MAGNETIC FIELD OF HIGH VOLTAGE POWER LINES OF DIFFERENT DESIGN TAKING INTO ACCOUNT SPATIAL AND TEMPORAL DISTRIBUTION OF MAGNETIC FIELD

Purpose. ***Analyze the spatial and temporal distribution of the magnetic field of high voltage power lines with different design allowing and development of recommendations for the design of active screening systems by magnetic field of high voltage power lines.*** ***Methodology.*** ***Analysis of the spatial and temporal distribution of the magnetic field of high voltage power lines of different design allowing is made on the basis of Maxwell's equations solutions in the quasi-stationary approximation. Determination of the number, configuration, spatial arrangement and the compensation coil currents is formulated in the form of multiobjective optimization problem that is solved by multi-agent multiswarm stochastic optimization based on Pareto optimal solutions.*** ***Results*** ***of active screening system for the synthesis of various types of transmission lines with different numbers of windings controlled. The possibility of a significant reduction in the level of the flux density of the magnetic field source within a given region of space.*** ***Originality.*** ***For the first time an analysis of the spatial and temporal distribution of the magnetic field of power lines with different types and based on findings developed recommendations for the design of active screening system by magnetic field of high voltage power lines.*** ***Practical value.*** ***Practical recommendations on reasonable choice of the number and spatial arrangement of compensating windings of active screening system by magnetic field of high voltage power lines of different design allowing for the spatial and temporal distribution of the magnetic field. Results of active screening system synthesis of the magnetic field of industrial frequency generated by single-circuit 110 kV high voltage power lines with the supports have 330-1T «triangle» rotating magnetic field with full polarization in a residential five-storey building, located near the power lines. The system contains three compensating coil and reduces the level of induction of the magnetic field source to the sanitary standards of 0.5 μT in almost of all the house space.*** References 8, figures 5.

Key words: **high voltage power lines, spatial and temporal distribution of the power frequency technogenic magnetic field, active screening system**.

Проведен анализ пространственно-временного распределения техногенного магнитного поля, создаваемого различными воздушными линиями электропередачи (ВЛ ЛЭП) внутри заданной области пространства. Приведены рекомендации по проектированию систем активного экранирования магнитного поля ЛЭП. Приведены результаты синтеза системы активного экранирования магнитного поля, создаваемого одноцепной ЛЭП ВЛ 110 кВ с опорой типа «треугольник» вращающегося магнитного поля с полной поляризацией в жилом пятиэтажном доме, расположенном вблизи ЛЭП. Система содержит три компенсационные обмотки и позволяет снизить уровень индукции исходного магнитного поля до санитарных норм практически во всем рассматриваемом пространстве жилого дома. Эффективность системы активного экранирования составляет около 8. Библ. 8, рис. 5.

Ключевые слова: **воздушные линии электропередачи,** пространственно-временное распределение **магнитного поля промышленной частоты, система активного экранирования.**

Introduction. The most dangerous source of man-caused magnetic field (MF) of the power frequency for the population is high voltage power lines (PL) [2]. Without taking special measures, they create an intensive MF which has carcinogenic properties at distances up to 100 m from the PL. Therefore, sanitary norms [3] are tightened in the world according to the maximum permissible level of the flux density of the magnetic field of 50-60 Hz (less than 1 μT) and intensive work is carried out to provide them for the population. At present, strict sanitary norms for the flux density of MF (0.5 μT) are also introduced in the normative documents of the Ministry of Energy of Ukraine [7]. However, at the moment in Ukraine these norms are universally exceeded which poses a threat to the health of millions of people who live closer than 100 m from high voltage PL.

Problem definition. The complex experimental investigations of the operating aerial PL 10-330 kV carried out at the Institute of Technical Problems of Magnetism of the NAS of Ukraine showed [8] that their MF is 3-5 times higher than the normative level at the border of the previously formed sanitary zones by the electric field.

This situation requires urgent measures to reduce the existing power lines within the city limits of Ukraine by 3-5 times. A similar situation is typical for most of the industrialized countries of the world, but in these countries, technologies for normalizing the MF of the operating PL have been created and widely used [1-5].

The most effective technology is the re-construction of the power line by removing it to a safe distance from residential buildings, or by replacing an overhead power line with a cable line. However, such a reconstruction requires enormous material resources. Therefore, less costly methods for shielding MF of operating PL are more acceptable for Ukraine, of which the necessary active methods are provided by methods of active contour screening of the magnetic field.

The technology of active contour screening of the existing PL is developed and used in developed countries for more than 10 years, for example in the USA and Israel [1-5]. In Ukraine, at the present time, both this technology and the scientific foundations of its creation are lacking. This does not allow relatively inexpensive methods to protect the population from the technogenic MF of the power frequency created by the power line. Therefore, the creation of scientific foundations of the domestic technology of active screening of industrial frequency MF in homes to a safe level is an actual scientific and technical problem.

The goal of the work is analysis of spatial and temporal distribution of MF PL of different design and development of recommendations for the design of active screening systems for high voltage PL.

Analysis of the spatial and temporal distribution of the magnetic field of the PL of various design. As the first example we consider a PL with a support ЛБ 330-3, in which current conductors are located in the horizontal plane, the photograph of which is shown in Fig. 1,*a*. The layout of the current conductors and the points at which the hodographs of the MF will be considered are shown in Fig. 1,*b*, and Fig. 1,*c* shows the hodographs of the MF vectors in the three points under consideration.

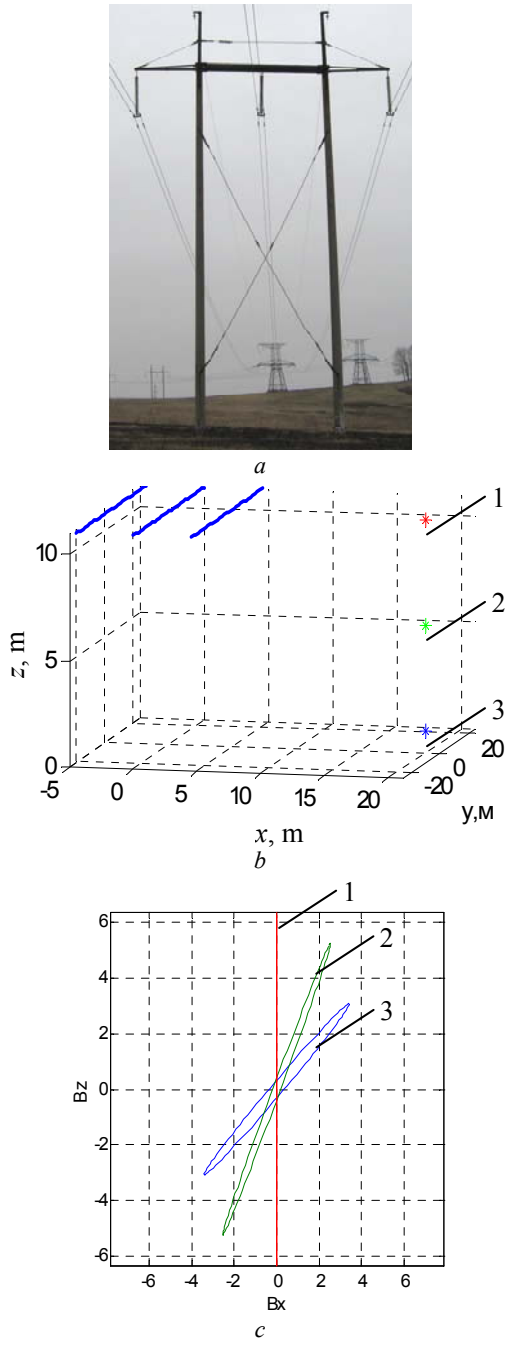

Fig. 1. Single-circuit PL with support ЛБ 330 – 3

As can be seen from Fig. 1, the hodographs of the MF represent strongly elongated ellipses, and at point 1 the coefficient of ellipticity (the ratio of the smaller semiaxis of the ellipse to the larger semiaxis) is generally zero, so that the hodograph of the vector of the MF is stretched into a vertical line.

As the second example, we consider a single-circuit PL with a support У 330 in which current conductors are located one below the other in a vertical plane, as shown in Fig. 2,*a*. The layout of the current conductors and the points in which the hodographs of the MP will be considered are shown in Fig. 2,*b*, and Fig. 2,*c* show the hodographs of the MF vector at the points under consideration.

As can be seen from Fig. 2, the hodographs of the MF of this PL also represent strongly elongated ellipses, and at point 1 the major axis of the ellipse is in the horizontal plane. In general, the hodographs of this PL are deployed with respect to the travel time curves shown in Fig. 1,*c*, by the angle $\pi/2$.

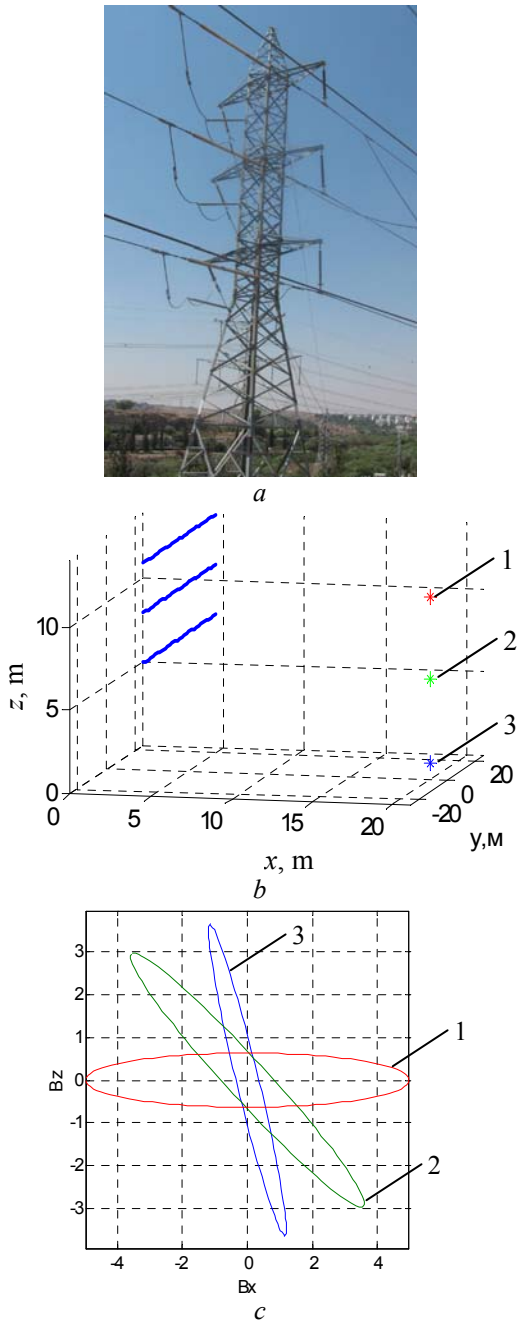

Fig. 2. Single-circuit PL with support У 330

As the third example, let us consider the most widespread version of a double-circuit PL with supports of type У 330-2 of the «barrel» type, in which the current conductors are arranged in a form resembling a barrel, whose photograph is shown in Fig. 3,*a*.

The layout of the current conductors and the points at which the hodographs of the MF will be considered are shown in Fig. 3,*b*, and the hodographs of the MF vector at the three points under consideration are shown in Fig. 3,*c*. As can be seen from Fig. 3, the hodographs of this MF represent less elongated ellipses, in comparison with the hodographs of the MP, produced by the PL with supports: ЛБ 330 – 3 and У 330, which are shown in Fig. 1,*c* and Fig. 2,*c*, respectively.

a

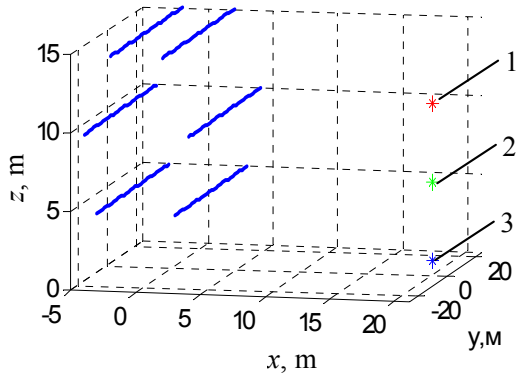

b

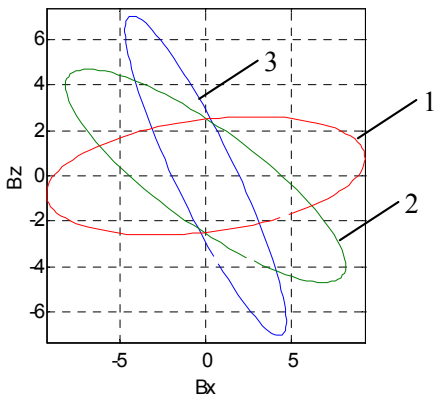

c

Fig. 3. Double-circuit PL with supports У 330 – 2 type «barrel»

As the fourth example, let us consider the most widespread version of a single-circuit PL with the У 330 – 1T support of the «triangle» type, the photograph of which is shown in Fig. 4,*a*, and Fig. 4,*b* shows the scheme of the arrangement of the current conductors and the points at which the hodographs of the MF will be considered, and Fig. 4,*c* shows the hodographs of the MF vector themselves. As can be seen from Fig. 4, the hodographs of this magnetic field are close to a circle, so that the coefficients of the ellipticity of the soil are equal to unity, and hence this MF is strongly polarized.

a

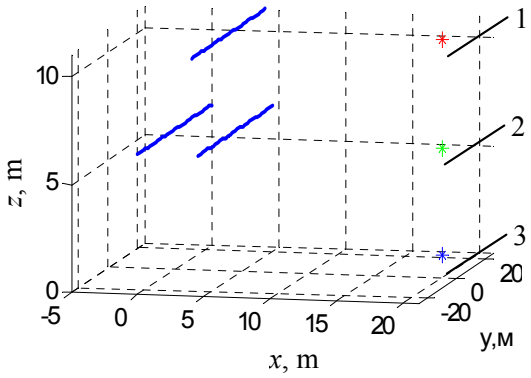

b

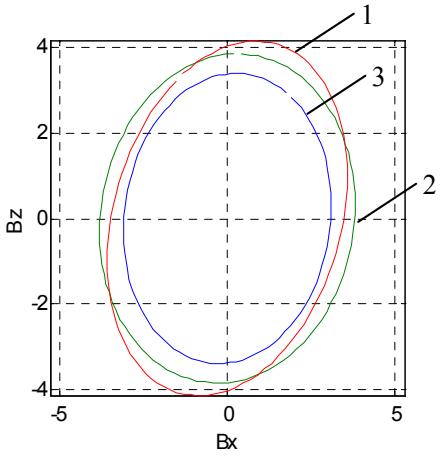

c

Fig. 4. Single-circuit PL with support У 330 – 1T type «triangle»

The principle of designing an active screening system. The essence of the method of active screening of PL consists in the formation of compensating windings with such a spatial and temporal structure whose superposition with a power line in the protection zone is minimized to the level of sanitary standards. The method is realized with the help of an active screening system which consists of compensating windings, by means of which a compensating magnetic field is formed. The currents in the compensation windings are automatically generated by a certain algorithm in the function of the signal from the MF sensors installed in the protection zone. The system contains a current source that receives energy from an external source.

When using only one compensation winding in the active shielding system, it is possible to create a compensating MF, the flux density vector of which is orthogonal to the winding plane and does not change its position with time. Therefore, using such a system, it is possible to compensate for the semimajor axis of the ellipse of the hodograph of the induction vector of the magnetic field and to obtain a sufficiently high screening efficiency for a weakly polarized MF. Such systems can be recommended to compensate for the weakly polarized magnetic field produced by the PL with supports ЛБ 330 – 3, У 330 and У 330 – 2 «barrel». It is for PL with these types of supports that the world's active screening system with one compensation winding is the most widely used [1, 2, 4].

To compensate for the highly polarized magnetic field, a power line with У 330 – 1Т «triangle» supports is required, at least two compensating windings are required.

The method of synthesis of effective closed systems of active screening of industrial frequency MF created by airPL in residential buildings was developed in [6]. The method is based on the solution of the multicriteria optimization problem in which the calculation of the vectors of the objective function and constraints is performed on the basis of the Maxwell equations in the quasi-stationary approximation, and the optimization problem is solved by the multi-stochastic stochastic multi-agent optimization method based on Pareto optimal solutions.

Results of computer modeling. As an example, let's consider the synthesis of the active screening system of a single-circuit PL of 110 kV «triangle» creating a rotating MF with full polarization in a residential five-story house located near the power line, the scheme of which is shown in Fig. 5,*a*. At the PL current of 1000 A, the initial flux density of the MF in the space under consideration is 4 μT which is 8 times higher than sanitary norms [7]. To compensate for this technogenic MF in the space under consideration, three compensation windings were required, the spatial arrangement of which is shown in Fig. 5,*a*. The estimated number of ampere-turns of compensating windings is 177, 195 and 199. The distribution of the resultant MF with the switched on active screening system is shown in Fig. 5,*b*. As can be seen from Fig. 5, with the help of the active screening system, it was possible to reduce the level of induction of the initial MF to sanitary standards in practically the entire considered space of the residential building. The efficiency of the active screening system is about 8.

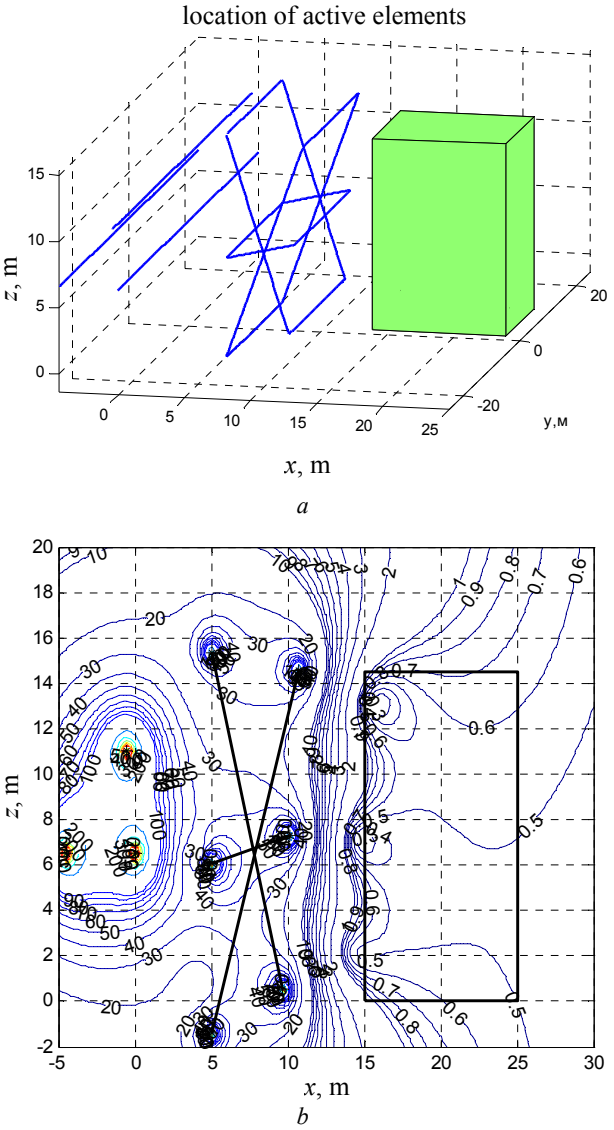

Fig. 5. The layout of PL, compensating windings and protected area (*a*) and distribution of the total magnetic field with the switched on system of active shielding (*b*)

Conclusions.

The analysis of the spatial and temporal distribution of the MF produced by the PL of various designs with ЛБ 330 – 3, У 330, У 330 – 2 «barrel» and У 330 – 1Т «triangle» supports is carried out.

The recommendations on the design of compensating windings for active screening systems for high voltage PL are developed. The results of the synthesis of the active shielding system for the magnetic field of the industrial frequency, a single-circuit power line of 110 kV with supports У 330 – 1Т «triangle», rotating MF with full polarization in a residential five-story house located near the power lines are presented.

The system contains three compensating windings and allows to reduce the level of induction of the initial MF to sanitary standards of 0.5 μT in almost the entire considered space of the living house. The efficiency of the active screening system is about 8.

REFERENCES

1. Active Magnetic Shielding (Field Cancellation). Available at: http://www.emfservices.com/afcs.html (accessed 10 September 2012).

2. Beltran H., Fuster V., García M. Magnetic field reduction screening system for a magnetic field source used in industrial applications. *9 Congreso Hispano Luso de Ingeniería Eléctrica (9 CHLIE)*, Marbella (Málaga, Spain), 2005, pp. 84-99.

3. Ter Brake H.J.M., Huonker R., Rogalla H. New results in active noise compensation for magnetically shielded rooms. *Measurement Science and Technology*, 1993, Vol. 4, Issue 12, pp. 1370-1375. **doi: 10.1088/0957-0233/4/12/010.**

4. Celozzi S., Garzia F. Active shielding for power-frequency magnetic field reduction using genetic algorithms optimization. *IEE Proceedings – Science, Measurement and Technology*, 2004, Vol.151, no.1, pp. 2-7. **doi: 10.1049/ip-smt:20040002**.

5. Shenkman A., Sonkin N., Kamensky V. Active protection from electromagnetic field hazards of a high voltage power line. *HAIT Journal of Science and Engineering. Series B: Applied Sciences and Engineering*, Vol. 2, Issues 1-2, pp. 254-265.

6. Kuznetsov B.I., Turenko A.N., Nikitina T.B., Voloshko A.V., Kolomiets V.V. Method of synthesis of closed-loop systems of active shielding magnetic field of power transmission lines. *Tekhnichna elektrodynamika*, 2016, no.4, pp. 8-10. (Rus).

7. *Pravila ulashtuvannya electroustanovok. Vyd. 3, pererob. i dop* [Electrical Installation Regulations. 3rd edition, revised and enlarged]. Kyiv, Minpalyvenergo of Ukraine Publ., 2010. 736 p. (Ukr).

8. Rozov V.Yu., Grinchenko V.S., Pelevin D.Ye., Chunikhin K.V. Simulation of electromagnetic field in residential buildings located near overhead lines. *Tekhnichna elektrodynamika*, 2016, no.3, pp. 6-8. (Rus).

Received 15.09.2016

B.I. Kuznetsov[1], *Doctor of Technical Science, Professor,*
T.B. Nikitina[2], *Doctor of Technical Science, Professor,*
A.V. Voloshko[1], *Candidate of Technical Science,*
I.V. Bovdyj[1], *Candidate of Technical Science,*
E.V. Vinichenko[1], *Candidate of Technical Science,*
B.B. Kobilyanskiy[1], *Candidate of Technical Science, Associate Professor,*
[1] State Institution «Institute of Technical Problems of Magnetism of the NAS of Ukraine»,
19, Industrialna Str., Kharkiv, 61106, Ukraine,
phone +38 050 5766900, e-mail: bikuznetsov@mail.ru
[2] Kharkov National Automobile and Highway University,
25, Petrovskogo Str., Kharkov, 61002, Ukraine,
e-mail: tatjana55555@gmail.com

How to cite this article:

Kuznetsov B.I., Nikitina T.B., Voloshko A.V., Bovdyj I.V., Vinichenko E.V., Kobilyanskiy B.B. Synthesis of active screening system of magnetic field of high voltage power lines of different design taking into account spatial and temporal distribution of magnetic field. *Electrical engineering & electromechanics*, 2017, no.2, pp. 29-33. **doi: 10.20998/2074-272X.2017.2.04.**

UDC 621.3.01 **doi: 10.20998/2074-272X.2017.2.05**

T.B. Nikitina

PARETO OPTIMAL SOLUTION OF MULTIOBJECTIVE SYNTHESIS OF ROBUST CONTROLLERS OF MULTIMASS ELECTROMECHANICAL SYSTEMS BASED ON MULTISWARM STOCHASTIC MULTIAGENT OPTIMIZATION

Purpose. *Developed the method for solving the problem of multiobjective synthesis of robust control by multimass electromechanical systems based on the construction of the Pareto optimal solutions using multiswarm stochastic multi-agent optimization of particles swarm, which reduces the time of determining the parameters of robust controls multimass electromechanical systems and satisfy a variety of requirements that apply to the work of such systems in different modes.* ***Methodology.*** *Multiobjective synthesis of robust control of multimass electromechanical systems is reduced to the solution of solving the problem of multiobjective optimization. To correct the above problem solving multiobjective optimization in addition to the vector optimization criteria and constraints must also be aware of the binary preference relations of local solutions against each other. The basis for such a formal approach is to build areas of Pareto-optimal solutions. This approach can significantly narrow down the range of possible solutions of the problem of optimal initial multiobjective optimization and, consequently, reduce the complexity of the person making the decision on the selection of a single version of the optimal solution.* ***Results.*** *The results of the synthesis of multi-criteria electromechanical servo system and a comparison of dynamic characteristics, and it is shown that the use of synthesized robust controllers reduced the error guidance working mechanism and reduced the system sensitivity to changes in the control parameters of the object compared to the existing system with standard controls.* ***Originality.*** *For the first time, based on the construction of the Pareto optimal solutions using a multiswarm stochastic multi-agent optimization particle algorithms improved method for solving formulated multiobjective multiextremal nonlinear programming problem with constraints, to which the problem of multiobjective synthesis of robust controls by multimass electromechanical systems that can significantly reduce the time to solve problems and meet a variety of requirements that apply to the multimass electromechanical systems in different modes.* ***Practical value.*** *Practical recommendations on reasonable selection of the target vector of robust control by multimass electromechanical systems. Results of synthesis of electromechanical servo system shown that the use of synthesized robust controllers reduced the error guidance of working mechanism and reduce the system sensitivity to changes of plant parameters compared to a system with standard controls.* References 9, figures 3.

Key words: **multimass electromechanical system, multiobjective synthesis, multiswarm stochastic multiagent optimization, Pareto optimal solution.**

Усовершенствован метод многокритериального синтеза робастного управления многомассовыми электромеханическими системами на основе построения Парето-оптимальных решений и с учетом бинарных отношений предпочтения локальных критериев с помощью алгоритмов многороевой стохастической мультиагентной оптимизации, что позволяет существенно сократить время решения задачи и удовлетворить разнообразным требованиям, которые предъявляются к работе систем в различных режимах. Приведены результаты сравнений динамических характеристик электромеханических систем с синтезированными регуляторами. Библ. 9, рис. 3.

Ключевые слова: **многомассовая электромеханическая система, многокритериальный синтез, многороевая стохастическая мультиагентная оптимизация, Парето-оптимальное решение.**

Introduction. When creating new generations of technology and new technologies, automatic control systems are required that can provide high accuracy in the presence of intense driving and disturbing influences, as well as changes in the structure and parameters of systems during their operation. Such control systems usually have very diverse and often contradictory requirements for the operation of the system in various modes and under various external influences: stepwise, linearly varying, harmonic, random, etc. [8, 9], so that the problem of synthesizing such systems in its formulation is multicriteria.

Problem definition. Multicriterion synthesis of robust control of multimass electromechanical systems can be reduced [8] to the solution of a multicriteria nonlinear programming problem in which the vector objective function

$$f(X)=[f_1(X), f_2(X)...f_k(X)]^T \quad (1)$$

and constraints on controls and variables

$$G(X)\le G_{\max},\ H(X)=0. \quad (2)$$

Components $f_i(X)$ of the vector criterion (1) are local optimization criteria for a multimass electromechanical system, such as the time of the first matching, the time of regulation, overshooting, etc.

The components of the vector of the required parameters X are the elements of the weight matrices, with the help of which the target vector of the robust control is formed [8].

The calculation of the vector objective function (1) and constraints (2) has an algorithmic character and is related to the solution of the problem of synthesizing robust regulators with the help of which the target vector H_∞ is minimized, and reduces to the calculation of four algebraic Riccati equations [8] for computing the robust regulator and Robust observer within the framework of four Riccati approach to the synthesis of robust systems. The solution of the problem of the synthesis of anisotropic regulators, by means of which the average anisotropy of the system is minimized, is reduced to the calculation of four algebraic Riccati equations, the

Lyapunov equation, and a special expression for calculating the anisotropy level of the input signal [9].

Solving the multicriteria optimization problem by collapsing the vector criterion into a scalar one using weight factors [4, 5] actually replaces the original problem of solving multicriteria optimization for the problem of choosing weight factors. Often the problem of correctly determining the weight factors in complexity is many times greater than the original problem of solving the multicriteria optimization problem, since to determine the weight factors it is necessary to solve the problem of scalar optimization repeatedly at the routine load of the decision-maker. In addition, the scalar target function obtained as a result of this transformation has sections of the «plateau» and «ravine» type, which requires special algorithms for solving it, while the scalar components of the vector objective function of the original multicriteria optimization problem are sufficiently smooth.

To date, the development of the theory of the correct solution of the original multicriteria optimization problem is completed on the basis of constructing Pareto-optimal solutions without the procedure for minimizing local criteria. In order to find a global optimum, in addition to specifying a vector objective function and constraints, it is also necessary to specify the binary relations of preferences for local optimization criteria that are components of the initial vector optimization criterion. To solve such a problem on the basis of Pareto-optimal solutions, algorithms of multi-stochastic stochastic multi-agent optimization are being used most successfully [1-3]. In this case, the problems of multicriteria optimization with the limitations [6, 7] are of greatest complexity. Let us consider one of the variants of constructing such an algorithm on the basis of nonlinear control laws.

The goal of the paper is improvement of the method of solving the problem of multicriteria synthesis of robust control multimass electromechanical systems by constructing a Pareto-optimal solutions, and taking into account the binary preference relations of local optimization criteria using multiswarm stochastic multi-agent optimization of particle swarm, which reduces the time of determining the parameters of robust controllers multimass electromechanical systems and meet the diverse requirements that apply to the such systems operation in different modes.

Search for the Pareto set on the basis of multiswarm stochastic multiagent optimization. In order to correctly solve the multicriteria optimization problem, in addition to the vector optimization criterion (1) and constraints (2), it is also necessary to have information about the binary relations of preferences of local solutions relative to each other [5]. The basis of such a formal approach is the construction of Pareto-optimal solutions. This approach allows us to significantly narrow the range of possible optimal solutions of the original multicriteria optimization problem and, consequently, to reduce the complexity of the person making the decision to choose the only variant of the optimal solution.

The problem of finding the minimum of the local criterion $f_i(X)$ in the space under consideration, as a rule, is multiextremal, containing local minima and maxima, therefore, it is expedient to use the stochastic multi-agent optimization algorithms to solve it [2]. Consider the algorithm for finding the set of Pareto-optimal solutions of multicriteria non-linear programming problems on the basis of stochastic multi-agent optimization. To date, a large number of algorithms have been developed for optimizing the swarm of particles – PSO algorithms based on the idea of collective intelligence of a swarm of particles, such as gbest PSO and lbest PSO algorithms [6]. The use of stochastic multi-agent optimization methods for solving multicriteria problems today causes certain difficulties and this direction continues to develop intensively [7]. To solve the original multicriteria nonlinear programming problem (1) with constraints (2), we construct an algorithm for stochastic multi-agent optimization based on the set of particle swarms, the number of which is equal to the number of components of the vector optimization criterion. In the standard optimization algorithm for swarms of particles, the particle velocities are varied according to linear laws [6]. To increase the speed of finding a global solution, special non-linear algorithms of stochastic multi-agent optimization proposed in [1] have recently been extended in which the motion of the i-th particle of the j-th swarm is described by the following expressions

$$v_{ij}(t+1) = w_j v_{ij}(t) + c_{1j} r_{1j}(t) H\left(p_{1j} - \varepsilon_{1j}(t)\right)\left[y_{ij}(t) - x_{ij}(t)\right] + \\ + c_{2j} r_{2j}(t) H\left(p_{2j} - \varepsilon_{2j}(t)\right)\left[y_j^*(t) - x_{ij}(t)\right], \quad (3)$$

$$x_{ij}(t+1) = x_{ij}(t) + v_{ij}(t+1), \quad (4)$$

where $x_{ij}(t)$, $v_{ij}(t)$ are the position and velocity of the i-th particle of the j-th swarm; c_1 and c_2 are the positive constants that determine the weights of the cognitive and social components of the velocity of the particle; $r_{1j}(t)$ and $r_{2j}(t)$ are the random numbers from the range [0, 1], which determine the stochastic component of the velocity component of the particle. Here $y_{ij}(t)$ and y_j^* are the best local – lbest and global – gbest positions of the i-th particle, found respectively by only one i-th particle and all the particles of the j-th swarm. The use of the inertia coefficient w_j makes it possible to improve the quality of the optimization process.

The Heaviside function is used as a function of switching H the particle motion to the local $y_{ij}(t)$ and the global $y_j^*(t)$ optimum, respectively. The parameters for switching cognitive p_{1j} and social p_{2j} components of the particle velocity to the local and global optimum, respectively; The random numbers $\varepsilon_{1j}(t)$ and $\varepsilon_{2j}(t)$ determine the parameters of the particle motion switching, respectively, to the local and global optimum. If $p_{1j} < \varepsilon_{1j}(t)$ и $p_{2j} < \varepsilon_{2j}(t)$, then the velocity of the i-th particle of the j-th swarm does not change at step t and the particle moves in the same direction as in the previous optimization step.

With the help of separate j-th swarms (3), (4), optimization problems for the scalar criteria $f_i(X)$ which are components of the vector optimization criterion (1), are solved. To find a global solution of the original multicriteria problem in the course of searching for optimal solutions of local criteria, individual swarms exchange information among themselves. In this case, to calculate the velocity of the particles of one swarm,

information is used about the global optimum found by the particles of another swarm, which makes it possible to isolate all potential Pareto-optimal solutions. For this purpose, at each step t of the motion of the i-th particle of the j-th swarm, the preferences functions of the local solutions obtained by all swarms are used. The solution $X_j^*(t)$ obtained by optimizing the objective function $f_i(X)$ with the j-th swarm is preferable to the solution $X_k^*(t)$ obtained by optimizing the objective function $f_j(X)$ with the help of the k-th swarm, i.e. $X_j^*(t) \succ X_k^*(t)$, if the binary preference condition is met. Moreover, as the global optimal solution $X_k^*(t)$ of the k-th swarm, a global solution $X_j^*(t)$ obtained by the j-th swarm is used that is preferable to the global solution $X_k^*(t)$ of the k-th swarm based on the preference relation.

In fact, with this approach, the basic idea of the method of successive narrowing of the field of compromises is realized: from the initial set of possible solutions, based on information about the relative importance of local solutions, all Pareto-optimal solutions that can not be selected according to the available information on binary preferences of local criteria are deleted successively. Removal is carried out until a globally optimal solution is obtained. As a result of applying this approach, no potentially optimal solution will be removed at each step of the contraction.

Usually, the initial position of the swarm agents is randomly assigned, and then the swarm moves to the global optimum starting from this position, which characterizes the stochastic properties of the optimization algorithm. The number of agents in the swarm can remain constant, or they will change as the swarm moves. With a constant number of swarm agents, the swarm topologies of the «ring», «square», «star» and «pyramid» types are most often used. In particular, the gbest PSO and lbest PSO algorithms use the swarm topologies of the «star» and «ring» type. If you change the number of agents in a swarm, the initial number of swarm agents is randomly assigned, and then from this number of agents, a random formation of a new number of agents and a new swarm topology begins.

When moving, the swarm particles try to improve the solution they found earlier and exchange information with their neighbors, thereby finding a global optimum for the fewer number of iterations. The advantage of these methods over the classical gradient optimization methods is that they do not require the calculation of the derivatives of the objective function, they are practically insensitive to the proximity of the initial position to the desired optimal solution, and it makes it easier to take into account various constraints in finding the global optimum.

Results of computer modeling. As an example, we consider the transient processes in the electromechanical servo system [9] with synthesized robust regulators. One of the characteristic modes of operation of the electromechanical servo system under consideration is the development of a given linearly varying angle of rotation of the working mechanism. To ensure a zero steady-state error of the system in this mode, a second order of the system's astaticism is required for the determining influence. In the existing system, PD controllers are used, since the introduction of the integral component leads to the emergence of undamped oscillations in the mode of working out the given angles of the position of the working member due to the presence of dry friction on the shafts of the drive motor and the working member. With the help of robust regulators it was possible to ensure a stable operation of the system taking into account all the essential nonlinearities inherent in the elements of this system when two integrating links are introduced into the control loop.

We perform a study of the sensitivity of such a robust system with second-order astatism, taking into account all the nonlinearities for three different values of the moment of inertia of the working member, which varies during the operation of the system.

Fig. 1 shows the transient processes: a) the rotation angle $\varphi(t)$ and b) the rotation speed $\omega_m(t)$ of the working mechanism when hovering at transfer speeds (35 deg/s).

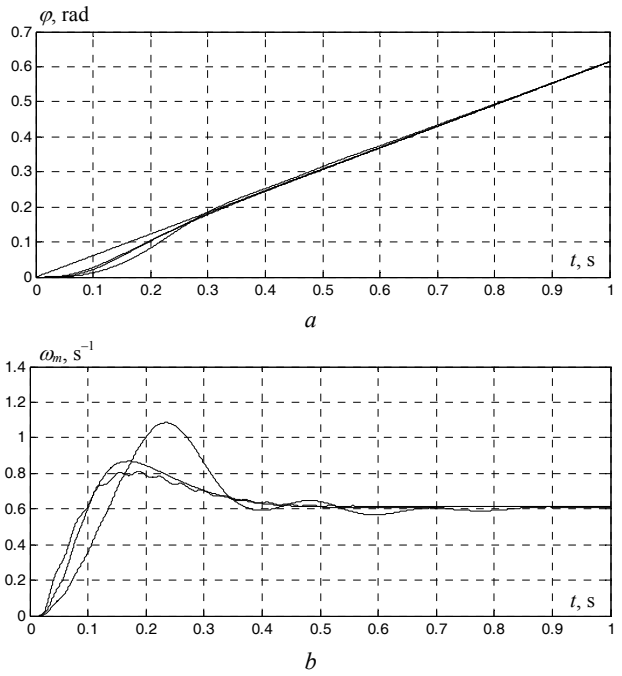

Fig. 1. Transient processes of:
a) rotation angle $\varphi(t)$; *b*) rotation speed $\omega_m(t)$ of the working mechanism when hovering at transfer speeds (35 deg/s)

The steady error in working out the given linearly varying rotation angle of the working mechanism is zero and, consequently, the synthesized system has a second-order astatism. Note that during the first 0.02 s. The working member remains stationary, since during this time the drive motor is stuck and then the shaft connecting the drive motor and the operating member is angled such that the elastic moment becomes greater than the dry friction moment of the working member. When the moment of inertia of the working mechanism changes, the transient processes change insignificantly, which confirms the weak sensitivity of the system being synthesized, and the steady-state velocities of the working mechanism coincide.

Fig. 2 shows the transient processes of the same state variables when the working mechanism is guided at low velocities (0.5 deg/s). At the same time, the working mechanism moves with jerks and with stops, but the steady error of the system is practically zero. It should be noted that in this mode the working element remains stationary during the first 0.08 s, which is four times longer than when the working member moves with a transfer speed, as shown in Fig. 1.

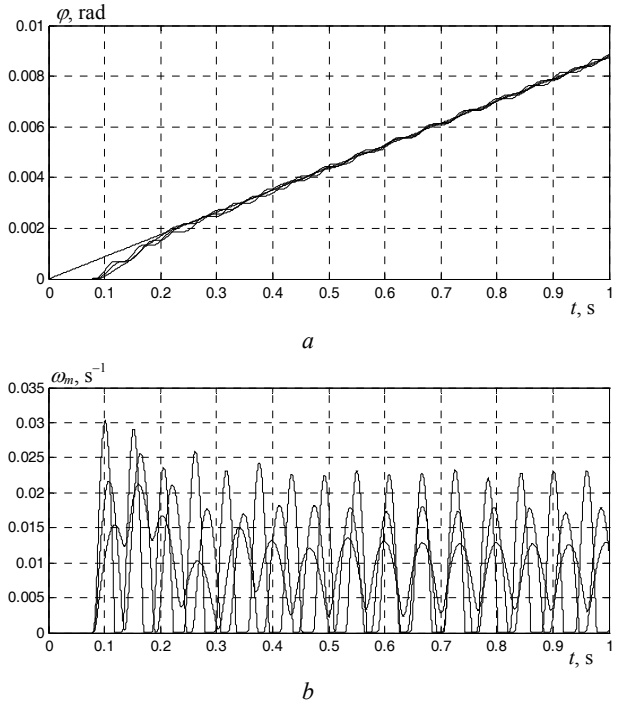

Fig. 2. Transient processes of:
a) rotation angle $\varphi(t)$; *b*) rotation speed $\omega_m(t)$ of the working mechanism when hovering at low speeds (0.5 deg/s)

Fig. 3 shows the transient processes of the same state variables when the working mechanism is guided at super small – creeping speeds (0.02 deg/s). We note that this mode of operation determines the potential accuracy of the electromechanical servo system under consideration and, in general, characterizes its tactical and technical characteristics [9]. In this mode, the working element remains stationary for the first 0.3 s, which is 15 times longer than when the working member moves at transfer speed. Such a long delay in the beginning of the movement of the working element is caused by the required time required for the appearance of an error in working out a given angle of the position of the working member and the generation of the corresponding motor moments and the moment of elasticity of the shaft connecting the drive motor with the working member necessary for friction, first the drive motor, and then Working member of the electromechanical servo system. At the same time, the working mechanism moves in jerks and contains sections like stopping, moving forward, stopping, moving backwards, and the system error in the steady state oscillates with respect to the zero value with an amplitude of $5 \cdot 10^{-4}$ rad.

The results of comparisons of the dynamic characteristics of the servo electromechanical system have shown that the use of synthesized robust controllers has made it possible to reduce the error in setting the working mechanism and to reduce the sensitivity of the system to changes in the parameters of the control object in comparison with the existing system with typical regulators.

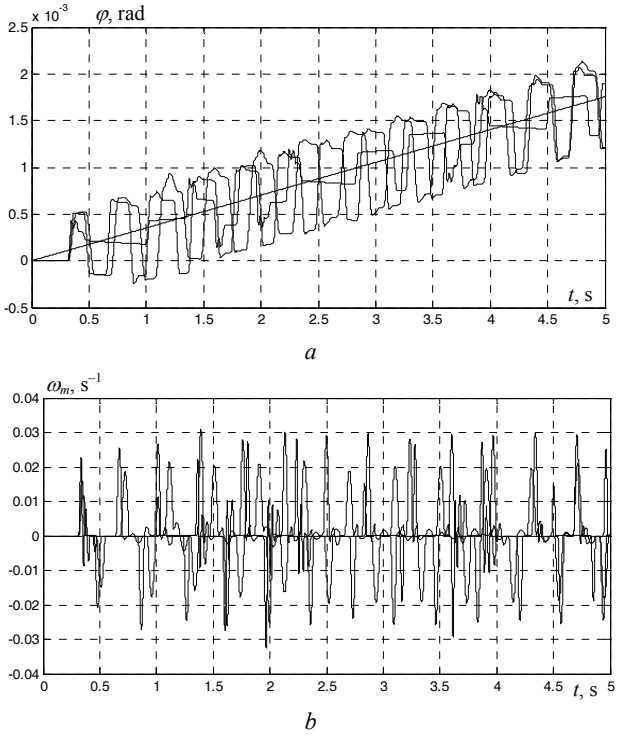

Fig. 3. Transient processes of:
a) rotation angle $\varphi(t)$; *b*) rotation speed $\omega_m(t)$ of the working mechanism when hovering at super small – creeping speeds (0.02 deg/s)

Conclusions.

On the basis of the construction of the Pareto-optimal solutions, and taking into account the binary preference relations of local criteria using stochastic multi-agent optimization particle by multiswarm algorithms improved method for solving formulated multiobjective multiextremal nonlinear programming problem with constraints, to which the problem of multicriteria synthesis of robust controllers multimass electromechanical systems that can significantly reduce the time for solving the problem and satisfy different requirements that apply to the work multimass electromechanical systems in various modes. It is shown that the use of synthesized robust controllers possible to reduce the pointing error of the working mechanism and reduce the sensitivity of the system to change control parameters of the object compared to a typical system regulators.

REFERENCES

1. Abido M.A. Two-level of nondominated solutions approach to multiobjective particle swarm optimization. *Proceedings of the 9th annual conference on Genetic and evolutionary computation – GECCO'07*. 2007, pp. 726-733. **doi: 10.1145/1276958.1277109**.

2. Clerc M. *Particle Swarm Optimization*. London, ISTE Ltd., 2006. 244 p. **doi: 10.1002/9780470612163**.

3. Fieldsend Jonathan E., Singh Sameer. A multi-objective algorithm based upon particle swarm optimization, an efficient data structure and turbulence. *Proceedings of the 2002 U.K. Workshop on Computational Intelligence*, 2002, pp. 37-44.

4. Gazi V., Passino K.M. *Swarm Stability and Optimization*. Springer, 2011. 318 p. **doi: 10.1007/978-3-642-18041-5**.

5. Hu Xiaohui, Eberhart R. Multiobjective optimization using dynamic neighborhood particle swarm optimization. *Proceedings of the 2002 Congress on Evolutionary Computation. CEC'02* (Cat. No.02TH8600). **doi: 10.1109/cec.2002.1004494**.

6. Nor Azlina Ab. Aziz, Mohamad Yusoff Alias, Ammar W. Mohemmed, Kamarulzaman Ab. Aziz. Particle Swarm Optimization for constrained and multiobjective problems: a brief review. *International Conference on Management and Artificial Intelligence IPEDR*. Bali, Indonesia, no.6, pp. 146-150.

7. Zizler Eckart. Evolutionary algorithms for multiobjctive optimizations: methods and applications. *Ph.D. Thesis Swiss Federal Institute of Technology*, Zurich, 1999. 122 p.

8. Nikitina T.B. *Mnogokriterial'nyj sintez robastnogo upravlenija mnogomassovymi sistemami* [Multicriterion synthesis of robust control by multimass systems]. Kharkiv, Kharkiv National Automobile and Highway University Publ., 2013. 432 p. (Rus).

9. Nikitina T.B. Multiobjective synthesis of robust control by multimass electromechanical systems based on Pareto-optimal solution. *Electrical engineering & electromechanics*, 2015, no.1, pp. 29-35. (Rus). **doi: 10.20998/2074-272X.2015.1.06.**

Received 20.11.2016

T.B. Nikitina, *Doctor of Technical Science, Professor,*
Kharkov National Automobile and Highway University,
25, Petrovskogo Str., Kharkov, 61002, Ukraine,
e-mail: tatjana55555@gmail.com

How to cite this article:

Nikitina T.B. Pareto optimal solution of multiobjective synthesis of robust controllers of multimass electromechanical systems based on multiswarm stochastic multiagent optimization. *Electrical engineering & electromechanics*, 2017, no.2, pp. 34-38. **doi: 10.20998/2074-272X.2017.2.05.**

UDC 621.315.2 **doi: 10.20998/2074-272X.2017.2.06**

V.S. Grinchenko, O.O. Tkachenko, N.V. Grinchenko

IMPROVING CALCULATION ACCURACY OF CURRENTS IN CABLE SHIELDS AT DOUBLE-SIDED GROUNDING OF THREE-PHASE CABLE LINE

This paper deals with the calculation of currents in shields of single-core cables at double-sided grounding of three-phase cable lines. We consider flat and trefoil cable lines and receive the analytical expressions for RMS currents in the shields of cables. These expressions allow reducing the shield current calculation error to value of 5 %. We analyze the known approximate expressions for RMS currents in the shields of cables and represent dependencies of corresponding calculation errors on cable line dimensionless parameters. These dimensionless parameters are determined by the distance between the axes of the cables, the radius and the resistance of shields. References 10, figures 4.

Key words: **cable line, shield of a cable, shield current, double-sided grounding.**

В работе рассмотрена задача расчета токов в экранах одножильных кабелей при двустороннем заземлении трехфазной кабельной линии. Для случаев прокладки кабелей в плоскости и треугольником получены аналитические выражения для действующих значений токов в экранах, позволяющие ограничить погрешность расчета на уровне 5 %. Проведен анализ приближенных выражений для токов в экранах кабелей. Представлены графики зависимостей погрешности приближенных выражений от производных безразмерных параметров кабельной линии, которые определяются расстоянием между осями кабелей, радиусом экранов и их активным сопротивлением. Библ. 10, рис. 4.

Ключевые слова: **кабельная линия, экран кабеля, ток в экране, двустороннее заземление.**

Introduction. When laying high-voltage cable power lines (CL), a necessary condition is the grounding of electrically conductive cable shields, one-sided or two-sided. The main advantage of single-sided grounding is the absence of longitudinal currents in the shields, which does not violate the thermal mode of the CL and ensures the maximum throughput of the CL. The disadvantage is the induced potential on the shield and, accordingly, the need to install protective devices against overvoltage [1]. When grounding shields at both ends with transposition of shields, longitudinal currents are also absent. However, the complexity and high cost of transposition limits its universal application. The simplest is the double-sided grounding of the cable shields, which provides no surge voltage and does not require the installation of additional protective devices [1]. In this case, the cable screens form closed contours along which the induced longitudinal currents flow [2-4]. On the one hand, this leads to a decrease in the magnetic field of the CL and contributes to solving the problems of the magnetic ecology; on the other hand, currents in the cable shields can disrupt the thermal mode of the CL and lead to a decrease in the line capacity [5, 6]. Therefore, the calculation of currents in the screens is an actual task.

The analysis of literature sources showed that for the calculation of induced currents in shields with their two-sided grounding, different approximate expressions are used. The normative document [7] contains expressions for calculating the currents in the shields when laying cables in the plane and with a triangle. These approximate expressions have a simple form and are used in practice when designing CL. In [8], the problem of thermal losses in cable screens is considered, and expressions for the current values of currents are given. For the case of laying cables in a triangle, the above expression is compact, but for the case of laying in the plane, expression are rather cumbersome. Therefore, to estimate the magnitude of the currents in the screens when laying cables in the plane, use a compact expression for laying with a triangle, assuming the distance between the cables is equal to the mean geometric interphase distance of the CL. In [9], this approach was used to analyze the inductance of three-phase CL for arbitrary arrangement of cables.

Approximate expressions are convenient for engineering calculations. However, as shown below, the error in calculating the currents in the shields with the help of approximate expressions can be more than 30%.

The goal of the paper is obtaining expressions for the effective values of currents in cable shields with their two-sided grounding, which makes it possible to limit the calculation error at the level of 5% with a real spread of the CL parameters.

Calculation of currents in the cable shields. In [10] an analytical model of the magnetic field of a three-phase CL with two-sided shielded single-core cables was developed. It is applicable under the following natural assumptions: the distribution of the induced current in the screen of each cable is uniform, and the thickness of the screen is much smaller than its radius. The model makes it possible to calculate the currents in the shields and the distribution of the magnetic induction of the field created by the CL for arbitrary arrangement of its cables. The scatter of the results of calculating the magnetic induction and experimental data [3, 4] does not exceed 5%.

In [10] analytical expressions for the complex amplitudes of currents induced in cable shields with their two-sided grounding are given. Calculating the modulus of these expressions, bringing such terms and dividing by, we obtain expressions for the effective values of the currents in the shields. As variables it is convenient to use the following dimensionless CL parameters:

$$Q = \frac{\mu_0 \omega}{2\pi R^*}, \quad \Delta = \frac{s}{r},$$

where $\omega = 2\pi \cdot 50$ s^{-1} is the frequency of the current; R^* is cable length unit length resistance, Ω/m; s is the distance between axes of adjacent cables, m; r is the radius of the shield section, m; $\mu_0 = 4\pi \cdot 10^{-7}$ H/m is the magnetic constant.

If the cables are laid in a plane, and the currents in the veins form a system of direct sequence, then the expressions for the current values of the currents in the shields with their bilateral grounding take the following form:

$$I_1^{\text{sh}} = I \cdot \sqrt{\frac{\left(Q \cdot \ln 2\Delta \cdot \ln \frac{\Delta^3}{2} + \sqrt{3} \cdot \ln 2\right)^2 + \ln^2 4\Delta^3}{\left(Q \cdot \ln 2\Delta \cdot \ln \frac{\Delta^3}{2} - \frac{3}{Q}\right)^2 + 4 \cdot \ln^2 2\Delta^3}},$$

$$I_2^{\text{sh}} = I \cdot \sqrt{\frac{Q^2 \cdot \ln^2 \frac{\Delta^3}{2}}{9 + Q^2 \cdot \ln^2 \frac{\Delta^3}{2}}}, \quad (1)$$

$$I_3^{\text{sh}} = I \cdot \sqrt{\frac{\left(Q \cdot \ln 2\Delta \cdot \ln \frac{\Delta^3}{2} - \sqrt{3} \cdot \ln 2\right)^2 + \ln^2 4\Delta^3}{\left(Q \cdot \ln 2\Delta \cdot \ln \frac{\Delta^3}{2} - \frac{3}{Q}\right)^2 + 4 \cdot \ln^2 2\Delta^3}},$$

where I is the effective current value in the conductors of the cables.

In the case of an inverse sequence of currents in the conductors, expressions for the currents in the shields of the first and third cables are interchanged in (1).

In the case of laying cables by a triangle, the current values of the currents in the screens with their two-sided grounding are equal to each other [8, 10]:

$$I^{\text{sh}} = I \cdot \sqrt{\frac{Q^2 \ln^2 \Delta}{1 + Q^2 \ln^2 \Delta}}. \quad (2)$$

In [7-9] various approximate expressions are given for calculating the effective values of the currents in the screens when laying cables in the plane. To determine the error of these expressions, we use (1). Quantitatively, the error is defined as follows:

$$\varepsilon = \sum_{k=1}^{3} \sqrt{\frac{1}{3}\left(1 - \frac{I_k^{approx}}{I_k^{sh}}\right)^2} \cdot 100\%, \quad (3)$$

where I_k^{sh} is the effective value of current in the k-th cable shield calculated by (1); I_k^{approx} is the effective value of current in the shield calculated by approximate expressions [7-9].

Analysis of the errors of approximate expressions for currents in shields when laying cables in a plane. In the normative document [7, p. 297] an approximate expression is presented for calculating the currents in the shields when laying cables in the plane. Writing it through Q, we get:

$$I_k^{approx} = I \cdot \sqrt{0.75 \cdot \frac{42.5 \cdot Q^2}{\pi^2 + 42.5 \cdot Q^2} + 0.25 \cdot \frac{25 \cdot Q^2}{\pi^2 + 25 \cdot Q^2}}. \quad (4)$$

We use (3) to find the error in calculating the currents with the help of (4). Fig. 1 shows the graphs of the dependences of the relative deviation of ε from the derivatives of the CL parameters. The curves are plotted for intervals of Q and Δ values, which are characteristic for CR, calculated for voltages of 45 ÷ 330 kV. Note that the values of Q equal to 0.15 and 0.35 are attained at values of the resistance R^* equal to $0.42 \cdot 10^{-3}$ Ω/m и $0.18 \cdot 10^{-3}$ Ω/m which in turn are characteristic for shields with cross-sections of 45 mm^2 and 105 mm^2, respectively.

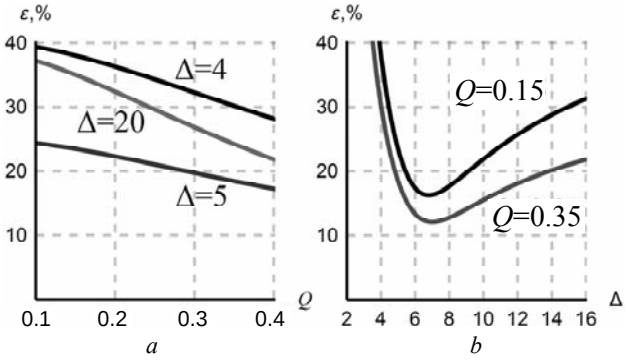

Fig. 1

From the presented graphs it is seen that the error ε as a whole is determined by the value Δ (Fig. 1,*b*), and the dependence of ε on Q, i.e. on the active resistance of the shield, can be ignored (Fig. 1,*a*). From Fig. 1,*b* it follows that an error of less than 20% is achieved in a rather narrow range for values of Δ greater than 5 and less than 10-12. If the distance between axes of adjacent cables is less than 4 or more than 20 screen radii, then the error of application (4) for calculating the currents in shields with their bilateral grounding may exceed 30%.

Using the approach presented in [9, p. 180], to calculate the currents in the screens when laying cables in the plane, one can use expression (2) with Δ replaced by, where is the geometric mean distance between the cable axes. Then, in terms of Q and Δ, the expression for determining the effective value of the current in the screen of each cable will have the following form:

$$I_k^{approx} = I \cdot \sqrt{\frac{Q^2 \cdot \ln^2 \Delta\sqrt[3]{2}}{1 + Q^2 \cdot \ln^2 \Delta\sqrt[3]{2}}}. \quad (5)$$

The error in applying this expression can be calculated using (3). The results of the calculation are shown in Fig. 2.

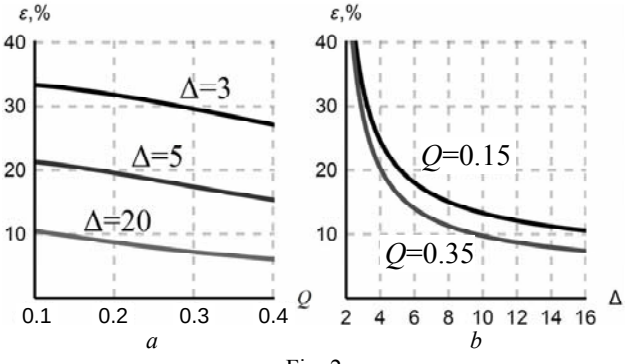

Fig. 2

As in the previous case, the error depends weakly on the parameter Q (Fig. 2,*a*) and essentially depends on the value of Δ (Fig. 2,*b*). The error of 20% is reached at Δ>5. For Δ<3, the error in applying expression (5) exceeds 30%.

Expressions for calculating the current values of currents in double-sided earthed shields when laying cables in the plane are also given in [8, p. 227]. In terms of Q and Δ, they can be written as follows:

$$I_1^{approx} = I \cdot \sqrt{0.75 \cdot \frac{Q^2 \ln^2 2\Delta}{1 + Q^2 \ln^2 2\Delta} + 0.25 \cdot \frac{Q^2 \ln^2 \frac{\Delta}{\sqrt[3]{2}}}{1 + Q^2 \ln^2 \frac{\Delta}{\sqrt[3]{2}}} + \frac{2}{\sqrt{3}} \cdot \frac{Q^3 \cdot \ln 2\Delta \cdot \ln \frac{\Delta}{\sqrt[3]{2}} \cdot \ln 2}{\left(1 + Q^2 \ln^2 2\Delta\right) \cdot \left(1 + Q^2 \ln^2 \frac{\Delta}{\sqrt[3]{2}}\right)}},$$

$$I_2^{approx} = I \cdot \sqrt{\frac{Q^2 \ln^2 \frac{\Delta}{\sqrt[3]{2}}}{1 + Q^2 \ln^2 \frac{\Delta}{\sqrt[3]{2}}}}, \qquad (6)$$

$$I_3^{approx} = I \cdot \sqrt{0.75 \cdot \frac{Q^2 \ln^2 2\Delta}{1 + Q^2 \ln^2 2\Delta} + 0.25 \cdot \frac{Q^2 \ln^2 \frac{\Delta}{\sqrt[3]{2}}}{1 + Q^2 \ln^2 \frac{\Delta}{\sqrt[3]{2}}} - \frac{2}{\sqrt{3}} \cdot \frac{Q^3 \cdot \ln 2\Delta \cdot \ln \frac{\Delta}{\sqrt[3]{2}} \cdot \ln 2}{\left(1 + Q^2 \ln^2 2\Delta\right) \cdot \left(1 + Q^2 \ln^2 \frac{\Delta}{\sqrt[3]{2}}\right)}}.$$

Let us investigate the error in calculating the currents with the help of (6). Fig. 3 shows the dependence of the error ε on Q and Δ calculated according to (3).

The greatest error is reached at $\Delta = 4$, and it does not exceed 15%. At the same time, for Q>0.25, the error exceeds the permissible value for engineering calculations of 10%.

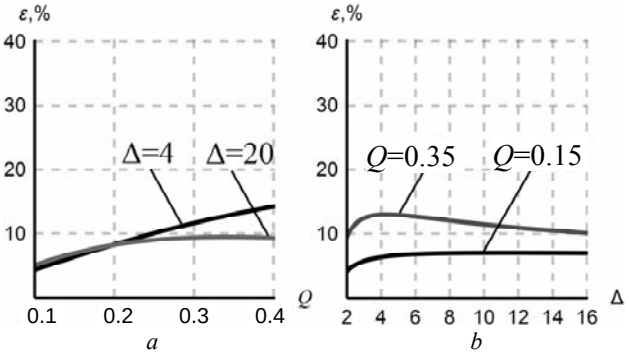

Fig. 3

Analysis of the error of the approximate expression for the currents in the shields when the cables are laid with a triangle. Separately, consider the case of laying cables in a triangle. In the normative document [7, p. 296], in order to calculate the effective currents in two-sided earthed shields, instead of (2) it is recommended to use the following expression:

$$I^{approx} = I \cdot \sqrt{\frac{0.0019}{R_{70}^2 + 0.0019}},$$

where R_{70} is the resistance of the shield of 1 km of the cable, Ω/km.

Rewriting it through the dimensionless parameter Q, we obtain:

$$I^{approx} = I \cdot \sqrt{\frac{4.75 \cdot Q^2}{\pi^2 + 4.75 \cdot Q^2}}. \qquad (7)$$

Since the effective values of the currents in the screens are equal when the triangle is laid, the error in applying the approximate expression (7) is defined as follows:

$$\varepsilon = \left|1 - \frac{I^{approx}}{I^{sh}}\right| \cdot 100\%,$$

where I^{sh} is calculated by (2), and I^{approx} is calculated by (7).

The graphs of the dependences of ε on Q and Δ are shown in Fig. 4. As can be seen from Fig. 4,*a*, the error varies only slightly with Q, which indicates an insignificant effect of the active resistance. From the dependence shown in Fig. 4,*b* we can conclude that the error of the approximate formula (7) does not exceed 20% only for Δ<2.4. At the same time, for Δ>5, the error ε exceeds 50%.

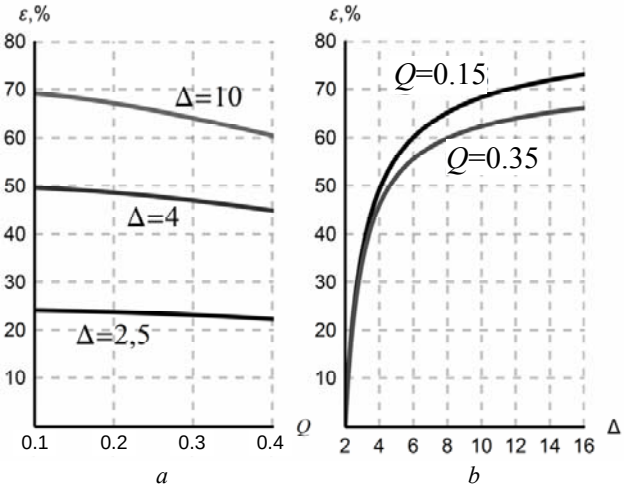

Fig. 4

Thus, when calculating the current values of currents in cable shields for bilateral grounding, it is recommended to use expressions (1) in case of laying cables in the plane and expression (2) in case of laying by triangle.

Conclusions.

1. Analytical expressions are obtained which, for cases of laying cables in the plane and with a triangle, allow calculating the effective values of currents in the cable shields with an error of 5% at their are double-sided grounding.

2. It is established that the error in calculating the effective values of the currents in the shields with the help of approximate expressions known from the literature sources exceeds 30% in a wide range of parameters of the cable line.

This work was supported by the State Fund for Fundamental Research of Ukraine under grant Ф70/18937.

REFERENCES

1. Bystrov A.V. *Razrabotka metodiki vybora energoeffektivnoi sistemy zazemleniia ekranov odnozhil'nykh silovykh kabelei s izoliatsiei iz sshitogo polietilena na napriazhenie 6-500 kV*. Autoref. diss. kand. techn. nauk [The development of selection methodology of energy efficient grounding systems of 6-500 kV XLPE insulated single-core power cable shields. Abstracts cand. tech. sci. diss.]. Moscow, 2014. 20 p. (Rus).

2. Grinchenko V.S. Increase of screening efficiency of technogenic magnetic field of underground high-voltage power cables. *Visnik Nacional'noi' akademii' nauk Ukrai'ni – Herald of the National Academy of Sciences of Ukraine*, 2014, no.8, pp. 71-76. (Ukr).

3. Rozov V.Yu., Dobrodeyev P.N., Erisov A.V., Tkachenko A.O. Increasing the efficiency of contour shielding of the magnetic field of high-voltage cable lines. *Tekhnichna Elektrodynamika*, 2016, no.4, pp. 5-7. (Rus).

4. Rozov V.Yu., Kvytsynskyi A.A., Dobrodeyev P.N., Grinchenko V.S., Erisov A.V., Tkachenko A.O. Study of the magnetic field of three phase lines of single core power cables with two-end bonding of their shields. *Electrical engineering & electromechanics*, 2015, no.4, pp. 56-61. (Rus). **doi: 10.20998/2074-272X.2015.4.11.**

5. Antonets T.Yu., Vepryk Yu.M., Shchebeniuk L.A. Heat tests of power cables with XLPE insulation at direct voltages up to 110 Kv. *Electrical engineering & electromechanics*, 2015, no.6, pp. 43-46. (Ukr). **doi: 10.20998/2074-272X.2015.6.07.**

6. Shchebeniuk L.A., Antonets T.Yu. Investigation of losses in insulation of high-voltage power cables with XLPE insulation. *Electrical engineering & electromechanics*, 2016, no.4, pp. 58-62. (Ukr). **doi: 10.20998/2074-272X.2016.4.08.**

7. *Pravila ulashtuvannya electroustanovok* [Electrical installation regulations]. Kharkiv, Minenergovugillya of Ukraine Publ., 2014. 793 p. (Ukr).

8. Larina E.T. *Silovye kabeli i vysokovoltnye kabelnye linii* [Power cables and high-voltage cable lines]. Moscow, Energoatomizdat Publ., 1996. 464 p. (Rus).

9. Kalantarov P.L., Tseytlin L.A. *Raschet induktivnostey* [Inductance calculations]. Leningrad, Energoatomizdat Publ., 1986. 488 p. (Rus).

10. Rozov V.Yu., Tkachenko A.O., Erisov A.V., Grinchenko V.S. Analytical calculation of magnetic field of three-phase cable lines with two-point bonded shields. *Tekhnichna Elektrodynamika*, 2017, no.2, pp. 13-18. (Rus).

Received 18.01.2017

V.S. Grinchenko[1]*, Candidate of Technical Science,*
O.O. Tkachenko[1]*, Postgraduate Student,*
N.V. Grinchenko[2]*, Candidate of Technical Science,*
[1] State Institution «Institute of Technical Problems of Magnetism of the NAS of Ukraine»,
19, Industrialna Str., Kharkiv, 61106, Ukraine,
phone +380 572 992162,
e-mail: vsgrinchenko@gmail.com, oleksandr.tk7@gmail.com
[2] Ukrainian State University of Railway Transport,
7, Feuerbach Sq., Kharkiv, 61050, Ukraine,
phone +380 57 7301055

How to cite this article:
Grinchenko V.S., Tkachenko O.O., Grinchenko N.V. Improving calculation accuracy of currents in cable shields at double-sided grounding of three-phase cable line. *Electrical engineering & electromechanics*, 2017, no.2, pp. 39-42. **doi: 10.20998/2074-272X.2017.2.06.**

UDC 679.7:678:544 **doi: 10.20998/2074-272X.2017.2.07**

E.V. Chuleyeva, V.M. Zolotaryov

STUDY OF THE INFLUENCE OF MAGNESIUM HYDROXIDE ON THE COMBUSTIBILITY PERFORMANCE OF POLYMER COMPOSITIONS BASED ON ETHYLENE VINYL ACETATE COPOLYMER

Purpose. To obtain the flame retardants polymer compositions for cables tested the effect of use EVA compositions with magnesium hydroxide, on indicators combustibility polymer. Methodology. We used the method of differential scanning calorimetry and defined heat flux dependence on the test time for each composition at temperatures from 20 ℃ to 600 ℃ rate of temperature rise: 50 ℃/min, 75 ℃/min, 100 ℃/min. Using the model of free kinetics we determined dependence of the activation energy from the conversion, a dependence of the conversion on the time of the test, the dependence of the time of the conversion from the temperature for each concentration. To comparison of these parameters for each composition we plotted the dependence of the time of the conversion from the temperature and the dependence the degree of conversion from the time of temperature exposure during the combustion of each of the compositions. Results. We obtained the kinetic characteristics, allowing to determine the composition, which provided the best results to reducing the kinetic parameters of flammability of polymeric compositions. Originality. For the first time we used the DSC and model-free kinetics to determine the effect properties of ingredients of the polymer compositions on the combustibility performance. Practical use. The research results can be used to develop polymer compositions for cable products. References 18, tables 3, figures 9.

Key words: **ethylene vinyl acetate copolymer, magnesium hydroxide, combustibility, polymeric composition, kinetics.**

Цель. Целью статьи является определение влияния дигидрата оксида магния на показатели горючести полимерных композиций на основе сополимера этилена с винилацетатом для разработки составов полимерных композиций для кабельной продукции с повышенными требованиями по пожарной безопасности. Методика. Мы применили метод дифференциальной сканирующей калориметрии (ДСК) и определили зависимость теплового потока от времени испытания для каждого состава при температурах от 20 ℃ до 600 ℃ и разной скорости подъема температуры: 50 ℃/мин, 75 ℃/мин, 100 ℃/мин. Используя модель свободной кинетики определили зависимость энергии активации от степени превращения, зависимость степени превращения от времени испытания, зависимость времени превращения от температуры для каждой концентрации. Для сравнения этих показателей для каждой композиции строили графики зависимости времени превращения от температуры и зависимости степени превращения от времени воздействия температуры при сгорании каждой из композиций. Результаты. Получены кинетические характеристики, позволяющие определить состав, обеспечивающий лучшие результаты по снижению кинетических показателей горючести полимерных композиций. Научная новизна. Впервые мы использовали ДСК и модель свободной кинетики для определения влияния свойств ингредиентов полимерных композиций на показатели горючести. Практическое применение. Результаты исследований могут быть использованы при разработке полимерных композиций для кабельной продукции. Библ. 18, табл. 3, рис. 9.

Ключевые слова: **сополимер этилена с винилацетатом, дигидрат оксида магния, горючесть, полимерная композиция, кинетика.**

Introduction.

Increasing the fire safety requirements for polymer compositions for the manufacture of cable products is given increasing importance due to the increasing application of the latter in a wide variety of technical and economic fields and tougher requirements for fire safety in construction, energy, nuclear energy, railway transport [1-4].

One of the ways to reduce the combustibility of polymer materials based on polyolefins is the introduction of filler-flame retardants into the polymer composition. Inorganic fillers-fire retardants, in particular magnesium hydroxides are used. These materials not only increase fire resistance by absorbing a large amount of heat, but also neutralize acid gases, which leads to a reduction in smoke formation [5-9].

The heating of polymeric materials to temperature at which a sharp increase in the rate of exothermic oxidation reactions takes place, results in the appearance of smoldering. Smoldering is the flameless burning of a solid material at relatively low temperatures (400-600) °C often accompanied by the emission of smoke.

The cable products are required to meet the burning performance: an exothermic reaction with an oxidizer, heat of combustion, combustion temperature, energy of heat release, burning rate. Data on these parameters for polymer compositions based on the ethylene-vinyl acetate copolymer and magnesium oxide are absent [10, 11]. Therefore, it is expedient to investigate these processes when developing and assessing the fire hazard of polymer materials for cable products.

The goal of investigations is study of the effect of magnesium dihydrates on the flammability of polymer compositions based on ethylene vinyl acetate copolymer.

Experimental investigations.

Carrying out investigations we used ethylene copolymers with vinyl acetate (CVA), the characteristics of which are given in Table 1.

Table1

CVA characteristics

Indicator name	CVA 1	CVA 2
Density, kg/m^3	939	951
Melt flow index, 2.16 kg, g/10 min	2.5	5
Content of vinyl acetate, %	18	28

Magnesium dihydrates the characteristics of which are given in Table 2 were they used as retardants fillers.

Table 2

Characteristics of retardant fillers

Name of indicators	$Mg(OH)_2$	
	Sample No. 1	Sample No. № 2
Mass fraction, %		
$Mg(OH)_2$	> 93	> 93.2
SiO_2	< 0.05	2.2 ± 0.2
Fe_2O_3	< 0.3	0.12 ± 0.02
Na_2O	< 0.05	–
CaO	–	2.2 ± 0.2
Median particle diameter, μm:		
average (D_{50})	3.0	3.7
maximal (D_{98})	20.0	12.5
minimal (D_{10})	1.0	1.1

Polymer compositions are presented in Table 3.

Table 3

Polymer compositions

Polymer composition	Components, %			
	CVA 1	CVA 2	$Mg(OH)_2$	$Mg(OH)_2$
			Sample No. 1	Sample No. 2
1a	60		40	
2a		60	40	
3a	60			40
4a		60		40
1b	50		50	
2b		50	50	
3b	50			50
4b		50		50
1c	40		60	
2c		40	60	
3c	40			60
4c		40		60

Thermal, temperature and kinetic characteristics were determined from the data obtained on the TGA/DSC 1/1100 SF device for differential scanning calorimetry from METTLER TOLEDO Company at temperature from 20 °C to 650 °C and heating rate (β) of 50 °C /min, 75 °C/min and 100 °C /min.

Differential scanning calorimetry is based on the well-known principle of Boersma, or the principle of heat flow, in accordance with which the heat fluxes of the sample and the reference measurement are compared.

TGA/DSC 1 is a highly sensitive measuring instrument of thermogravimetric analysis (TGA). The main node TGA/DSC 1 is a measuring cell which includes a furnace and a balance. In addition to the mass of the sample, which is measured with the built-in high-precision balance, TGA/DSC 1 provides a sample temperature measurement. Together with the value of the reference temperature, these values form the basis of the thermogravimetric analysis of the sample. In addition, TGA/DSC 1 allows the measurement of the heat flux signal, thereby providing the use of differential scanning calorimetry (DSC). The sample temperature and the heat flux signal are determined based on the readings of the temperature sensors, which is measured directly with a thermocouple mounted in the crucible holder.

The heat flux is calculated from the DTA (differential thermal analysis) signal, which is the difference between the sample temperature and the temperature set in the temperature program. The module transmits the measurement data to the software, which determines the amount of heat flow from the formulas:

$$\varphi = E_{(T)} SDTA,$$

$$SDTA = T_s - T_{set},$$

where φ is the heat flux, $E_{(T)}$ is the calorimetric sensitivity, T_s is the measured sample temperature, T_{set} is the temperature value given in the temperature program [12].

Kinetic calculations were performed using the model of free kinetics [13-18]. The model of free kinetics is based on the temperature dependence and the degree of transformation. Each transformation gives the calculated value of the activation energy. The reaction rate for a fixed degree of conversion depends only on temperature. The Arrhenius temperature function is used.

For the analysis, three dynamic temperature curves were used for each polymer composition (Fig. 1). Dynamic, isothermal and combined temperature programs were used.

The processing of kinetic experiments is based on the theoretical equation of S. Vyazovkin:

$$\frac{d\alpha}{dt} = ke^{-E/RT} f(\alpha),$$

where $\frac{d\alpha}{dt}$ is the reaction speed, s^{-1}; k is the speed constant; E is the activation energy, J/mol; R is the universal gas constant, J/(mol×K); T is the temperature, K; α is the degree of transformation, %.

The activation energy $E(\alpha)$ is constant for a certain degree of transformation (the isoconversion method).

The rate of chemical reaction depends on the degree of transformation (α), temperature (T) and time (t). The reaction speed depends on the degree of transformation $f(\alpha)$. For each process, speed is own and is determined experimentally.

Based on the DSC obtained using the above programs, we obtain graphical data on the dependence of the activation energy $E(\alpha)$ on the degree of conversion (in our case, the degree of combustion); the dependence of the degree of transformation (α) on the test time (t) at fixed temperature (T) and the dependence of the transformation time (t) on temperature at fixed degree of transformation (α) (Fig. 1).

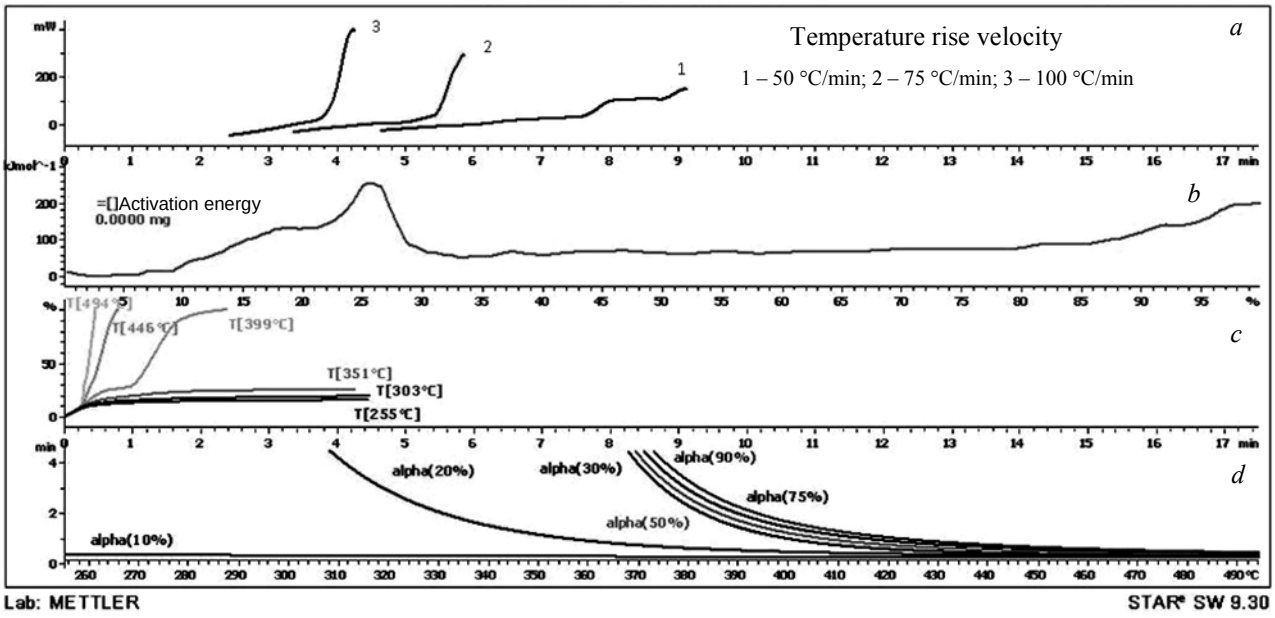

Fig. 1. Thermal, temperature and kinetic characteristics:
a – the dependence of the heat flux on the test time;
b – dependence of the activation energy on the degree of transformation;
c – dependence of the degree of transformation on the test time;
d – dependence of the transformation time on temperature

To determine the effect of the ingredients of the polymer compositions on the kinetic characteristics, graphs were constructed of the dependence of the transformation time on temperature at a constant conversion degree (α = 75%). The results are shown in Fig. 2-5.

From the analysis of the obtained data it follows that the kinetic characteristics of the polymer compositions essentially depend on the properties of both CVA 1 and CVA 2 as well as fillers.

The transformation time decreases when exposed to elevated temperatures. At the same time, in the temperature range close to combustion temperatures (430 °C), the conversion time is higher for the polymer composition based on CVA 1 and flame retardant (sample No. 1). As the temperature rises to 520° C, the transformation time decreases.

An analogous dependence is observed for polymer compositions based on CVA 2.

However, the transformation time is of greater importance than for CVA 1 based polymer compositions.

The dependence of the degree of conversion on the time of exposure to an elevated temperature close to the combustion temperature of polymer compositions was studied.

For this purpose, graphical dependencies of these characteristics were constructed at a temperature of 440 °C (Fig. 6-9).

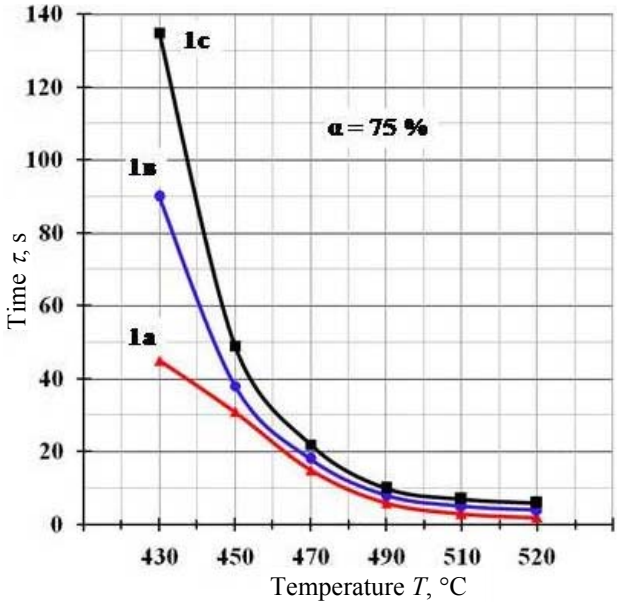

Fig. 2. Dependence of the transformation time on temperature for polymer compositions 1a, 1b, 1c

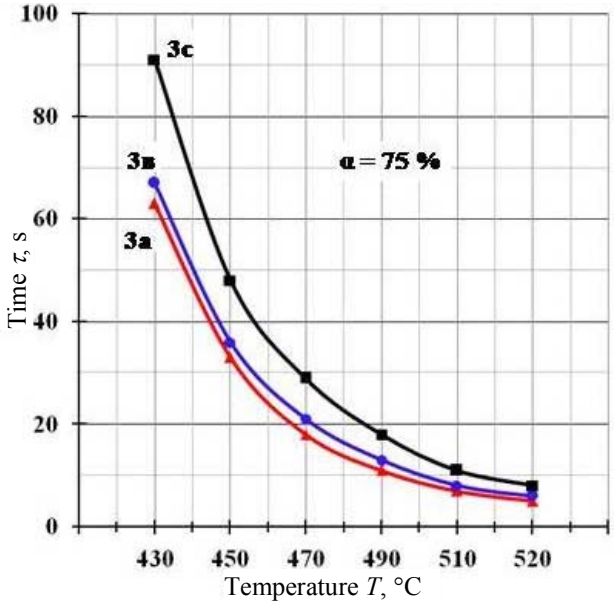

Fig. 3. Dependence of the transformation time on temperature for polymer compositions 3a, 3b, 3c

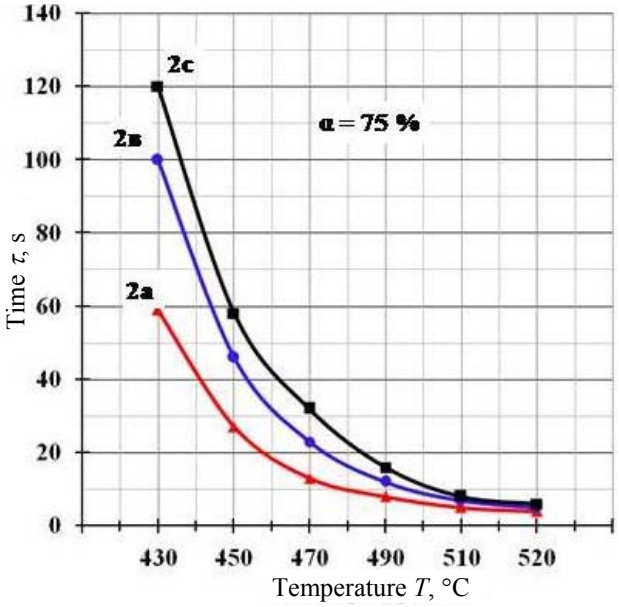

Fig. 4. Dependence of the transformation time on temperature for polymer compositions 2a, 2b, 2c

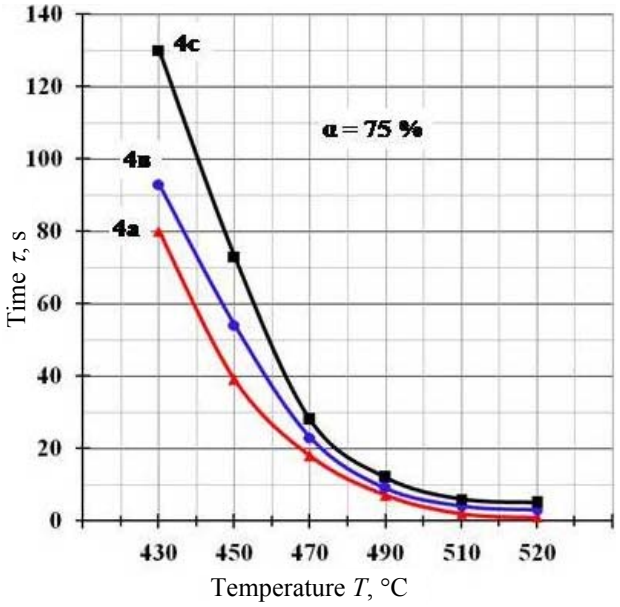

Fig. 5. Dependence of the transformation time on temperature for polymer compositions 4a, 4b, 4c

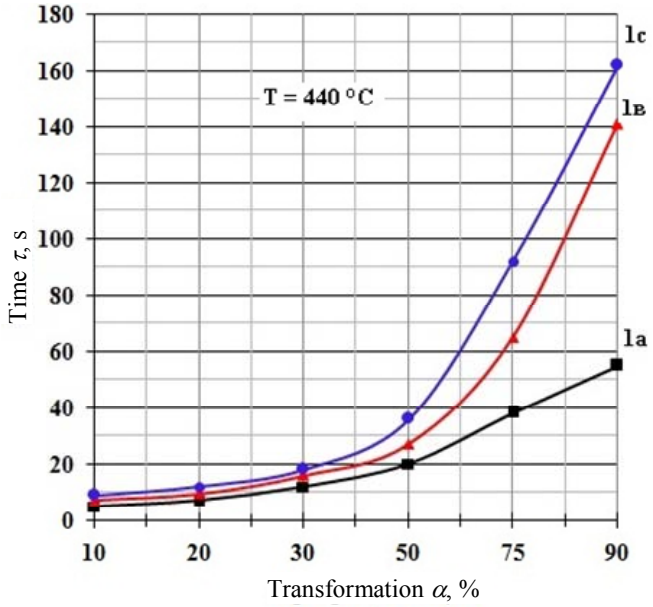

Fig. 6. Dependence of the degree of transformation on the temperature influence time for compositions 1a, 1b, 1c

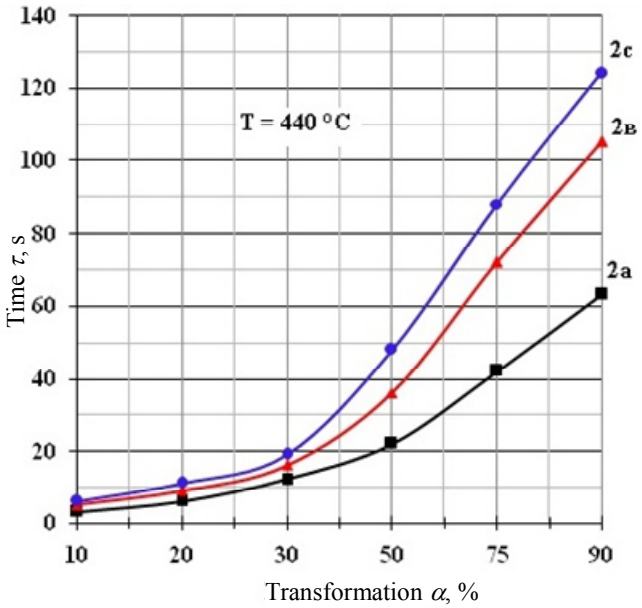

Fig. 7. Dependence of the degree of transformation on the temperature influence time for compositions 2a, 2b, 2c

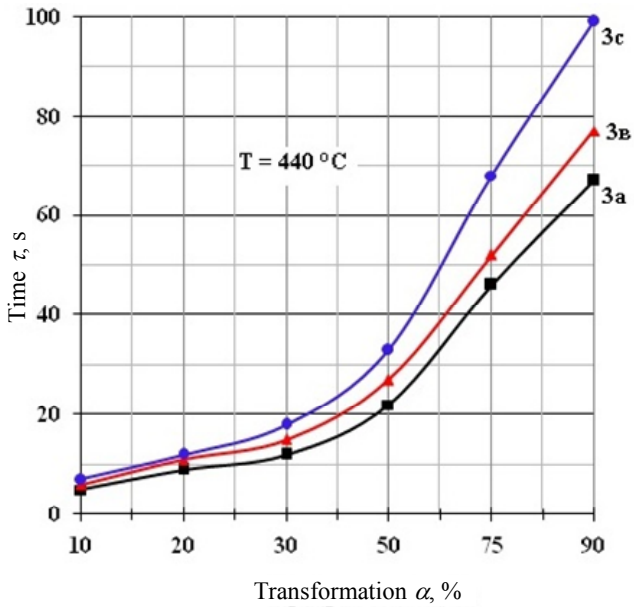

Fig 8. Dependence of the degree of transformation on the temperature influence time for compositions 3a, 3b, 3c

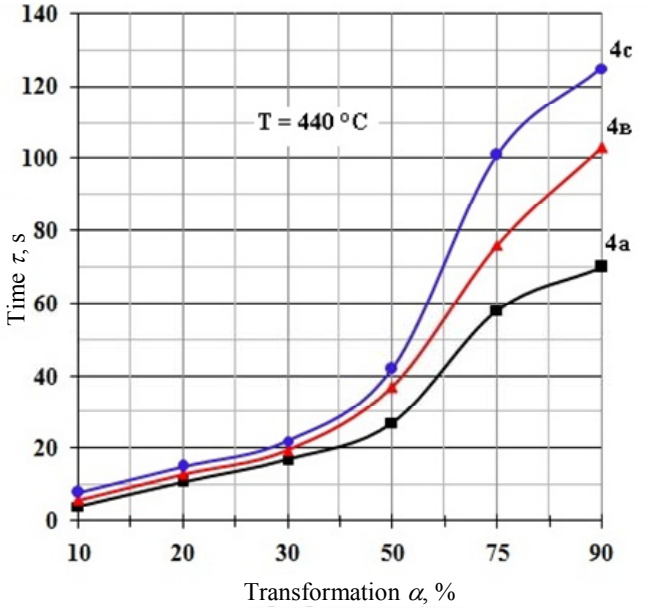

Fig. 9. Dependence of the degree of transformation on the temperature influence time for compositions 4a, 4b, 4c

From the data presented, it follows that the degree of transformation α increases with the time of exposure to an elevated temperature.

In this case, the exposure time should be significantly increased for polymer compositions based on CVA 2 and filler (sample No. 2).

Conclusions.

1. Kinetic characteristics are obtained for polymer compositions based on CVA using magnesium oxide dihydrate as an excipient for retardant.

2. The composition based on CVA2 (with high content of vinyl acetate and a high melt flow index) with a filler (sample No. 2) with smaller maximum particle diameter and largest content of SiO_2 guarantees better results to reduce flammability indicators.

REFERENCES

1. *DSTU EN 50363-7:2010. Materialy dlya izolyatsiyi, obolonok i zovnishnikh pokryviv nyz'konapruzhnykh sylovykh kabeliv. Chastyna 7. Bez·halohenni termoplastychni izolyatsiyni kompozytsiyi* [State Standard of Ukraine EN 50363-7:2005. Insulating, sheathing and covering materials for low voltage energy cables. Part 7: Halogen-free, thermoplastic insulating compounds]. Kyiv, 2013. p. 4. (Ukr).

2. *DSTU EN 50363-5:2010. Materialy dlya izolyatsiyi, obolonok i zovnishnikh pokryviv nyz'konapruzhnykh sylovykh kabeliv. Chastyna 5. Bez·halohenni vulkanizovani izolyatsiyni kompozytsiyi* [State Standard of Ukraine EN 50363-5:2005. Insulating, sheathing and covering materials for low voltage energy cables. Part 5: Halogen-free, cross-linked insulating compounds]. Kyiv, 2013. p. 4. (Ukr).

3. *DSTU EN 50363-6:2010. Materialy dlya izolyatsiyi, obolonok i zovnishnikh pokryviv nyz'konapruzhnykh sylovykh kabeliv. Chastyna 6. Bez·halohenni vulkanizovani kompozytsiyi obolonok* [State Standard of Ukraine EN 50363-6:2005. Insulating, sheathing and covering materials for low voltage energy cables. Part 6: Halogen-free, cross-linked sheathing compounds]. Kyiv, 2013. p. 4. (Ukr).

4. Peshkov I.B. *Materialy kabel'nogo proizvodstva* [Materials of cable production]. Moscow, Mashinostroenie Publ., 2013. 456 p. (Rus).

5. Tirelli D. Flame retardants for composites. *The Chemical Journal*, 2013, no.1-2, pp. 42-45. (Rus).

6. Overview mineral flame retardants, halogen-free cable for hydroxide compositions. *Kabel-News*, 2009, no.8, pp. 41-43. (Rus).

7. Mikhalin Y.A. Criteria of plastics fire resistance and methods of their testing. *Polimernye materialy*, 2011, no.7, pp. 26-31. (Rus).

8. Herbiet R. Mineral Flame Retardants: Market Outlook and Latest Developments. *High Performance Filler*, 2005, pap. 4, p. 20.

9. Innes J., Innes A. Plastic Flame Retardants: Technology and Current Developments. *Rapra Review Reports*, 2004, vol.14, no.12, report 168, p. 148.

10. EN 13501-6:2014 (E) Fire classification of construction products and building elements – Part 6: Classification using data from reaction to fire tests on electric cables.

11. EN 50399:2011 Common test methods for cables under fire conditions –Heat release and smoke production measurement on cables during flame spread test –Test apparatus, procedures, results.

12. STAR^e thermal analysis system, operating instructions to the TGA/DSC 1. Switzerland, Mettler Toledo AG, 2007.

13. Tips on model free kinetics. *METTLER TOLEDO Thermal Analysis UserCom 8*, 1998, pp. 1-3.

14. Vyazovkin S., Wight C.A. Model-free and model-fitting approaches to kinetic analysis of isothermal and nonisothermal data. *Thermochimica Acta*, 1999, no.340-341, pp. 53-68. **doi: 10.1016/S0040-6031(99)00253-1.**

15. Vyazovkin S. What can model free kinetics tell us about reaction mechanisms? *METTLER TOLEDO Thermal Analysis UserCom.10*, 1999, pp. 9-10.

16. Schawe J. Kinetic studies of complex reactions. Part 1: model free kinetics. *METTLER TOLEDO Thermal Analysis UserCom 18*, 2003, pp. 13-16.

17. Varankina G.S., Vysotskii A.V. Effective low toxic aluminosilicate fillers for phenol formaldehyde adhesives for plywood and particleboard. *Adhesives in woodworking Industry*, 1997, pp. 114-120.

18. Vyazovkin S. Evaluation of activation energy of thermally stimulated solid-state reactions under arbitrary variation of temperature. *Journal of Computational Chemistry*, 1997, vol.18, no.3, pp. 393-402. **doi: 10.1002/(SICI)1096-987X(199702)18:3<393::AID-JCC9>3.0.CO;2-P.**

Received 10.01.2017

E.V. Chuleyeva[1]*, Candidate of Technical Science,*
V.M. Zolotaryov[1]*, Doctor of Technical Science,*
[1] Private Joint-stock company Yuzhcable works,
7, Avtogennaya Str., Kharkiv, 61099, Ukraine,
phone +380 57 7545312;
e-mail: echuleeva@mail.ru

How to cite this article:
Chuleyeva E.V., Zolotaryov V.M. Study of the influence of magnesium hydroxide on the combustibility performance of polymer compositions based on ethylene vinyl acetate copolymer. *Electrical engineering & electromechanics*, 2017, no.2, pp. 43-48. **doi: 10.20998/2074-272X.2017.2.07.**

UDC 621.314 **doi: 10.20998/2074-272X.2017.2.08**

V.E. Bondarenko, O.V. Shutenko

DEVELOPMENT OF FUZZY NEURAL NETWORK FOR THE INTERPRETATION OF THE RESULTS OF DISSOLVED IN OIL GASES ANALYSIS

Purpose. The purpose of this paper is a diagnosis of power transformers on the basis of the results of the analysis of gases dissolved in oil. Methodology. To solve this problem a fuzzy neural network has been developed, tested and trained. Results. The analysis of neural network to recognize the possibility of developing defects at an early stage of their development, or growth of gas concentrations in the healthy transformers, made after the emergency actions on the part of electric networks is made. It has been established greatest difficulty in making a diagnosis on the criterion of the boundary gas concentrations, are the results of DGA obtained for the healthy transformers in which the concentration of gases dissolved in oil exceed their limit values, as well as defective transformers at an early stage development defects. The analysis showed that the accuracy of recognition of fuzzy neural networks has its limitations, which are determined by the peculiarities of the DGA method, used diagnostic features and the selected decision rule. Originality. Unlike similar studies in the training of the neural network, the membership functions of linguistic terms were chosen taking into account the functions gas concentrations density distribution transformers with various diagnoses, allowing to consider a particular gas content of oils that are typical of a leaky transformer, and the operating conditions of the equipment. Practical value. Developed fuzzy neural network allows to perform diagnostics of power transformers on the basis of the result of the analysis of gases dissolved in oil, with a high level of reliability. References 16, tables 3, figures 9.

Key words: **diagnostics of transformers, analysis of dissolved gases in oil, peculiarities of gas content, concentration levels, fuzzy neural networks, membership function, Weibull distribution, network training, fuzzy conclusion, wrong decisions.**

Разработана и обучена нечеткая нейронная сеть для интерпретации результатов хроматографического анализа растворенных в масле газов. Предложено определять функции принадлежности лингвистических термов с учетом функций плотностей распределения концентраций газов для трансформаторов с различным состоянием. Выполнено тестирование обученной сети на независимой выборке. Проанализированы возможности нейронных сетей распознавать развивающиеся дефекты на ранней стадии их развития, или рост концентраций газов в исправных трансформаторах, после аварийных воздействий со стороны электрических сетей. Библ. 16, табл. 3, рис. 9.

Ключевые слова: **диагностика трансформаторов, анализ растворенных в масле газов, особенности газосодержания, уровни концентраций, нечеткие нейронные сети, функции принадлежности, распределение Вейбулла, обучение сети, нечеткий вывод, ошибочные решения.**

Introduction. One of the ways to increase the operational reliability of high-voltage electric power equipment especially that operated outside the normative service life is to improve existing methods and means of monitoring for obtaining diagnostic information, development of mathematical models and algorithms for assessing the technical condition of electrical equipment. The most promising, according to the authors, the direction of such an improvement is the development of computer systems for technical diagnostics using the apparatus of fuzzy logic and neural networks, which can provide an increase in the reliability of recognition and prediction of the technical condition and resource of the object.

Analysis of publications. At present, the mathematical apparatus of fuzzy logic and neural networks is widely used to detect developing defects and to recognize their type both by domestic [1-6] and foreign [7-11] researchers. In most of the published works, international, national or departmental standards or techniques for interpreting the results of chromatographic analysis of dissolved gases in oil (CADG) are used as a decisive rule. When using the fuzzy logic device, the membership function type as well as their numerical characteristics, are determined based on expert estimates or from existing standards. As a rule, when learning and testing the developed systems of fuzzy inference or neural networks, either the results of the CADG are used, corresponding to the working or defective condition of the equipment. But at the same time, the peculiarities of the gas content of oils in serviceable transformers were not taken into account, which are determined by the features of the design, operating conditions and a number of other factors. In addition, despite a rather large number of publications on the use of neural networks to interpret the results of CADG, a number of issues remain uninformed. In particular, issues related to the ability of neural networks to recognize developing defects at an early stage of their development, or the growth of gas concentrations in serviceable transformers, after emergency actions on the part of electrical networks, have not been considered. The latter circumstances served as an excuse for writing this paper.

The goal of the work is the development, training and testing of fuzzy neural network, for diagnostics of power transformers based on the results of CADG, and also analysis of the possibility of this network to recognize developing defects at an early stage of their development and growth of gas concentrations in serviceable transformers as a result of external influences.

Initial data for the network training. To train the network, the results of CADG were used in Donetsk, Luhansk, Sumy and Kharkiv regions, Ukraine. In total, the results of observations of 426 transformers with voltage of 110 and 330 kV, an unpressurized version, were analyzed. Analyzed transformers differ both in voltage class, and in nominal power, and in design, and most importantly – in terms of operation, i.e. by the values of the load, by the frequency and level of action of short-circuit currents, by the multiplicity of the effects of overvoltages, etc. All this leads to the fact that the values of gas concentrations vary in a fairly wide range of values. For the convenience of analysis, the values of the gas concentrations were the concentration levels recommended in [12] were used to diagnose the state of high voltage equipment with voltages up to 330 kV. Values of gas concentrations corresponding to different levels are given in Table 1. According to [12], if the values of the gas concentrations correspond to level 1, this indicates a normal, defect-free state of the equipment. If the concentration of at least one of the gases corresponds to level 2, then the decision on the state of the equipment is taken based on the analysis of the values of the rates of increase in the sum of the hydrocarbon series gases (the defect is considered «present» if this rate exceeds 30 ml/day). If the concentration of at least one of the gases corresponds to level 3, then the presence of a defect without taking into account the rate of increase in gas concentrations is predicted.

Table 1

Levels of the state of oil-filled equipment by values of gas concentrations

Concentration level	Gases dissolved in oil				
	H_2	CH_4	C_2H_6	C_2H_4	C_2H_2
1	<0.01	<0.005	<0.005	<0.0015	<0.00005
2	0.01-0.015	0.005-0.012	0.005-0.01	0.0015-0.01	0.00005-0.001
3	>0.015	>0.012	>0.005	>0.0015	>0.001

The performed analysis showed that out of 7393 results of measurements of hydrogen concentrations 5161 (H_2) the value or 69.81% did not exceed the detection limit of the chromatograph. Another 2106 values (28.49%) of concentrations did not exceed the value of the analytical recognition threshold (0.005% by vol.) regulated in [12]. Only 71 values (0.96%) corresponded to level 1 (less than 0.01% by vol.). Level 2 (0.01-0.015% by vol.) corresponded to 26 values (0.35%), and to level 3 (more than 0.015% by vol.) – 29 values (0.39%).

The concentrations of methane (CH_4) below the detection limit by the chromatograph were found in 2,304 oil samples, which is 31.6% of all observations for this gas; another 3,342 (45.2%) concentrations of methane were below the analytical recognition threshold (0.0015% by vol.). 1160 values (15.69 %) corresponded to level 1 (up to 0.005% by vol.), level 2 (0.005-0.012% by vol.) – 367 values (4.96%), and to level 3 (more than 0.012) – 220 values (2.98%).

The ethane concentrations (C_2H_6) do not exceed the detection limit of the chromatograph in 1957 samples (26.47%), in 4485 oil samples (60.67%), the ethane concentrations did not exceed the analytical recognition threshold (0.0015% by vol.). 619 concentrations (8.37%) corresponded to level 1 (up to 0.005% by vol.), level 2 (0.005-0.01% by vol.) – 153 values (4.96%), and level 3 (more than 0.01 % by vol.) – 179 values (2.42%).

Of the 7393 ethylene concentrations (C_2H_4), 1090 values (14.74%), 3763 (50.90%) were found below the detection limit by the chromatograph, did not exceed the analytical recognition threshold (which is 0.0015% by vol.). It should be noted that for ethylene, the values of the analytical recognition level coincide with the value of the upper limit of level 1. Therefore, in the future for ethylene, all values corresponding to level 1 are assigned to values not exceeding the analytical recognition threshold. In 1914 samples, the values of ethylene concentrations (25.89%) correspond to level 2 (0.0015-0.01% by vol.), And 626 ethylene values (8.47%) correspond to level 3 (more than 0.01% by vol.).

The concentrations of acetylene (C_2H_2) not exceeding the detection limit by the chromatograph were found in 4551 oil samples, which is 61.56% of all observations for this gas. Another 1602 values (21.67%) of acetylene concentrations were below the analytical recognition threshold. Due to the fact that for acetylene the recognition level (0.0003% by vol.) exceeds the upper limit of level 1 (0.00005% by vol.) acetylene values with concentrations above the analytical recognition threshold, but below level 3 are assigned to level 2 (from 0.00005 to 0.001% by vol.). Level 2 corresponded to 982 values (13.28%), and to level 3 (more than by 0.001% by vol.) – 258 values (3.49%).

Thus, on the basis of the analysis, it is established that, in serviceable transformers of a leaky design, gas concentrations, upper limit values of level 2, can be exceeded, which can be interpreted as a defect. The greatest probability of exceeding the boundary value of level 2 was found in ethylene, then acetylene, methane, ethane and least of all hydrogen.

At the same time, the greatest probability of realization of gas concentrations below the analytical detection threshold is hydrogen, then acetylene, ethane and methane. For ethylene, this probability is the lowest. The maximum number of values with concentrations above the analytical recognition threshold is C_2H_4 (2540 values or 34.36%). Then follows CH_4 (1747 values or 23.63%), then C_2H_2 (1240 values or 16.77%). The lowest values with concentrations above the analytical detection threshold were found in C_2H_6 (951 or 12.86%) and H2 (126 values or 1.70%).

The received results allow to draw a conclusion that in serviceable transformers, the concentration values can correspond to the values characteristic for the defective state (level 3). As shown by the analysis performed in [13, 14], one of the main reasons for exceeding the gas concentrations of boundary values, fault-free transformers

are emergency actions from electrical networks (short circuits, overvoltages, overloads, etc.).

To train the neural network, the results of CADG were used for defective equipment, which were obtained both as a result of cooperation of authors with Ukrainian energy companies, and from open domestic and foreign literary sources. The total amount of sampling values was 1103 measurements. The distribution of sample values by types of defects is given In Table 2. As can be seen from the table in the sample presented to the analysis, different types of defect have a different volume of sample values, i.e. Different probability of their occurrence. The greatest number of defects is due to overheating in the temperature range above 700 °C (in the Table is designated as superheating of high temperatures) and overheating in the high temperature region, which are accompanied by electric discharges. The lowest number of observations is for electric discharges of low energy and overheating, which turn into an arc discharge. The performed analysis showed that in defective equipment, the values of gas concentrations substantially depend on the stage of defect development, while in the initial stages the concentration values may not exceed the boundary values corresponding to level 3 [12], but as the defect develops, the values of the concentrations increase. Another important factor affecting the values of the concentrations of individual gases is the type of defect. As a rule, the maximum values of concentrations are observed in gases characteristic for this type of defects. For concomitant gases, the concentrations are somewhat less. At the same time, the values of the concentrations of gases that are not characteristic for this type of defect have values corresponding to either levels 1 or 2, or they do not exceed the detection limit of the chromatograph.

Table 2

Distribution of sample values by types of defects

No.	Defect type	Scope of the sample
1	Partial discharge	115
2	Partial discharges of high intensity	15
3	Spark and creeping discharges	81
4	Low-energy discharges	17
5	Arc discharge (H_2)	67
6	Arc discharge (C_2H_2)	43
7	Discharges of high energy (C_2H_2)	53
8	Overheating of low temperatures (CH_4)	48
9	Overheating of low temperatures (C_2H_6)	57
10	Overheating of average temperatures (CH_4)	68
11	Overheating of average temperatures (C_2H_4)	81
12	Overheating of high temperatures (C_2H_4)	260
13	Overheating of low temperatures and discharges	35
14	Overheating in the arc (CH_4)	16
15	Overheating transitions into discharges (C_2H_6)	27
16	Overheating of high temperatures and discharges	120

Note: the gas with the maximum concentration is shown in brackets.

Each result of measurements of gas concentrations was assigned a code corresponding to the concentration levels from Table 1. The coding of transformer diagnoses is given in Table 3.

Table 3

The coding of transformer diagnoses

Code	Diagnosis
1	Working condition
2	Suspicious condition
3	Defective condition

Fuzzy neural network training. Next, a fuzzy neural network topology was developed, which is shown in Fig. 1. The created network has 15 inputs, three inputs for each of the gases. The number of learning cycles created by the fuzzy neural network was 300 epochs.

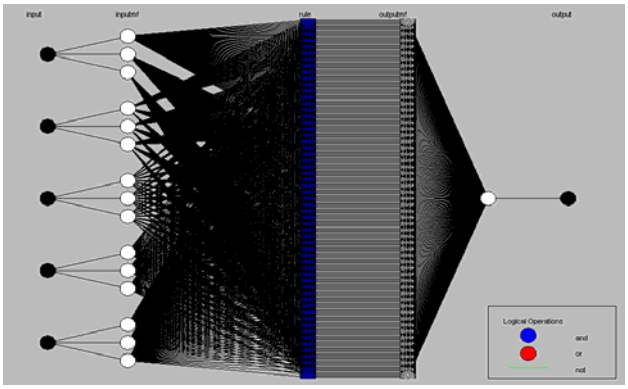

Fig. 1. Fuzzy neural network topology

Fig. 2 shows the dependence of the learning error on the number of training cycles.

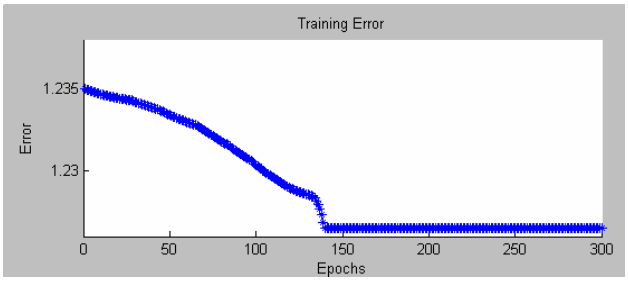

Fig 2. Dependence of the learning error of a fuzzy neural network on the number of training cycles

As can be seen from Fig. 2, the decrease in the learning error is observed approximately to the middle of the training interval. Further increase in the number of training cycles does not lead to an increase in the reliability of recognition. To reduce the error, the fuzzy logic apparatus was used.

Stage of fuzzification. At this stage, the input linguistic variables were identified:

LV_{inp1}: <hydrogen concentration>

LV_{inp2}: <methane concentration>

LV_{inp3}: <ethane concentration>

LV_{inp4}: <ethylene concentration>

LV_{inp5}: <acetylene concentration>

Further, LV_{inpi} is divided into several linguistic

terms LT_{ij} characterizing the peculiarities of the state of a given variable:

$$LT_{ij}, j=1\ldots n,$$

where: j is the number of term LV_{inpi}, n is the number of terms into which LV_{inpi} is divided.

The dividing into term for each of the gases was the following:

LV_{inp1} is divided into three LT
- LT_{11}: < concentration within normal limits – **1**>
- LT_{12}: < suspicious concentration – **2**>
- LT_{13}: < defective concentration – **3**>

LV_{inp2} is divided into three LT
- LT_{21}: < concentration within normal limits – **1**>
- LT_{22}: < suspicious concentration – **2**>
- LT_{23}: < defective concentration – **3**>

LV_{inp3} is divided into three LT
- LT_{31}: < concentration within normal limits – **1**>
- LT_{32}: < suspicious concentration – **2**>
- LT_{33}: < defective concentration – **3**>

LV_{inp4} is divided into three LT
- LT_{41}: < concentration within normal limits – **1**>
- LT_{42}: < suspicious concentration – **2**>
- LT_{43}: < defective concentration – **3**>

LV_{inp5} is divided into three LT
- LT_{51}: < concentration within normal limits – **1**>
- LT_{52}: < suspicious concentration – **2**>
- LT_{53}: < defective concentration – **3**>

The definition of membership functions is quite a challenge. To ensure that the selected membership functions and their boundaries most adequately describe the results of chromatographic analysis, the functions of the density distribution of gas concentrations for serviceable and defective states were used [15]. As an example, Fig. 3, the Weibull theoretical density distributions are given for methane concentrations obtained for serviceable transformers ($\boldsymbol{D_1}$), serviceable transformers after emergency actions from electrical networks ($\boldsymbol{D_{12}}$) and transformers in which a defect ($\boldsymbol{D_2}$) is detected.

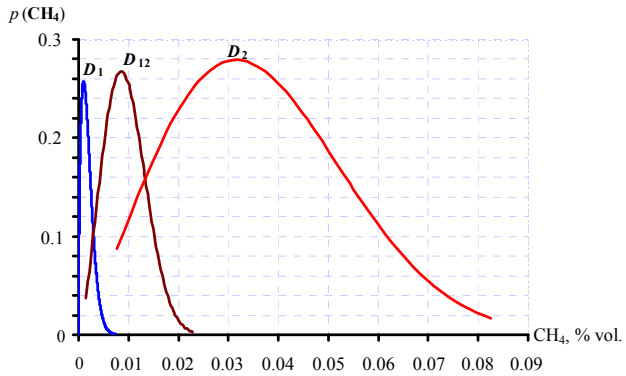

Fig. 3. Density of theoretical methane distributions for transformers with different state

As a membership function, it is very convenient to use a trapezoidal function, the degree of belonging to which has a maximum value in the middle of the interval and decreases along its edges. As borders for $\mathbf{LT_1}$ of all linguistic variables, the boundaries corresponding to the functions of the density distribution of gas concentrations were chosen for transformers with different states (see Fig. 3). The boundary values for $\mathbf{LT_2}$ and $\mathbf{LT_3}$ of all linguistic variables were chosen on the basis of the functions of the distribution densities. Fig. 4 shows the functions of methane for three linguistic terms. As can be seen from Fig. 4 membership functions are chosen in such a way as to take into account both the recommendations of СОУ-Н ЕЕ 46.501:2006, and the operational experience reflected in the form of density distribution functions.

Output linguistic variables have the form:

LV_{out1}: < Concentrations within normal limits – **1**>

LV_{out2}: < Concentrations above normal – **2**>

LV_{out3}: < The concentration values correspond to the presence of a defect – **3**>

The dividing into term was the following:

LV_{out1} is divided into two LT
- LT_{11}: <Corresponds – *Y*>
- LT_{12}: <Does not correspond – *N*>

LV_{out2} is divided into two LT
- LT_{21}: <Corresponds – *Y*>
- LT_{22}: <Does not correspond – *N*>

LV_{out3} is divided into two LT
- LT_{31}: <Corresponds – *Y*>
- LT_{32}: <Does not correspond – *N*>

As the membership functions for each of the terms, a triangular function was chosen.

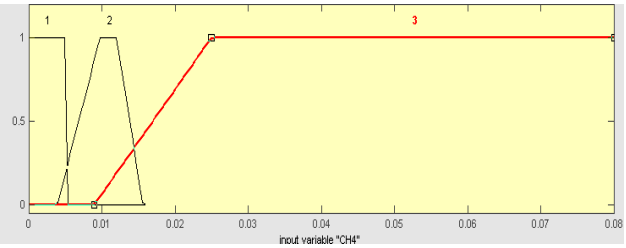

Fig. 4. The membership functions of three linguistic terms for, linguistic variable content of methane in oil

Stage of calculating the rule. A system with fuzzy logic should have a rules base, which, in essence, is the empirical knowledge of the expert about the control mechanism. To calculate the rules, the fuzzy inputs received from the fuzzification block and the rules in the knowledge base are used. In the left part of the rules, possible situations at the input of the system are sorted, and on the right-hand side it is indicated which LV describes the correct reaction of the system. As a decisive rule, the recognition technique was regulated in [9]. In short, the rules base can be represented in the form:

Rule 1: **IF** [H_2∈1] **AND** [CH_4∈1] **AND** [C_2H_6∈1] **AND** [C_2H_4∈1] **AND** [C_2H_2∈1] **THEN** [**D∈ 1**];

Rule 2: **IF** [H_2∈2] **AND** [CH_4∈1] **AND** [C_2H_6∈1] **AND** [C_2H_4∈1] **AND** [C_2H_2∈1] **THEN** [**D∈ 2**];

Rule 3: **IF** [H_2∈1] **AND** [CH_4∈2] **AND** [C_2H_6∈1] **AND** [C_2H_4∈1] **AND** [C_2H_2∈1] **THEN** [**D∈ 2**];

…

Rule 6: **IF** [$H_2 \in 1$] **AND** [$CH_4 \in 1$] **AND** [$C_2H_6 \in 1$] **AND** [$C_2H_4 \in 1$] **AND** [$C_2H_2 \in 2$] **THEN** [**D∈ 2**];

Rule 7: **IF** [$H_2 \in 2$] **AND** [$CH_4 \in 2$] **AND** [$C_2H_6 \in 1$] **AND** [$C_2H_4 \in 1$] **AND** [$C_2H_2 \in 1$] **THEN** [**D∈ 2**];

…

Rule 17: **IF** [$H_2 \in 1$] **AND** [$CH_4 \in 1$] **AND** [$C_2H_6 \in 1$] **AND** [$C_2H_4 \in 2$] **AND** [$C_2H_2 \in 2$] **THEN** [**D∈ 2**];

Rule 18: **IF** [$H_2 \in 2$] **AND** [$CH_4 \in 2$] **AND** [$C_2H_6 \in 2$] **AND** [$C_2H_4 \in 1$] **AND** [$C_2H_2 \in 1$] **THEN** [**D∈ 2**];

…

Rule 27: **IF** [$H_2 \in 1$] **AND** [$CH_4 \in 1$] **AND** [$C_2H_6 \in 2$] **AND** [$C_2H_4 \in 2$] **AND** [$C_2H_2 \in 2$] **THEN** [**D∈ 2**];

Rule 28: **IF** [$H_2 \in 2$] **AND** [$CH_4 \in 2$] **AND** [$C_2H_6 \in 2$] **AND** [$C_2H_4 \in 2$] **AND** [$C_2H_2 \in 1$] **THEN** [**D∈ 2**];

…

…

Rule 48: **IF** [$H_2 \in 1$ **OR** $H_2 \in 2$] **AND** [$CH_4 \in 1$ **AND** $CH_4 \in 2$] **AND** [$C_2H_6 \in 1$ **OR** $C_2H_6 \in 2$] **AND** [$C_2H_4 \in 3$] **AND** [$C_2H_2 \in 3$] **THEN** [**D∈ 3**];

Rule 49: **IF** [$H_2 \in 3$] **AND** [$CH_4 \in 3$] **AND** [$C_2H_6 \in 3$] **AND** [$C_2H_4 \in 1$ **OR** $C_2H_4 \in 2$] **AND** [$C_2H_2 \in 1$ **OR** $C_2H_2 \in 2$] **THEN** [**D∈ 3**];

…

Rule 63: **IF** [$H_2 \in 1$ **OR** $H_2 \in 2$] **AND** [$CH_4 \in 3$] **AND** [$C_2H_6 \in 3$] **AND** [$C_2H_4 \in 3$] **AND** [$C_2H_2 \in 3$] **THEN** [**D∈ 3**];

Rule 64: **IF** [$H_2 \in 3$] **AND** [$CH_4 \in 3$] **AND** [$C_2H_6 \in 3$] **AND** [$C_2H_4 \in 3$] **AND** [$C_2H_2 \in 3$] **THEN** [**D∈ 3**];

Stage of defuzzification. At this stage, the fuzzy information contained in the form of the authenticity of the linguistic term is transformed into a clearly defined meaning. The defuzzification is made according to the figure obtained by adding all the membership functions of the terms of the input variable. As a method of defuzzification, the right modal value method was adopted, which provides the greatest reliability in determining the degree of belonging of the output variables.

Testing of fuzzy neural network. The trained network was tested on an independent sample (values that were not used in training). For the convenience of analysis, the test data was broken according to known diagnoses into three groups. Test results for serviceable transformers whose concentration values do not exceed the values for level 1, from Table 1 are shown in Fig. 5.

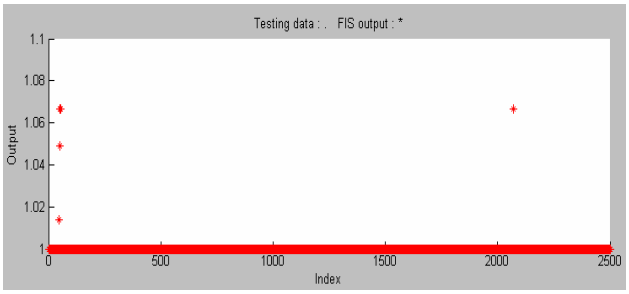

Fig. 5. Results of testing fuzzy neural network for CADG results of transformers not having defect

As can be seen from Fig. 5, the fuzzy neural network unambiguously classified the data presented to the recognition to level 1. Further, the trained neural network was presented to recognize the values of concentrations of dissolved gases that correspond to level 2. The test results are shown in Fig. 6.

Fig. 6 shows that the network accurately, but with varying degrees of belonging, carried all the results of the CADG to the level 2 submitted to the input. At the last stage of the testing for the input of the fuzzy neural network, the results of CADG were submitted, for equipment in which defects of various types were detected. It should be noted that in the sampling network fed to the input, the concentration of at least one of the gases corresponded to level 3.

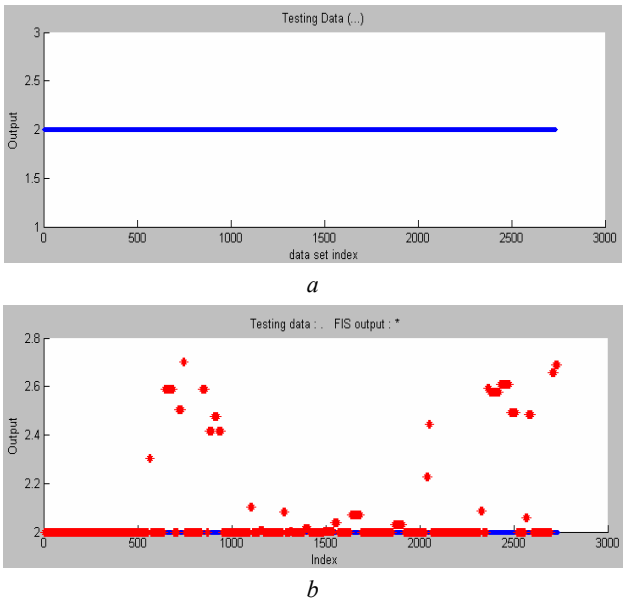

a

b

Fig. 6. Results of testing fuzzy neural network for the results of CADG transformers, whose gas concentrations correspond to level 2 (*a* – initial data, *b* – test results)

The test results are shown in Fig. 7.

As you can see from the Figure, the fuzzy neural network correctly recognized the defective condition of the transformers, too.

Analysis of the possibilities of a fuzzy neural network. Further, the results of CADG of serviceable transformers were submitted to the input of the fuzzy neural network, in which the gas concentrations corresponded to level 3. The reason for the increase in gas concentrations was the emergency operation of electrical networks (short-circuit, overvoltage, transformer overloading effects [13, 14]). And violations by operational personnel in the selection, transportation and storage of oil samples, as well as during testing. The results of the network are shown in Fig. 8.

As can be seen from Fig. 8, out of 541 the results of CADG applied to the input to the defect-free state, the network classified only 5.

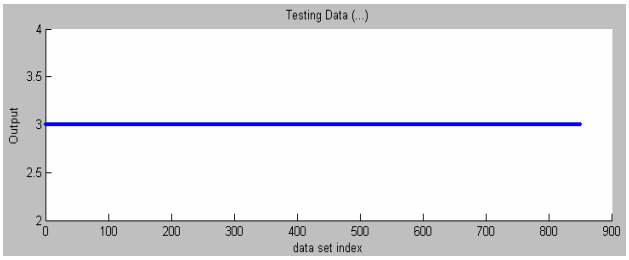

a

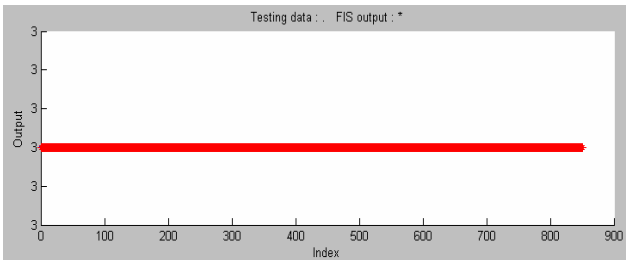

b

Fig. 7. Results of testing fuzzy neural network for the results of CADG defective transformers (*a* – initial data, *b* – test results)

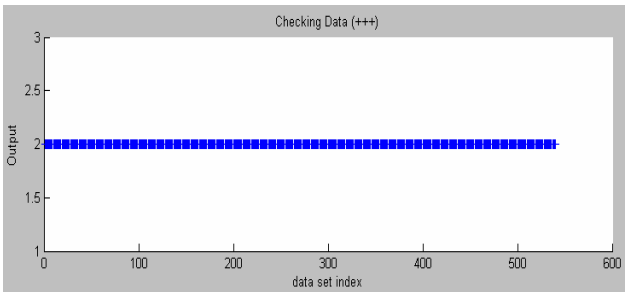

a

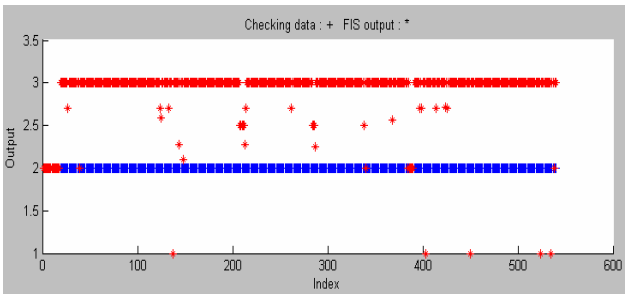

b

Fig. 8. Results of testing fuzzy neural network for the results of CADG defect-free transformers, in which gas concentrations corresponded to level 3 (*a* – initial data, *b* – test results)

The analysis performed showed that in these five oil samples the levels 3 corresponded to the values of only one of the five gases. The values of the concentrations of the remaining four did not exceed the detection limit by the chromatograph (conditionally equal to zero). Such gas content is not characteristic for a defective state, i.e. In the training sample, such data were not available, which probably allowed the network to make this diagnosis. Another 27 CADG results were attributed to the suspicious state by the network, i.e. level 2. In these oil samples, the concentration of only one of the five gases corresponded to level 3. The concentrations of the remaining four did not exceed the detection limit by the chromatograph or corresponded to level 1. All other results of the CADG presented to recognition were attributed to state 3 by the network, i.e. mistakenly recognized as defective, which is error of the first kind (false alarm).

No less interesting are the results of the operation of the fuzzy network, with the recognition of the state of the transformers based on the results of the CADG defective equipment, which are obtained in the early stages of defect development, when the gas concentrations do not exceed the upper limit of level 2. The results of the operation of the electric network are shown in Fig. 9. As can be seen from Fig. 9 out of 51 results submitted to the network input for only 15, the network was diagnosed a defective condition. For 25 samples of oils, with varying degrees of belonging, the network was diagnosed with a suspicious condition (level 2). It is noteworthy that the results of the CADG transformers of the Nelson River hydropower station, Northern Canada [16], which were received for 10 months and 5 days before their damage (1 and 2 results, respectively) were attributed to level 2 by the network. It should be noted that the expert system used by the company could not prevent damage to these transformers. However, according to the results of CADG, the fuzzy neural network has definitely not determined the defective state in these transformers, but only classified the results obtained as a result of the state of «suspicious concentrations». For 11 results of CADG, the fuzzy neural network diagnosed the absence of a defect, which is error of the second kind (missed target).

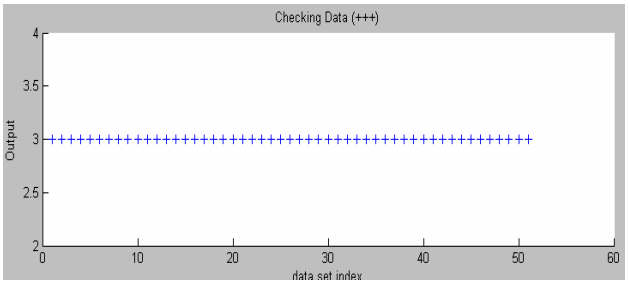

a

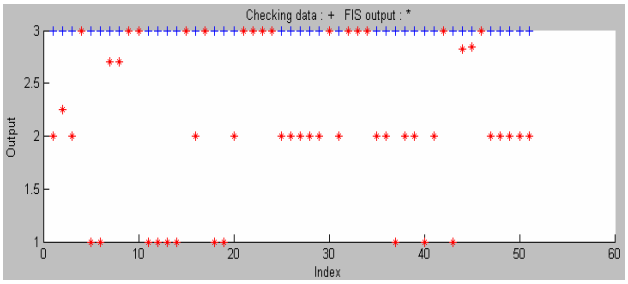

b

Fig. 9. Results of testing fuzzy neural network for the results of CADG defective transformers, in which the gas concentrations did not exceed the boundary values of level 2 (*a* – the initial data, *b* – the test results)

Analyzing the obtained results, it is necessary to recognize that the developed and trained neural network

had to solve the mutually exclusive problem. On the one hand, in order to recognize the defects of equipment at an early stage of their development, the membership function for the defective state must be shifted to the lower range, on the other hand, to recognize the effect of emergency operation of the network, the membership function for the faulty state must be shifted to higher values. However, even in such a situation, a fuzzy neural network has successfully coped with the task, especially considering that an unmistakable recognition of emergency influences and defects at an early stage of development, based on the use of only the values of gas concentrations, is fundamentally impossible. At the same time, as shown in [6], the use as a criterion for the development of a defect, the nature of changes in gas concentrations in time, allows solving this problem with almost 100% certainty. Thus, the reliability of the diagnosis of a neural network is significantly influenced by both the diagnostic features used to make the diagnosis, and the decision rule.

In addition, the reliability of the diagnosis, which puts the neural network, is substantially limited by the peculiarities of the CADG method. This was clearly demonstrated by the example of recognition of a condition caused by an emergency response from the power grid or personnel errors. Since both the development of the defect, and the effect of abnormally high currents, voltages or temperatures, due to emergency operation of the network, lead to an increase in gas concentrations, then on the basis of an analysis of only the values of gas concentrations, it is not possible to determine the cause of gas evolution. Therefore, to expect an error-free diagnosis from the neural network would be extremely improper.

Conclusions:

1. A fuzzy neural network has been designed, trained and tested to interpret the results of CADG. In contrast to similar investigations, when training a neural network, the functions of belonging to linguistic terms were chosen taking into account the functions of the density distribution of gas concentrations for transformers with different states, which allowed to take into account both the peculiarities of the gas content of oils characteristic for non-hermetically sealed transformers and the operating conditions of this equipment.

2. Based on the results of the network check on an independent sample, it was found that the greatest difficulty in diagnosing by the boundary gas concentration criterion is the results of CADG obtained for serviceable transformers in which the concentrations of dissolved gases in the oil exceed their boundary values, as well as for defective transformers on early stage of defect development.

3. The performed analysis showed that the reliability of recognition of fuzzy neural networks has limitations that are determined by the features of the CADG method, the diagnostic features used and the chosen decision-making rule.

REFERENCES

1. Kosterev M.V., Bardik E.I. *Pytannya pobudovy nechitkykh modeley otsinky tekhnichnoho stanu ob»yektiv elektrychnykh system* [The issue of building fuzzy models evaluate the technical condition of the objects of electrical systems]. Kyiv, NTUU «KPI» Publ., 2011. 654 p. (Ukr).

2. Lezhnjuk P.D., Rubanenko O.Є., Zhuk I.A. Diagnosis of power transformers using fuzzy sets. *Visnyk of Vinnytsia Politechnical Institute*, 2005, no.1, pp. 43-51. (Ukr).

3. Kosterev M.V., Bardik Є.I., Vozhakov R.V., Bolotnij M.P. Technical condition evaluation and prediction of the resource operability of power transformers based on the theory of fuzzy sets. *Visnyk of Vinnytsia Politechnical Institute*, 2012, no.2, pp. 83-87. (Ukr).

4. Kosterev N.V., Bardik E.I. Fuzzy modeling of electrical equipment for the evaluation of the technical condition and deciding on further exploitation strategy. *Tekhnichna elektrodynamika. Tem. vypusk «Problemy suchasnoyi elektrotekhniky»*, 2006, no.3, pp. 39-43. (Rus).

5. Denisova N.V., Sahapov A.A. Neural network as a tool for diagnosis power oil transformers. *Archivarius*, 2016, no.3(7), pp. 33-37. (Rus).

6. Shutenko O.V. Formation of fuzzy inference procedures to detect emerging defects in high-voltage transformers. *Bulletin of NTU «KhPI»*, 2008, no.44, pp 162-177. (Rus).

7. Ahmed M.R., Geliel M.A., Khalil A. Power transformer fault diagnosis using fuzzy logic technique based on dissolved gas analysis. *21st Mediterranean Conference on Control and Automation*, Jun. 2013, pp. 584-589. **doi: 10.1109/MED.2013.6608781.**

8. Hongzhong Ma, Zheng Li, P. Ju, Jingdong Han, Limin Zhang. Diagnosis of power transformer faults on fuzzy three-ratio method. *2005 International Power Engineering Conference, 2005*. **doi: 10.1109/ipec.2005.206897.**

9. C.-H. Liu, T.-B. Lin, L. Yao, S.-Y. Wang. Integrated power transformer diagnosis using hybrid fuzzy dissolved gas analysis. *IEEJ Transactions on Electrical and Electronic Engineering*, Oct. 2015, vol.10, no.6, pp. 689-698. **doi: 10.1002/tee.22148.**

10. M. A. A. Siddique, S. Mehfuz. Artificial neural networks based incipient fault diagnosis for power transformers. *2015 Annual IEEE India Conference (INDICON)*, Dec. 2015. **doi: 10.1109/indicon.2015.7443174.**

11. C. H. Liu, L. T. Yao, T. B. Lin, S. Y. Wang. Innovated Fault Diagnosis for Power Transformer Using Hybrid Fuzzy Dissolved Gas Analysis. *Applied Mechanics and Materials*, Jan. 2013, vol.284-287, pp. 1082-1086. **doi: 10.4028/www.scientific.net/amm.284-287.1082.**

12. *SOU-N EE 46.501: Diagnostika maslonapovnenogo transformatornogo obladnannja za rezul'tatami hromatografichnogo analizu vil'nih gaziv, vidibranih iz gazovogo rele, i gaziv, rozchinenih ui zoljacijnomu masli* [SOU-N EE 46.501: Diagnosis oil-filled transformer equipment based on the results of chromatographic analysis of free gas with gas relay selected, i gases dissolved in insulating oil]. Kiïv, 2007, 92p.(Ukr).

13. Shutenko O.V. Research of influence of operational factors on results of chromatographic analysis of the gases dissolved in oil. *Bulletin of Kharkiv Petro Vasylenko*

National Technical University of Agriculture, 2008, vol.1, no.73, pp. 45-48. (Ukr).

14. Shutenko O.V., Baklay D.N., Ostrikova T.A., Melnik N.Y. Analysis of the causes of gassing in the power transformer, based on a study of correlations between dissolved in oil gases. *Lighting Engineering and Power Engineering*, 2012, no.3, pp. 72-81. (Rus).

15. Shutenko O.V., Baklay D.M. Analysis of gases concentration distribution laws, dissolved in oil of high voltage transformers unpressurized of execution. *Bulletin of NTU «KhPI»*, 2014, no.60(1033), pp.136-150. (Ukr).

16. Aksenov Yu.P. *Monitoring tekhnicheskogo sostoianiia vysokovol'tnoi izoliatsii elektrooborudovaniia energeticheskogo naznacheniia v ekspluatatsii i pri remontakh* [Technical condition monitoring of high-voltage insulation of electrical energy purposes in the operation and repairs]. Moscow, Nauchtekhlitizdat Publ., 2002. 338 p. (Rus).

Received 25.01.2017

V.E. Bondarenko[1]*, Doctor of Technical Science, Professor,*
O.V. Shutenko[1]*, Candidate of Technical Science, Associate Professor,*
[1] National Technical University «Kharkiv Polytechnic Institute», 2, Kyrpychova Str., Kharkiv, 61002, Ukraine,
phone +38 057 7076246,
e-mail: bond@kpi.kharkov.ua, o.v.shutenko@gmail.com

How to cite this article:
Bondarenko V.E., Shutenko O.V. Development of fuzzy neural network for the interpretation of the results of dissolved in oil gases analysis. *Electrical engineering & electromechanics*, 2017, no.2, pp. 49-56. **doi: 10.20998/2074-272X.2017.2.08.**

UDC 621.316.9 **doi: 10.20998/2074-272X.2017.2.09**

S.S. Rudenko, D.G. Koliushko, O.V. Kashcheyev

DETERMINATION OF DIRECTION TO RECONSTRUCTION OF GROUNDING SYSTEM

Purpose. In paper the most efficient and economical way for bringing the grounding system of power facilities into compliance with requirements of normative parameters was determined. Methodology. The determination was based on the comparison of the calculated values of touch voltage and length of additional electrodes for reconstruction of grounding system by two ways. To calculate the software based on the method of point current source which located in the three-layer soil, method guidance potential, Gauss method and the method of ordinary least squares was used. Results. For three possible cases amount of material and labor costs for the reconstruction and modernization of the grounding system while maintaining the equipotent grounding system and allowable touch voltage was defined. Originality. For the first time the effectiveness the reconstruction of grounding system for requirements of touch voltage, not to her of resistance, both in terms of electrical safety and in terms of material and labor costs proved. Practical value. The implementation of results saves a national scale funds for modernization and reconstruction of existing grounding systems of power facilities. References 3, tables 8, figures 6.
Key words: **grounding system, electrical safety, reconstruction, material and labour costs.**

На основании расчетного эксперимента проанализированы возможные случаи несоответствия заземляющих устройств нормативным требованиям и способы их реконструкции по требованиям к напряжению прикосновения и сопротивлению. Определена эффективность указанных направлений реконструкции как с точки зрения электробезопасности, так и материально-трудовых затрат. Библ. 3, табл. 8, рис. 6.
Ключевые слова: **заземляющее устройство, электробезопасность, реконструкция, материально-трудовые затраты.**

Introduction. Substations (SS) operated in Ukraine, most were designed for the requirements of the permissible value of resistance of grounding device (GD). Since these energy facilities were built over 30 years ago, it has undergone significant changes GD influenced corrosion processes, replacement and reconstruction of high-voltage equipment and so on. Therefore, at this time you need to choose the best option of GD modernization according to one of its normalized parameters (NP). To bring the current GD in line with current regulations [1] uses electromagnetic diagnostics (EMD) of the state of GD [2] which aims to determine the NP of GD and development of recommendations on reconstruction and modernization of GD.

Reconstruction of GD of electrical installation for voltage above 1 kV in power grids with dull grounded neutral, as well as the design can be done in two ways [2]: according to the requirements of the GD allowable resistance values or the permissible touch voltage. Existing investigations [3] have repeatedly noted that in some cases of GD realization according to its resistance can not guarantee the electrical safety of staff and provide a valid value of touch voltage. But this time estimate material and labor costs, taking into account the values of NP to select the optimal arrangement direction of GD is not performed.

The goal of the work is determining the optimal direction of reconstruction and modernization of electrical grounding device of electrical installations of voltage above 1 kV working in a network with dull grounded neutral.

Materials of investigation. We consider two methods of reconstruction of existing grounding device: the first one – the requirements for its resistance, the second one – the requirements to touch voltage. Analysis of the development of recommendations by these two ways to perform the reconstruction of GD we carry out on the example of electrical substation of voltage class of 110 (150) kV. It was considered three options:

1) before the reconstruction of exceeding the permissible touch voltage observed in 50% of the equipment after the reconstruction of both the first and second contact means voltage does not exceed the permissible value;

2) before the reconstruction of exceeding the permissible touch voltage observed on all equipment to ensure acceptable touch voltage in the reconstruction of both the first and second insulating layer methods used in the field of surgical equipment maintenance;

3) before the reconstruction of contact voltage and impedance GD do not exceed the allowable values and during the reconstruction of the first and second method required only made constructive recommendations.

We consider these options in detail:

1) After the reconstruction of two ways of contact voltage does not exceed the permissible value.

We execute analysis on the example of existing substation, the results of which EMD state GD are shown in Fig. 1, 2. This thick solid black line marked grounding located underground. The real name of the research facility is changed to conditional – SS No. 1.

Initial data for determining NP of GD were: real circuit GD SS No. 11, in use, the electrical characteristics (ECH) of ground (electrical resistivity (ER) I layer – 42.65 Ω·m, II layer – 25.37 Ω·m and thickness of the first layer – 0.82 m), the value of current single-phase short circuit (SC) – 1.957 kA. It should be noted that the implementation of reconstruction GD exceeding the allowable contact voltage (65 V at the time of operation of reserve protection with more than 1.0) was observed in 50% of the equipment where possible operational switching (namely: BI T-1, BI T-2, S T-1, S T-2 and SC-1), while the resistance value GD does not exceed the allowable value of 0.5 Ω.

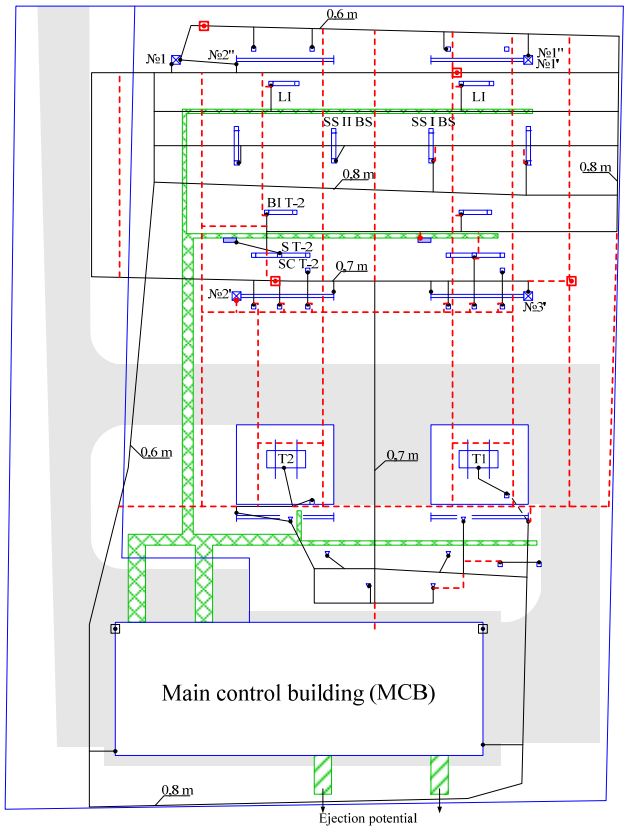

Fig. 1. Circuit of the GD of the SS No. 1 complied with the permissible resistance value

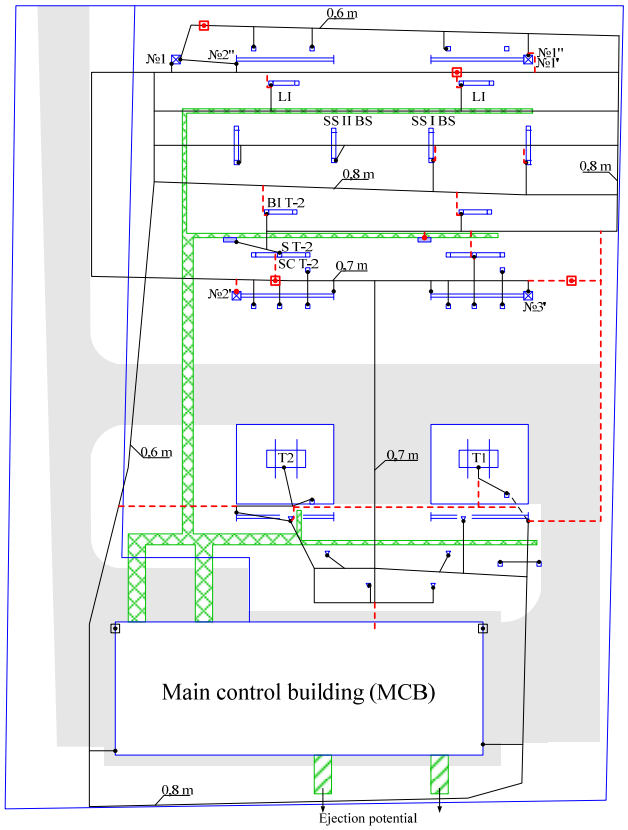

Fig. 2. Circuit of the GD of the SS No. 1 complied with the permissible touch voltage value

According to the item 1.7.106 of the Standard [1] the distance between the transverse horizontal grounding (HG) for GD performed the requirements for its resistance, it is recommended to take upward from the periphery to the center grounding grid. In this case, the first and following distance from the periphery should not exceed respectively 4.0; 5.0; 6.0; 7.5; 9.0; 11.0; 13.5; 16.0; 20.0 m. The depth should be laying HG (0.5 – 0.7) m. Fig. 1 shows the GD of the substation with introduced recommendations necessary to bring embodiment of the GD to the requirements of its resistance R_G (additional HG are indicated by dotted line).

According to the item 1.7.105 of the above standard for GD performed according to the requirements to touch voltage U_t we must place the longitudinal and transverse HG to perform protective potential equalization considering permissible touch voltage value and convenience joining grounded equipment, laying depth must be not less than 0.3 m. Thus, in comparison with GD, meet the requirements for its resistance requirements for a design less stringent.

Fig. 2 shows GD with recommendations necessary to bring it into compliance with the allowable voltage to ground. Calculation of parameters was performed using mathematical tools developed in [4]. Compare the value (see Table 1) and a voltage variation of contact for both versions of the GD. From Table 1 it follows that the voltage of touch with the first mode of implementation will be somewhat less important, but in both cases touch voltage does not exceed the permissible value of 65 V, and variations in the voltage of contact is approximately the same for both cases, i.e. in the first and in the second case will be equipotential grounding grid.

Table 1

Equipment name	Values of U_t, V		Deviations of U_t from mean value, %	
	GD with requirements for R_G	GD with requirements for U_t	GD with requirements for R_G	GD with requirements for U_t
SS II BS	26.1	38.3	12.8	9.9
SS I BS	23.5	33.8	1.6	–2.9
BI T-2	22.0	32.4	–4.9	–7.0
S T-2	21.1	27.5	–8.8	–21.1
SC T-2	20.6	31.6	–10.9	–9.3
SC T-1	21.2	34.2	–8.3	–1.8
right LI	25.6	39.8	12.4	2.8
left LI	26.6	37.1	–19.6	–13.9

When performing the first method of reconstruction GD material and labor costs (see Table 2) will be significantly higher (more than five times).

Table 2

Name and type of works		GD with requirements for R_G	GD with requirements for U_t
Laying additional HG in soil of 3 group, m		349	66
Laying additional HG in soil of 5 group, m		151	33
Fulfillment of punctures under roads or pass on the asphalt-concrete massive	amount	9	2
	length, m	60	10

2) For permissible touch voltage in the reconstruction of both the first and the second insulating layer methods used in the field of surgical equipment maintenance.

We execute analysis on the example of existing substation, the results of which EMD state GD are shown in Fig. 3, 4. This thick solid black line marked grounding located underground. The real name of the research object changed to conditional – SS No. 2.

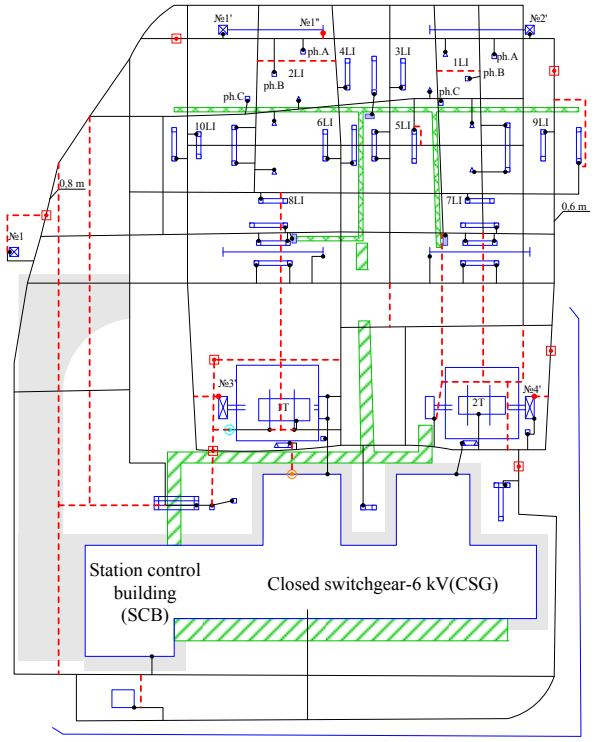

Fig. 3. Circuit of the GD of the SS No. 2 complied with the permissible resistance value

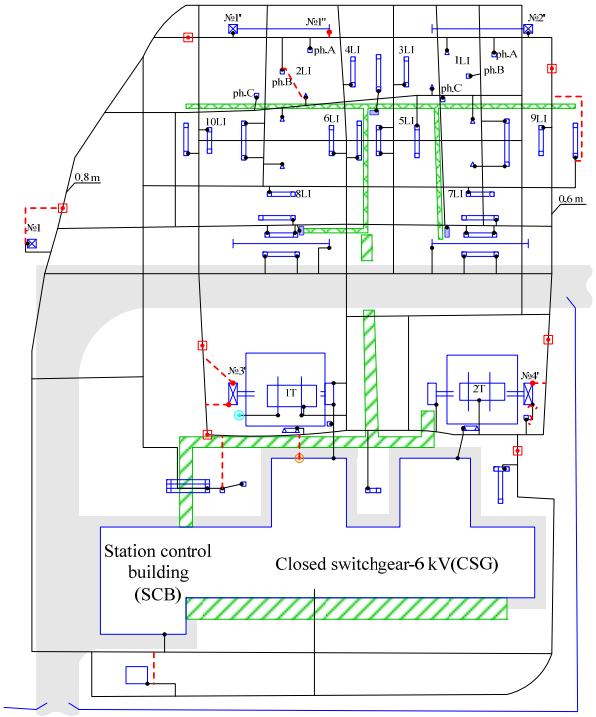

Fig. 4. Circuit of the GD of the SS No. 2 complied with the permissible touch voltage value

Initial data for determining NP GD were: real circuit GD SS No. 2, in use, ECH ground (ER layer I – 33 Ω·m, II layer – 4.6 Ω·m and thickness of the first layer – 1.97 m, the value of current single-phase circuit – 10.784 kA. It should be noted that the implementation of reconstruction GD exceeding the allowable contact voltage (65 V at the time of operation of reserve protection 0.1 s) was observed on all equipment where possible rapid switching, although the resistance value of GD does not exceed the permissible 0.5 Ω.

Fig. 3 shows the GD of the substation with introduced recommendations necessary to bring embodiment of the GD to the requirements of its resistance GD (additional HG are indicated by dotted line).

Fig. 4 shows the GD with the recommendations necessary to bring it into compliance with the allowable voltage to ground.

We compare the value and variation (see Table 3) of touch voltage for both versions of the GD.

From Table 3 we can see that the voltage of contact for both methods of reconstruction exceeds the permissible value of 65 V. Therefore the use of the insulating layer required for the reconstruction of both methods in the field of equipment maintenance, thus reducing to acceptable U_t.

Table 3

Equipment name	Values of U_t, V		Deviations of U_t from mean value, %	
	GD with requirements for R_G	GD with requirements for U_t	GD with requirements for R_G	GD with requirements for U_t
1LI ph. A	195.5	208.5	16.2	8.4
1LI ph. B	137.4	198.4	–18.3	3.2
1LI ph. C	134.5	155.8	–20.1	–19.0
2LI ph. A	152.7	217.3	–9.3	13.0
2LI ph. B	191.9	185.9	14.0	–3.3
2LI ph. C	196.6	214.0	16.8	11.3
3LI	173.4	189.1	3.0	–1.7
4LI	180.8	200.7	7.4	4.4
5LI	127.5	174.2	–24.2	–9.4
6LI	185.7	203.4	10.4	5.8
7LI	155.7	168.3	–7.5	–12.5
8LI	171.3	198.8	1.8	3.4
9LI	190.2	201.9	13.0	5.0
10LI	162.7	175.8	–3.3	–8.6

Variations in the contact pressure will be roughly the same for both cases.

In this case, when performing the first reconstruction GD way of material and labor costs for the construction of additional HG (see Table 4) will be significantly higher (more than six times). For improvement include operational service in both cases used without metal reinforcement plate with a total impedance of 3500 Ω.

3) Touch voltage does not exceed the permissible values, and during reconstruction included only the necessary constructive recommendations.

We execute analysis execute on the example of existing substations, the results of which EMD state GD are shown in Fig. 5, 6. This thick solid black line marked grounding located underground. The real name of the research object changed to conditional – SS No. 3.

Table 4

Name and type of works		GD with requirements for R_G	GD with requirements for U_t
Laying additional HG in soil of 3 group, m		199	32
Laying additional HG in soil of 5 group, m		78	12
Fulfillment of punctures under roads or pass on the asphalt-concrete massive	Amount	8	1
	length, m	63	3
Number of places of stacking plates without reinforcement with the area of 1 m^2, pieces		16	16

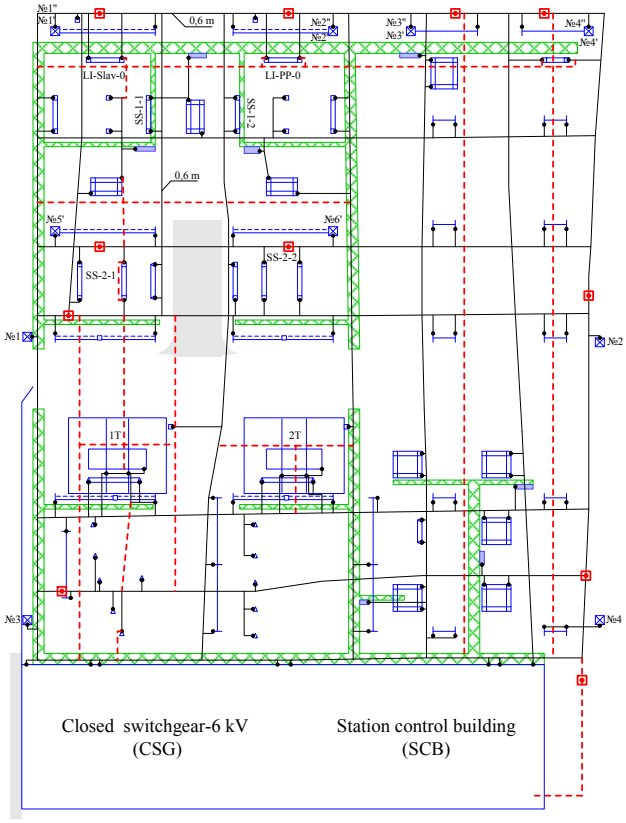

Fig. 5. Circuit of the GD of the SS No. 3 complied with the permissible resistance value

Initial data for determining the NP were: the real circuit of GD SS No. 3 (see Fig. 5), which is in operation, ECH ground (ER I layer – 12.1 Ω·m, II layer – 15.1 Ω·m, the first layer thickness – 1.15 m), the value of current single-phase circuit – 3.798 kA. It should be noted that the implementation of reconstruction touch voltage does not exceed the permissible value (65 in operation at the time of backup protect more than 1.0 s) on all equipment. GD resistance value was also lower than the allowable 0.5 Ω.

Fig. 5 shows the GD of the substation with introduced recommendations necessary to bring embodiment of the GD to the requirements of its resistance GD (additional HG are indicated by dotted line).

Fig. 6 shows GD with recommendations necessary to bring it into compliance with the allowable voltage to ground. As seen from the circuit, GD installation requires only vertical grounding connections and lightning at SCB. We compare the value and variation U_t (see Table 5) for both versions of the GD.

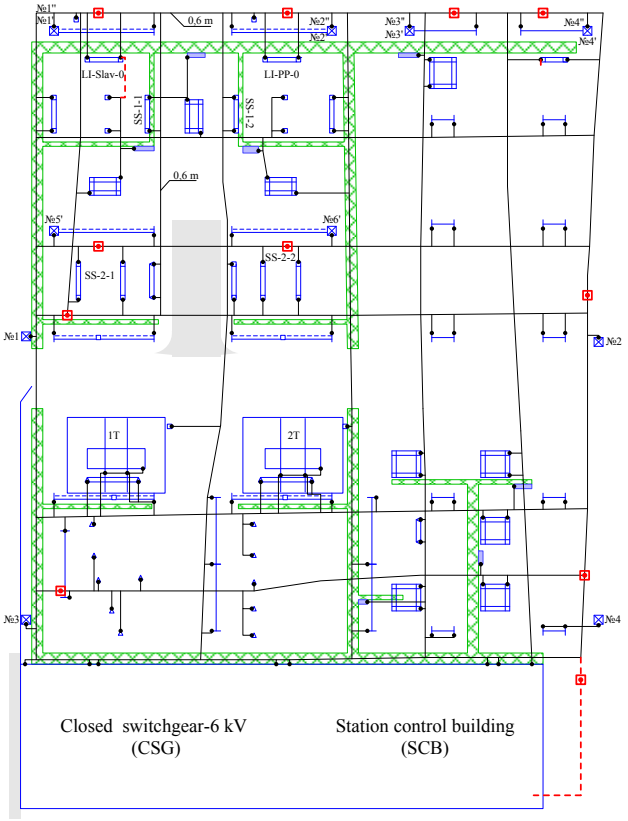

Fig. 6. Circuit of the GD of the SS No. 3 complied with the permissible touch voltage value

Table 5

Equipment name	Values of U_t, V		Deviations of U_t from mean value, %	
	GD with requirements for R_G	GD with requirements for U_t	GD with requirements for R_G	GD with requirements for U_t
LI-Slav-0	26.2	35.1	13.7	14.3
SS-1-1	23.9	28.2	3.8	–8.1
LI-PP-0	21.7	37.9	–5.8	23.5
SS-1-2	25.2	28.5	9.4	–7.2
SS-2-1	18.7	30.2	–18.8	–1.6
SS-2-2	22.5	24.3	–2.3	–20.8

From Table 5 follows that of contact voltage as in the first and in the second mode of execution does not exceed the permissible value of 65 V. Also, variations in the U_t will be approximately the same for both cases. In this case, when performing the first reconstruction GD way of material and labor costs for the construction of additional HG (see Table 6) will be almost 8 times higher.

It should be noted that the reconstruction of the GD by requirements for R_G reduces resistance value GD only 3-6% compared to GD reconstruction the requirements to touch voltage (see Table 7).

Table 6

Name and type of works		GD with requirements for R_G	GD with requirements for U_t
Laying additional HG in soil of 3 group, m		321	38
Laying additional HG in soil of 5 group, m		125	16
Fulfillment of punctures under roads or pass on the asphalt-concrete massive	Amount	5	-
	length, m	28	-

Table 7

Substation name	R_G before GD reconstruction, Ω	R_G after GD reconstruction, Ω:	
		with requirements for R_G	with requirements for U_t
SS No. 1	0.309	0.235	0.251
SS No. 2	0.088	0.083	0.087
SS No. 3	0.133	0.119	0.123

According to the Standard ДСТУ Б Д.1.1-1-2013, the analysis of the cost of reconstruction of GD in two directions for the object (see Table 8) to the cost of construction of HG in the soil of different groups, and arranging the insulating layer in the event necessary, on-site equipment maintenance.

Table 8

Substation name	Cost of the GD reconstruction, thousand UAH:	
	with requirements for R_G	with requirements for U_t
SS No. 1	42.504	8.915
SS No. 2	29.423	4.640
SS No. 3	45.781	5.168

Thus, cost-effectiveness of reconstruction and modernization of existing power facilities GD with requirement for allowable contact voltage is proven.

Conclusions.

1. Implementation of the GD with requirements for its resistance does not guarantee electrical safety of the electrical maintenance personnel in case of emergency, i.e. the resistance value of the GD does not allow one to judge the suitability of the GD for further use.

2. Reconstruction of existing GD should be carried out according to the requirements to touch voltage that will ensure electrical safety of service personnel and reliability of operating the equipment in all modes of electrical installations.

3. Implementation of modernization and reconstruction of the GD in the direction of providing acceptable touch voltage has high economic efficiency: the average savings in the reconstruction of power facilities of voltage classes of 110 kV and 150 kV is about 33 thousand UAH for each object.

The authors during the period 2015 – 2016 have developed recommendations for modernization and reconstruction of the GD as required for touch voltage of 10 substations of the voltage class of 150 kV and 20 substations of voltage class 110 kV. That said introduction of the indicated direction of reconstruction allowed even for a fairly small number of substations saving more than 1 million UAH for Ukrainian energy sector.

REFERENCES

1. *Natsional'nyy standart Ukrayiny. Pravila ulashtuvannya electroustanovok* [National Standard of Ukraine. Electrical Installation Regulations]. Kharkiv, Minenergovugillya Ukrayiny Publ., 2014. 793 p. (Ukr).

2. *Natsional'nyy standart Ukrayiny. SOU 31.2-21677681-19:2009. Viprobuvannya ta kontrol' prystroyiv zazemlennya elektroustanovok. Tipova instruktsiya.* [National Standard of Ukraine SOU 31.2-21677681-19:2009. Test and control devices, electrical grounding. Standard instruction]. Kyiv, Minenergovugillya Ukrayiny Publ., 2010. 54 p. (Ukr).

3. Koliushko D.G., Koliushko G.M., Rudenko S.S. Statistical analysis according grounding grid the power stations and substations for of normalized parameters. *Energetic and electrification*, 2015, no.6, pp. 3-7. (Rus).

4. Koliushko D.G., Rudenko S.S. Mathematical model of grounding connection of a power plant with under layer. *Electronic modeling*, 2014, vol.36, no.2, pp. 89-97. (Rus).

Received 13.02.2017

S.S. Rudenko[1], *Research Associate,*
D.G. Koliushko[1], *Candidate of Technical Science, Senior Research Associate,*
O.V. Kashcheyev[1], *Candidate of Technical Science, Senior Research Associate,*
[1] National Technical University «Kharkiv Polytechnic Institute», 2, Kyrpychova Str., Kharkiv, 61002, Ukraine,
e-mail: nio5_molniya@ukr.net

How to cite this article:
Rudenko S.S., Koliushko D.G., Kashcheyev O.V. Determination of direction to reconstruction of grounding system. *Electrical engineering & electromechanics*, 2017, no.2, pp. 57-61. **doi: 10.20998/2074-272X.2017.2.09.**

UDC 629.56:064.5+620.9+629.5 **doi: 10.20998/2074-272X.2017.2.10**

V.V. Budashko

DESIGN OF THE THREE-LEVEL MULTICRITERIAL STRATEGY OF HYBRID MARINE POWER PLANT CONTROL FOR A COMBINED PROPULSION COMPLEX

Purpose. *Efficiency of hybrid ships power plants (SPP) combined propulsion complexes (CPC) by various criteria for energy management systems strategies.* ***Methodology.*** *Based on the classification system topologies SPP CPC for mechanical, electrical and hybrid types of motors schematic diagrams of management strategies for the criterion of minimum power consumption are defined. Changing the technical component of the traditional approach to building hybrid ships electric power systems (SEPS) SPP CPC the principle of modifying the structure of SEPS is applied with the integration of additional static alternative power source as dynamic reserve, which allowed to meet modern requirements for energy efficiency, levels of vibration, noise and degradation effects produced to SPP CPC, in all areas of the energy for the transfer of power from energy to propellers. Modeling of power transmission of energy to propellers in MatLab/Simulink is conducted, using blocks of optimization library and definition of identity markers.* ***Results.*** *Major advantages and disadvantages SPP CPC depending on the topology of energy distribution systems are determined. According to the chosen structure system electricity characteristics were obtained in the process of power transmission SPP CPC and power systems and their control strategies in terms of increased efficiency and eliminate these drawbacks. And finally, mathematical apparatus for research in terms of the development of methods for designing and managing SPP hybrid CPC to reduced fuel consumption, emissions into the environment and improving maintainability, flexibility and comfort level are improved.* ***Originality.*** *The methodology for improving SPP CPC implementation by developing methods of identification markers mutually influencing processes in SPP CPC and the development of implementing these methods of settlement and information systems.* ***Practical value.*** *The method enables iterative optimization parameters SPP CPC, it can be used as a means of intelligent design, which is the result of the application of improved performance SPP CPC.* References 49, table 1, figures 12.

Key words: **ship power plants, combined propulsion complexes, energy management system, control strategy.**

На основании системной классификации топологий судовых энергетических установок (СЭУ) комбинированных пропульсивних комплексов (КПК) были систематизированы основные преимущества и недостатки СЭУ КПК в зависимости от топологии системы управления распределением энергии. Были получены характеристики процессов передачи мощности в СЭУ КПК и системах энергоснабжения, и их стратегий контроля с точки зрения повышения эффективности и устранения указанных недостатков. Усовершенствован математический аппарат для проведения исследований с точки зрения разработки методов проектирования и управления гибридными СЭУ КПК с сокращением потребления топлива, выбросов в окружающую среду и повышении ремонтопригодности, маневренности и уровня комфорта. Разработанный метод дает возможность итерационной оптимизации параметров СЭУ КПК, что позволяет использовать его как средство интеллектуального проектирования, результатом применения которого является усовершенствованные эксплуатационные характеристики СЭУ КПК. Библ. 49 табл. 1, рис. 12.

Ключевые слова: **судовая энергетическая установка, комбинированный пропульсивной комплекс, система управления энергопотреблением, стратегия управления.**

Introduction.

Minimizing the additional costs of changing the operating mode of ship power plant (SPP) combined propulsive complex (CPC) is achieved by providing stable power of SPP and the loadof middle-rotating diesel generators (MRDG) under perturbation of the environment through optimal in terms of minimum criteria consumed power management options in the SPP CPC. In order summarized forgiveness performance SPP CPC with various of architecture-Circuit decision structures, the use of this or other intellectual management strategies based to determining the effectiveness of setting governmental regulators MRDG and frequency converters (FC) feeding rowing electric motors (REM) of under-steering device (USD) in terms of compliance with the appropriate level of specific fuel consumption (SFC) depending on the load on propellers and MRDG (Fig. 1).

Despite the diversity of structures SPP CPC they may be grouped by similar advantages and disadvantages (Table 1) analyzing what can be concluded that the main drawbacks of modern-these hybrid SPP CPC in terms of management efficiency and ensure operational modes, is the inability to adjust MRDG speed-intensive in accordance with the load on propellers and the need for alternative sources of energy (ASE).

Problem definition. On the first stage it is necessary to categorized topology of SPP CPC by mechanical, electrical or hybrid types of engines and power topology (thermal, electrochemical and hybrid).

Then, considering the processes at SPP CPC power systems and their control strategies, increase capacity and eliminate the disadvantages of these systems and their respective controls. Finally need to develop mathematical tools for research in terms of the development of methods for designing and managing SPP CPC hybrid with reduced fuel consumption, emissions into the environment and improving maintainability, flexibility and comfort level.

Investigations are conducted under the state budget research work «Concept of technology and ways of improvement of ship power plants of combined propulsive complexes» of the National University «Odessa Maritime Academy» (state registration number 0114*U*000340).

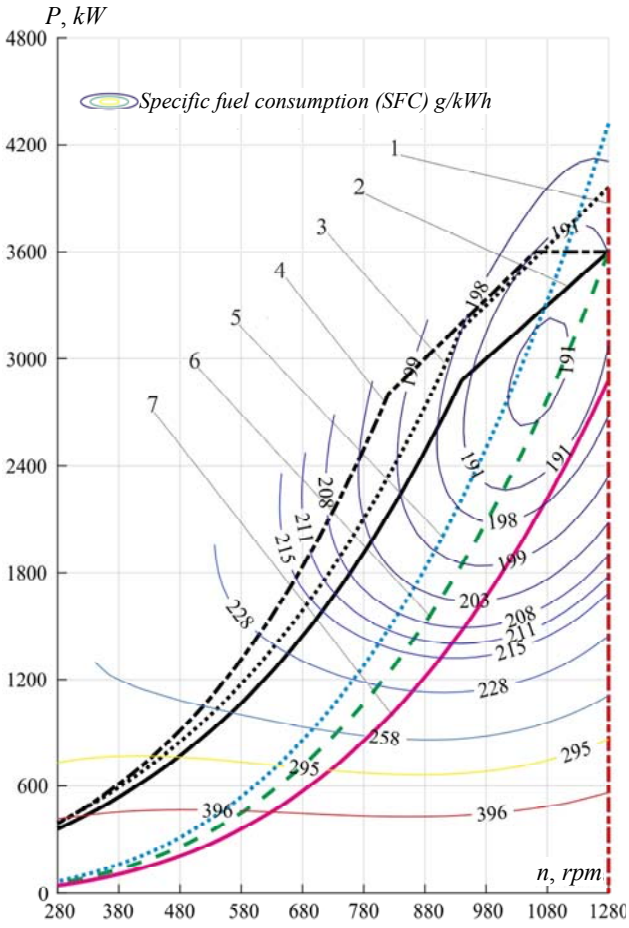

Fig. 1. Dependence of the specific fuel consumption of the load on MRDG and characteristics of propellers: 1–4 – MRDG characteristics; 1 – barrage; 2 – loading; 3 – loading with increased load rating; 4 – loading with sequential turbocharging; 5–6 – characteristics of propellers; 5 – calculated; 6 – on free water; 7 – testing

The goal of the paper is the increase of hybrid SPP CPC efficiency by combining criteria of control strategies of energy distribution.

Methods of investigations.

Hybrid SPP CPC with ASE using maximum efficiency of direct mechanical drive power and flexibility of a combination of combustion engine and the heat energy accumulated ASE is the most promising. At low power propulsive electric drive designed to bring vehicles in motion, REM provides the necessary power and excess capacity heat engine can be used as an auxiliary power supply from the shaft generator. Such SPP CPC typical architecture is shown in Fig. 2 [41, 42].

Note that MRDG equipped with automatic start-up, such as *PMR* (*Power Management Relay*) inside *PMS* (*Power Management System*) during the period of expectations are in «hot standby». This means that at least provides constant heating of the engine (for single HSPP liquid-cooled). Power station with automatic start-up can take the load after a few seconds after power failure at the main distribution board (MDB) it does not need additional time to warm the engine. In addition, there is no need to manually perform switching MDB - all necessary switching performed automatically and during MRDG carried automatic maintenance frequency output voltage and speed diesel. For particularly difficult conditions, special HSPP MRDG can work in this mode when the engine is constant, but the generator load is not connected or minimum. In this mode, fuel consumption, though not very big, but is also available. Remember that when switching to emergency mode, guaranteed job batteries. Therefore, during normal operation HSPP necessary to provide and charging batteries, in which also consumes fuel. It is clear that the total fuel consumption for the two partially loaded MRDG significantly higher than in other MRDG working under similar voltage.

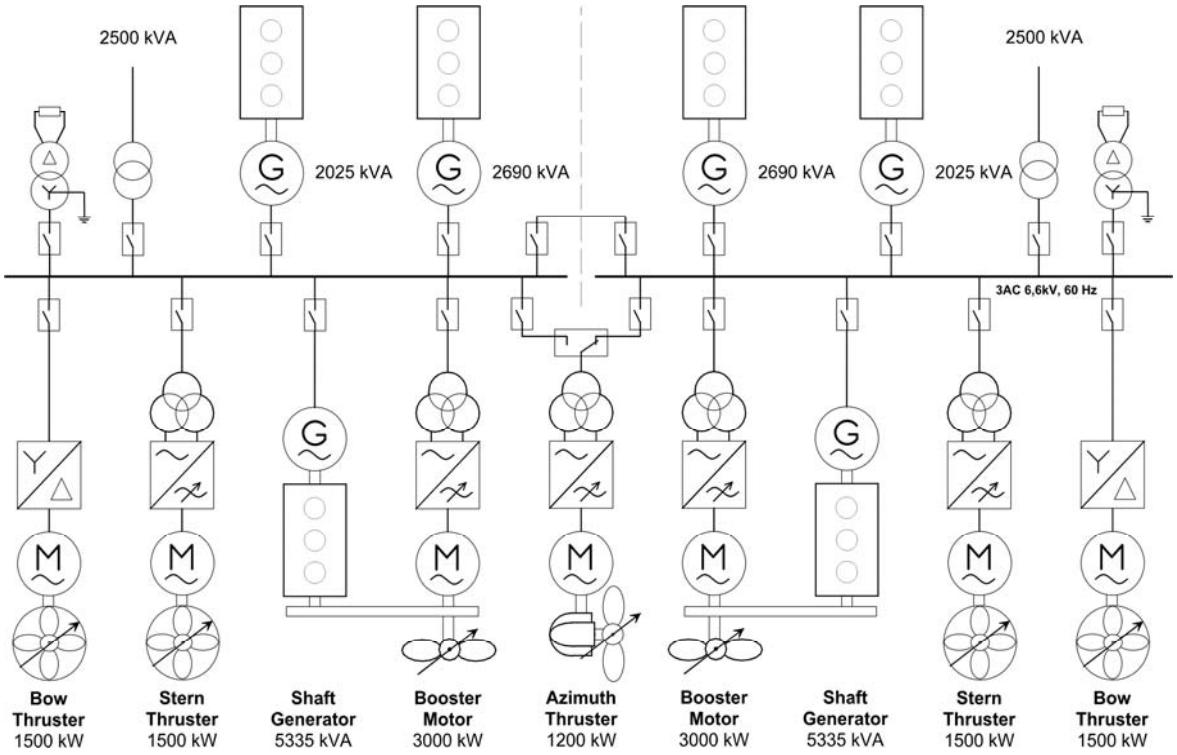

Fig. 2. One-linear circuit of the hybrid SPP CPC of the multipurpose vehicles with auxiliary USD of *L–Drive* type

Table 1

Advantages and disadvantages of motors and feeding systems techniques of SPP CPC

Technique	Advantages	Disadvantages	Source
Electromechanical CPC	Low power loss at the design power	Low efficiency at partial and peak loads	Fig. 1 [1, 2]
	Low CO_2 and NO_x emissions at the design power	High NO_x emission while reducing the load	[3, 4]
	Low loss of power conversion	Low reservation	[5]
		Increased noise	[6]
		Overloading diesel motors	[7, 8]
Disel electrical propulsion complex (DEPC)	The overload capacity	The constancy of rotational speed of MRDG	[9, 10]
	Consistency of load with MRDG	Losses at the design power	[11]
	High prospects	The risk of permanent instability of the load power	[12]
	Reduction of NO_x emission at low speed Potentially low noise		Fig. 2 [13]
Hybrid DEPC	Low power loss at the design power	The constancy of rotational speed of MRDG	[14]
	The overload capacity		[15, 16]
	Matching of load and REM at low-power	Difficulty of the system	[17]
	Potentially low noise of REM		[18, 19]
Hybrid DEPC with alternative sources of energy (ASE)	Independence from air quality	The limited power	[20, 21]
	Reduction of emission in air	Danger	[22]
	High efficiency and low noise	Failure to modernize	[23]
Hybrid ship electric power system (HSPP)	Independence from air quality	The limited power	[24, 25]
	Reducing of emission in air and low noise	Danger	
DEPC with HSPP	Load balancing	The constancy of rotational speed of MRDG	[26, 27]
	Zero noise and emission	Difficulty of the system	[28]
	Storing regenerated energy	The hazard of batteries maintenance	[29]
	The efficiency of backup power	Batteries cost	[30]
	Ability to pulse power ON	The need for control of each bathery	[31]
	Reduced fuel consumption and emission into the atmosphere	The possibility of failure in consequence recharging batteries	[32, 33]
	Absense of NO_x increase while increasing the load	Difficulty monitoring of batteries	Fig. 3 [34, 35]
DEPC with AC HSPP and system of energy storage (SES)	REM variable rotation speed and load	Difficulty of the system	[36]
	Optimal REM load	The cost and loss in power electronics	[37]
	Reducing noise and vibration of the motor	The increase in NO_x due to the variable power	[38]
	Reduced fuel consumption and CO_2 emission	The need for energy conservation while reducing power	[39]
	Ability to pulse power ON	Complexity control	[40]

Changing the technical component of the traditional approach to building hybrid HSPP SPP CPC suitable for use in many types of vehicles, based on the principle of modifying the structure of the HSPP many practical cases, operational modes, which work main MRDG can be carried out with loads of up to 80% of the nominal value, and dynamic reserve of energy provided from additional static ASE.

This approach is known, but its technical implementation to date has been virtually impossible because of the lack of highly static energy, which markedly exceeds the technical and operational characteristics of classic batteries and provides a high degree of reserve and peak load electricity.

It is proposed to use in the hybrid HSPP SPP CPC additional of ASE which consists with e*lectric double–layer capacitor* – (*EDLC*).

Flowchart of classical control strategy of the hybrid SPP CPC based on the shown in Fig. 2 *EDLC* using the criterion of minimum power consumption is shown in Fig. 3.

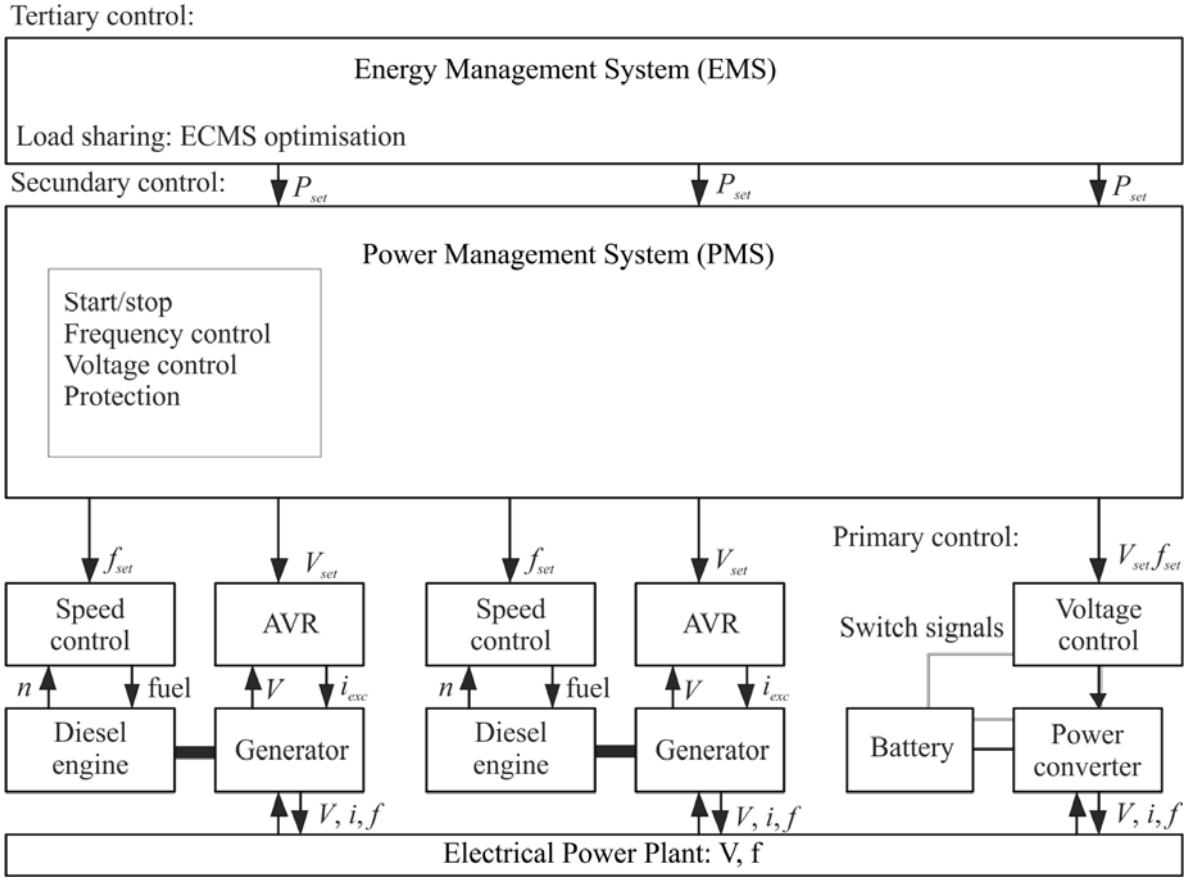

Fig. 3. Flowchart of control of hybrid SPP CPC by criterion of minimum power consumption: AVR - automatic voltage regulation; X_{set} – setpoint; P – power; f – frequency of voltage; V – voltage; n – rotational speed of MRDG; i_{exc} – generators excitation current; I – current of MRDG

The core of monitoring and and control of the joint HSPP SPP CPC with *EDLC* as a dynamic source of power is the evaluation module of voltage *EDLC* and the degree of excess charge. Because the relationship between voltage and current value *EDLC* degree charge is approximately linear, therefore, the detection accuracy of the voltage on the capacitor will directly determine the accuracy of the information about the state of *EDLC*.

The energy discharge capacitor modules in the SPP CPC features disturbing forces parameterization actions are determined by the equations (1) and (2), provided of all the USD in the coordinate plane direct regulation since given by equation (3) to assess the integration of the total area all modules *EDLC* surface galvanic curve during discharge or charge:

$$\begin{cases} U_S(t) = I_S(t) \cdot Z_{SE} + t_{EM} \cdot \bar{\upsilon}_S(t), \\ F_S(t) = I_S(t) \cdot t_{ME} + Z_{SM} \cdot \bar{\upsilon}_S(t), \end{cases} \quad (1)$$

where Z_{SE} is the impedance of the converter from the electric side, [Ω]; Z_{SM} is the impedance of the converter from the mechanical side, [Ω]; t_{EM} is the time constant of the electromechanical transformation, [s]; t_{ME} is the time constant of the mechanical-electrical transformation, [s]

$$\begin{cases} \bar{\boldsymbol{U}}_S(\boldsymbol{Z}) = \bar{\boldsymbol{I}}_S(t) \cdot \boldsymbol{Z}_{SE} + t_{EM} \cdot \bar{\upsilon}_S(t), \\ \bar{\boldsymbol{F}}_S(\boldsymbol{Z}) = \bar{\boldsymbol{I}}_S(t) \cdot t_{ME} + \boldsymbol{Z}_{SM} \cdot \bar{\upsilon}_S(t), \\ (m_{cS} + m_{ncS}) \cdot \dfrac{d\bar{\upsilon}_S(t)}{dt} + \mu_S \bar{\upsilon}_S(t) + \mu_R \int_{\varepsilon_0}^{\varepsilon} \bar{\upsilon}_S(t) dt = \bar{\boldsymbol{F}}_S(\boldsymbol{Z}), \end{cases} \quad (2)$$

where $\boldsymbol{F}_S(\boldsymbol{Z}) = (\boldsymbol{F}_{S1}(\boldsymbol{Z}^1), \boldsymbol{F}_{S2}(\boldsymbol{Z}^2), \boldsymbol{F}_{S3}(\boldsymbol{Z}^3), \boldsymbol{F}_{S4}(\boldsymbol{Z}^4), \ldots, \boldsymbol{F}_{Si}(\boldsymbol{Z}^m))^{Tmatrix(i)}$; complex impedance is defined by

matrices of active and inductive components of the equivalent circuit complex load $\boldsymbol{Z}^m = \boldsymbol{R}^m + p_i j\boldsymbol{L}^m$; $T_{matrix(i)}$ is the thruster matrix of configuration parameters of devices, where $(i = 0\ldots k)$ is the number of the corresponding configuration regarding Table 1 and selected technique of the SPP CPC [43, 44].

$$E_{int/SOC}(t) = I_{EDLC} \int_{U_{EDLC\_max}}^{U_{EDLC\_min}} U_S(t)dt \qquad (3)$$

Equation (3) permits to calculate the power charger needed to ensure the required level of charge *EDLC* for a particular operating mode SPP CPC during dynamic loading. Whence all capacity capacitor modules will be determined by the formula:

$$C_{int/EDLC} = \frac{2E_{int/SOC}}{(U_{EDLC\_max})^2}. \qquad (4)$$

Power capacitors of *EDLC* of hybrid DEPC are formed in the modules by determining the necessary energy charge/discharge capacity calculated in chargers. Considering the large number of power devices, high-voltage and high-power lines between modules and HSPP SPP CPC, electromagnetic environment is complicated. The program operation monitoring system should consist of two parts: a control system (CS) and integrated control unit monitoring capacity. The integrated control unit will be responsible for tracking and signal processing modules of *EDLC*, for example, the total capacity voltage level of the charging and discharge currents about ambient temperature and so on. CS will monitor algorithms and data storage in *EDLC* modules, system status monitoring and control, power management devices and schemes of the man-machine interface.

To exchange information in various control devices as a communication center in SPP CPC it is planned to use the *network* in order to send commands to the monitoring unit of *EDLC* modules on the system bus and receive data downloads. Each unit monitoring modules *EDLC* responsible for: receiving a signal state of one *EDLC* by voltage and temperature.

To select the number and capacity of *EDLC* according to the type and characteristics of SPP CPC operating mode at the start according to the components of complex impedance matrix parameters determine the active and inductive components integrated load equivalent circuit $\boldsymbol{Z}^m = \boldsymbol{R}^m + p_i j\boldsymbol{L}^m$ (Fig. 4). And for the value of the stop mode direct control point forward coefficients matrix configuration parameters of thruster devices $T_{matrix(i)}$, where $(i = 0\ldots k)$ is the number of the configuration.

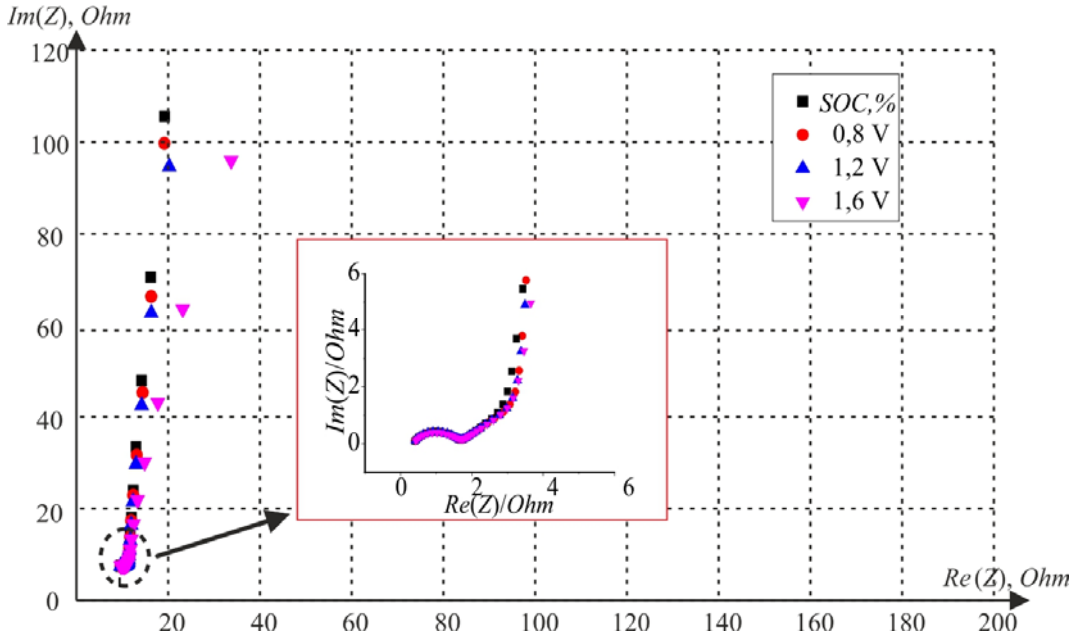

Fig. 4. Parameters for determining integrated load of capacitance of *EDLC* for a particular operating mode of the SPP CPC: the degree of charge of *EDLC* (*State–of–Charge – SOC*)

For example, for the circuit of the SPP CPC (Fig. 2) [45, 46] on the ship are two main classic screw the left and right sides of the stern of the ship; two feed tunnel USD; one azimuthal USD that slides out from the hull in the bow of the vessel, which can be rotated to any angle α_A (Fig. 8) relative to centreline of the ship; two bow tunnel USD ($u_{T1,2}$ – the main focuses of classic screws; $u_{T3,4}$ – the focuses of feeding tunnel USD; u_{T5} – focus of support azimuth USD, $u_{T6,7}$ – the focuses of nasal USD):

$$T_{matrix} = \begin{pmatrix} 1 & 1 & 0 & 0 & cos\alpha_{A5} & 0 & 0 \\ 0 & 0 & 1 & 1 & sin\alpha_{A5} & 1 & 1 \\ l_{T1} & -l_{T2} & -l_{T3} & -l_{T4} & l_{T5}sin\alpha_{A5} & l_{T6} & l_{T7} \end{pmatrix}, \qquad (5)$$

where l_{Ti} $(i = 1\ldots 7)$ is the arm strength or distance from the application of USD to focus this effort τ_T vector projection onto the plane of the ship.

Then, according to the type of *EDLC* we calculate frequency response (FR) (Fig. 5) and the initial parameters of the charge/discharge of the prescribed limits of *SOC* (Fig. 6).

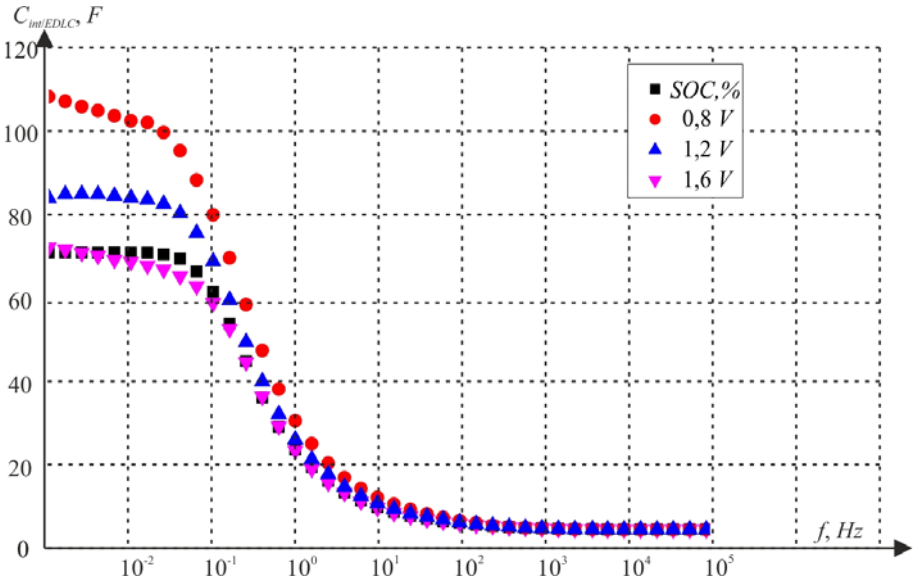

Fig. 5. Frequency response of the selected *EDLC*

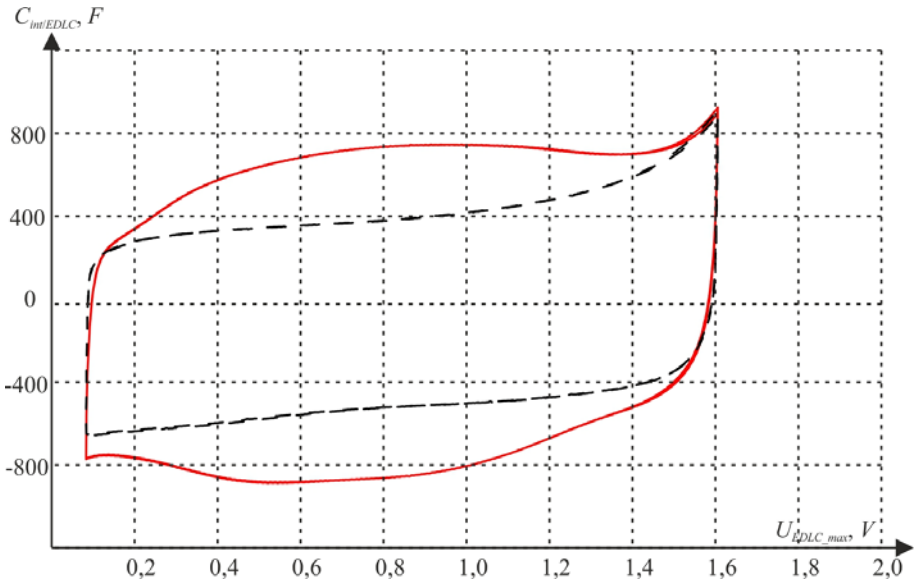

Fig. 6. Charge/discharge parameters of the selected *EDLC* in the prescribed limits of *SOC*

And, finally, the calculated effectiveness of the proposed configuration of SPP CPC handheld dynamic type *EDLC* power supply for a particular operating mode (Fig. 7), taking into account situational factors set of the operating mode SPP CPC of the particular ship, single-line diagram of which is presented in Fig. 2. These factors are taken into account in the task of solving local problems identifying operational mode, each of which corresponds to a composition of effective variables [47, 48].

Results of investigations. Based on the proposed method we improved the control strategy of SPP CPC by criterion of minimum power consumption by introducing criterion for maximum alternative energy and regulating the degree battery of SES using ASE to minimize fuel consumption.

Compliance with other criteria such as noise, vibration, emission into the environment or maintenance of MRDG (see Table 1) is primarily dependent on the operating point of MRDG (Fig. 1) and ASE (Fig. 7) and is determined by adjusting the control system of distribution electricity (Fig. 3).

Thus, similar to the cost function depending on the mode of MRDG can be obtained on these criteria, as well as the overall optimal power of SPP CPC can be determined from the weighted cost function on several criteria.

Improvement strategies criterion for obtaining the maximum alternative energy and regulating the degree battery of SES using ASE is a promising approach to improve SPP CPC compared with many features for future developments [49].

Ultimately, further research must move by combining management strategies in terms of integrated approach. Block diagram of one embodiment of improved management strategies integrated system with hybrid DEPC and joint HSPP is shown in Fig. 8.

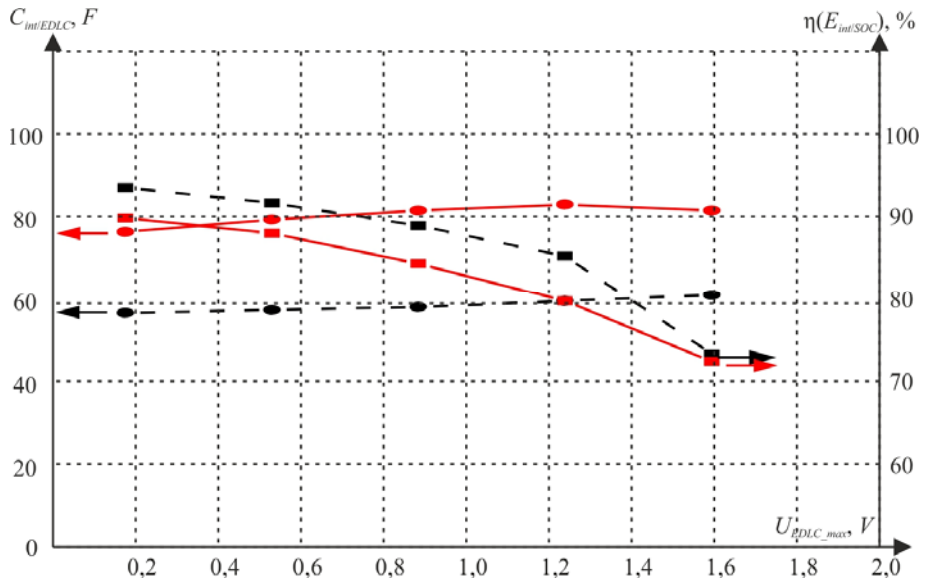

Fig. 7. Comparative characteristics of effective charge/discharge cycles of *EDLC* for proposed configuration of SPP CPC dynamic sources of power for two operating modes: fully equipped – 4 MRDG (red solid line); partially equipped – 3 MRDG (black dotted line)

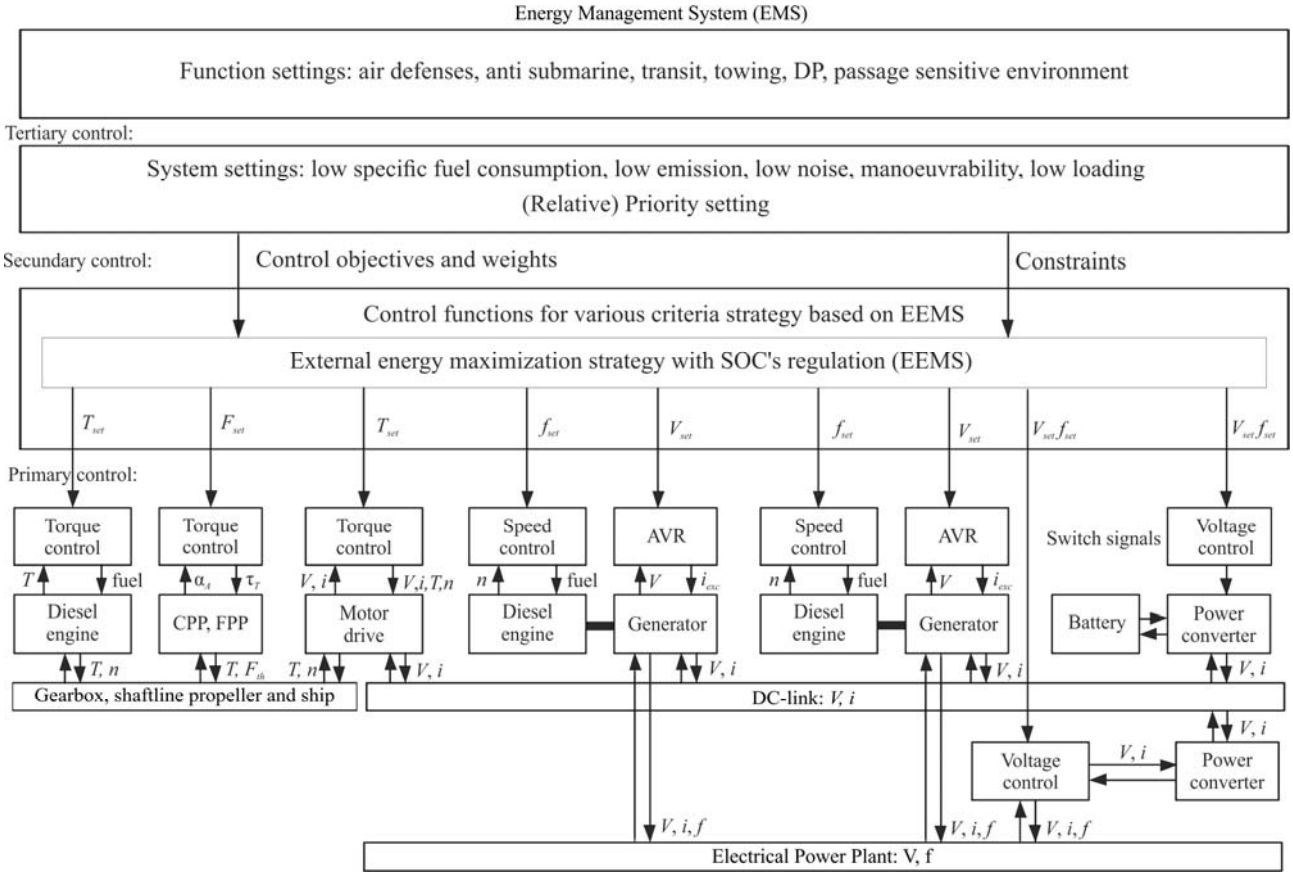

Fig. 8. Block diagram of the control strategy of SPP CPC by criterion of maximum regulation and alternative energy of the battery charge of the SES: AVR – automatic voltage regulation; VPP – variable pitch propeller; FPP – fixed pitch propeller; X_{set} - setpoint; T – focus (torque); F – force of push the propeller; f – frequency of voltage; V – voltage; n – rotational speed of MRDG; i_{exc} – generators excitation current; i – current; τ_T – resulting force vector projection onto the plane of the ship; α_A – angle of rotation relative to ship centreline

Fig. 9 - 12 show obtained dependences of modeling processes in hybrid power transmission DEPC. Simulations are conducted in *MatLab/Simulink*. Since the beginning of the transient (t = 0 s), the load is powered from the main MRDG. SES of the hybrid DEPC plug for charging batteries and is preparing for a possible breakdown of the ship.

On the 40th second the vessel is de-energized and the system of power switches with power MRDG on ASE. This request excesses capacity provided by the DC link, which implemented energy recovery from consumers, working in generator mode, as *EDLC* power increases slowly.

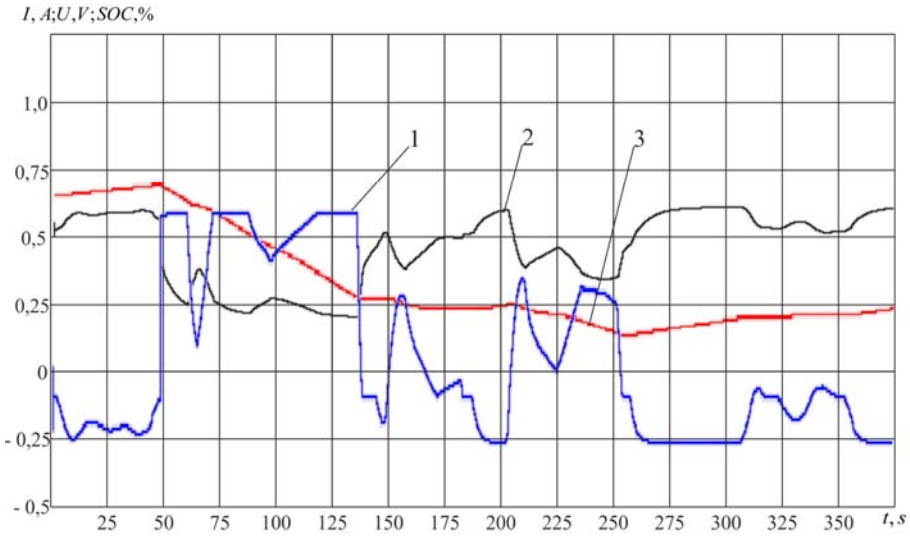

Fig. 9. Energy characteristics of SES: 1 – maximum current value corresponding to 400 A; 2 –- maximum voltage value corresponding to 48 V; 3 –maximum level of charge corresponds to 100%

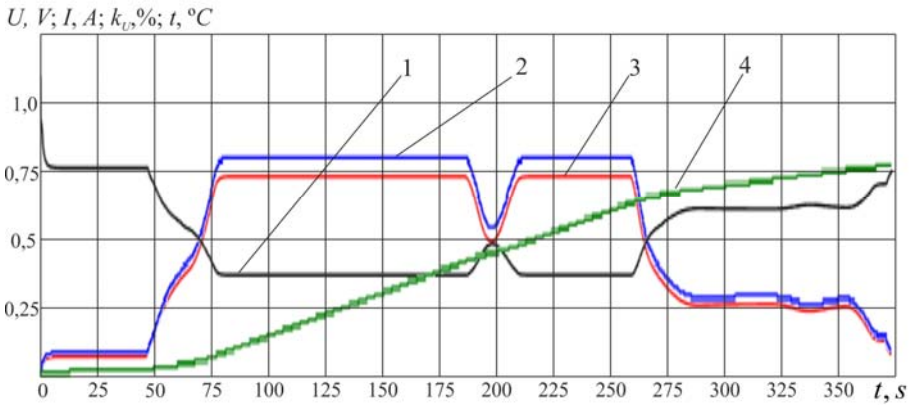

Fig. 10. Energy characteristics of *EDLC*: 1 – maximum voltage value corresponds to 180 V; 2 – maximum current value corresponds to 270 A; 3 – the maximum voltage in relation to the *EDLC* circuit voltage corresponding to value of 1; 4 – maximum temperature of *EDLC* corresponds to value of 50 ºC

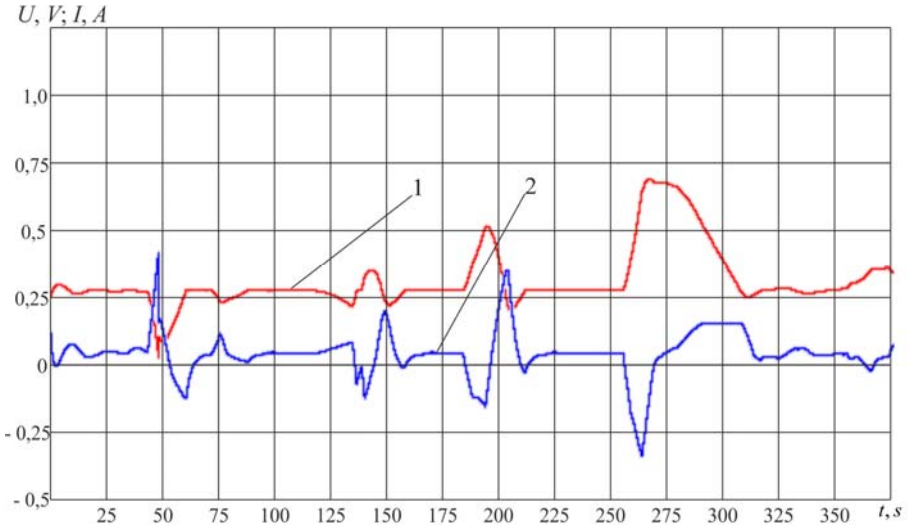

Fig. 11. Dependencies of voltage and current in the DC link: 1 – maximum voltage value corresponds to 450 V; 2 – maximum current value corresponds to 1150 A

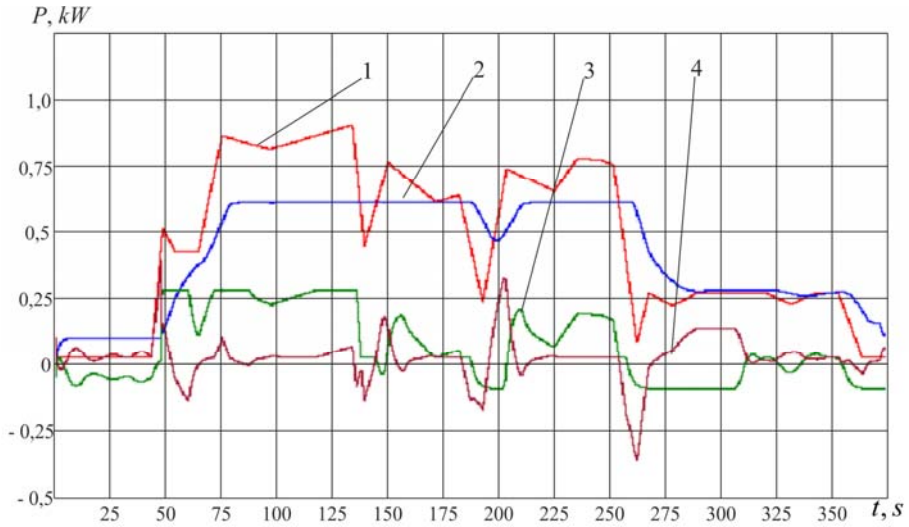

Fig. 12. Energy characteristics of hybrid DEPC: 1 – maximum power load value corresponds to 1000 kW; 2 – maximum power on SES corresponds to 10 kW; 3 – maximum power on SES corresponds to 20 kW; 4 – maximum power for *DC-Link* corresponds to the value of 300 kW

At t = 45 s the voltage on the DC link has reached the lowest level (280 V) and SES is connected to its bus and feeds up to 450 V, the voltage at which on the 47th second increases to the required level and Sneh limits the capacity gradually to zero. *EDLC* provides the necessary power their needs and continue to fuel the bus DC link, which connected on the 55th second customers operating in emergency mode. On the 62nd second SES is turned on supporting bus voltage DC to 450 V to help *EDLC* to provide additional load power loading.

After the 80th seconds the power of *EDLC* reaches the maximum value that the set point is limited to 10 kW maximum output voltage of the converter *DC/AC*. Therefore, the required power load their needs provided Sneh, whose maximum power is reached at t = 120 s (20 kW) and load power is provided via the bus of the DC link.

On the 130th second request of power load is reduced below capacity on which *EDLC* designed. Due to the fact that *EDLC* low inherent dynamic characteristics during transient additional power consumers is switched to the DC link.

The results of investigations of processes of power transmission in hybrid SPP CPC give reason to believe that the solution of the problem of increase of efficiency of last ones is possible by combining the classic control strategy of power distribution with strategy to control the degree of charge of alternative power sources. The set of proposed strategies allows to design flexible multipurpose electric power systems that are integrated into hybrid SPP CPC as an integral component.

Taking into account that the degree of adjustment of charge of *EDLC* is insignificant in relation to the consumption of reactive power, and voltage and power converters with low harmonic creates a problem of recovery of electric power we can say that reactive power compensation occurs mainly due to the transfer of MRDG to the compensator mode by corresponding adjustment of PID compensators regulators.

Conclusions. In the paper a scientific and applied problem of SPP CPC improvement by developing an integrated three-level multicriterial control strategy of energy distribution is solved.

The proposed method meets the modern requirements for energy efficiency, levels of vibration, noise and degradation effects imposed on the SPP CPC in all areas of the energy process of the transfer of power from energy to propellers. This allows parameterization of propulsive and power characteristics of SPP CPC depending on changes in operating modes, hydrodynamic characteristics and environmental conditions.

What is important is the possibility of iterative optimization of SPP CPC parameters that allows to use the method developed as a means of intelligent design which results in enhanced performance of SPP CPC.

REFERENCES

1. Geertsma R.D., Negenborn R.R., Visser K., Hopm J.J. Design and control of hybrid power and propulsion systems for smart ships: A review of developments. *Applied Energy*, 2017, v.194, pp. 30-54. **doi: 10.1016/j.apenergy.2017.02.060**.

2. Kim D.H., Paik J.K. Ultimate limit state-based multi-objective optimum design technology for hull structural scantlings of merchant cargo ships. *Ocean Engineering*, 2017, v.129, pp. 318-334. **doi: 10.1016/j.oceaneng.2016.11.033**.

3. Gonca G., Sahin B., Parlak A., Ust Y., Ayhan V., Cesur İ., Boru B. Theoretical and experimental investigation of the Miller cycle diesel engine in terms of performance and emission parameters. *Applied Energy*, 2015, v.138, pp. 11-20. **doi: 10.1016/j.apenergy.2014.10.043**.

4. Ko J., Jin D., Jang W., Myung C.-L., Kwon S., Park S. Comparative investigation of NOx emission characteristics from a Euro 6-compliant diesel passenger car over the NEDC and WLTC at various ambient temperatures. *Applied Energy*, 2017, v.187, pp. 652-662. **doi: 10.1016/j.apenergy.2016.11.105**.

5. Baldi F., Johnson H., Gabrielii C., Andersson K. Energy Analysis of Ship Energy Systems – The Case of a Chemical Tanker. *Energy Procedia*, 2014, v.61, pp. 1732-1735. **doi: 10.1016/j.egypro.2014.12.200**.

6. Vrijdag A., Stapersma D., van Terwisga T. Control of propeller cavitation in operational conditions. *Journal of Marine Engineering & Technology*, 2010, v.9, pp. 15-26. **doi: 10.1080/20464177.2010.11020228**.

7. Natale F.D., Carotenuto C. Particulate matter in marine diesel engines exhausts: Emissions and control strategies.

Transportation Research Part D: Transport and Environment, 2015, v.40, pp. 166-191. **doi: 10.1016/j.trd.2015.08.011**.

8. Zhao F., Yang W., Tan W.W., Yu W., Yang J., Chou S.K. Power management of vessel propulsion system for thrust efficiency and emissions mitigation. *Applied Energy*, 2016, v.161, pp. 124-132. **doi: 10.1016/j.apenergy.2015.10.022**.

9. Bassam A.M., Phillips A.B., Turnock S.R., Wilson P.A. An improved energy management strategy for a hybrid fuel cell/battery passenger vessel. *International Journal of Hydrogen Energy*, 2016, v.41, iss.47, pp. 22453-22464. **doi: 10.1016/j.ijhydene.2016.08.049**.

10. Symington W.P., Belle A., Nguyen H.D., Binns J.R. Emerging technologies in marine electric propulsion. *Proceedings of the Institution of Mechanical Engineers, Part M: Journal of Engineering for the Maritime Environment*, 2014, v.230, iss.1, pp. 187-198. **doi: 10.1177/1475090214558470**.

11. Kwatny H.G., Bajpai G., Miu K., Yasar M. Fuel Optimal Control With Service Reliability Constraints for Ship Power Systems. *IFAC Proceedings Volumes*, 2014, v.47, iss.3, pp. 6386-6391. **doi: 10.3182/20140824-6-ZA-1003.01773**.

12. Chuang S.-J., Hong C.-M., Chen C.-H. Improvement of integrated transmission line transfer index for power system voltage stability. *International Journal of Electrical Power & Energy Systems*, 2016, v.78, pp. 830-836. **doi: 10.1016/j.ijepes.2015.11.111**.

13. Vernengo G., Gaggero T., Rizzuto E. Simulation based design of a fleet of ships under power and capacity variations. *Applied Ocean Research*, 2016, v.61, pp. 1-15. **doi: 10.1016/j.apor.2016.09.003**.

14. Lützen M., Mikkelsen L.L., Jensen S., Rasmussen H.B. Energy efficiency of working vessels – A framework. *Journal of Cleaner Production*, 2017, v.143, pp. 90-99. **doi: 10.1016/j.jclepro.2016.12.146**.

15. McCoy T.J. Trends in ship electric propulsion. *IEEE Power Engineering Society Summer Meeting*, 2002, v.1, pp. 243-346. **doi: 10.1109/PESS.2002.1043247**.

16. Zivi E. Design of robust shipboard power automation systems. *Annual Reviews in Control*, 2005, v.29, iss.2, pp. 261-272. **doi: 10.1016/j.arcontrol.2005.08.004**.

17. Castles G., Reed G., Bendre A., Pitsch R. Economic benefits of hybrid drive propulsion for naval ships. *IEEE Electric Ship Technologies Symposium*, 2009. **doi: 10.1109/ESTS.2009.4906560**.

18. Baldi F., Ahlgren F., Melino F., Gabrielii C., Andersson K. Optimal load allocation of complex ship power plants. *Energy Conversion and Management*, 2016, v.124, pp. 344-356. **doi: 10.1016/j.enconman.2016.07.009**.

19. Sulligoi G., Castellan S., Aizza M., Bosich D., Piva L., Lipardi G. Active front-end for shaft power generation and voltage control in FREMM frigates integrated power system: Modeling and validation. *International Symposium on Power Electronics Power Electronics, Electrical Drives, Automation and Motion*, 2012, pp. 452-457. **doi: 10.1109/SPEEDAM.2012.6264570**.

20. Bigdeli N. Optimal management of hybrid PV/fuel cell/battery power system: a comparison of optimal hybrid approaches. *Renewable and Sustainable Energy Reviews*, 2015, v.42, pp. 377-393. **doi: 10.1016/j.rser.2014.10.032**.

21. Choi C.H., Yu S., Han I.-S., Kho B.-K., Kang D.-G., Lee H.Y., Seo M.-S., Kong J.-W., Kim G., Ahn J.-W., Park S.-K., Jang D.-W., Lee J.H., Kim M. Development and demonstration of PEM fuel-cell-battery hybrid system for propulsion of tourist boat. *International Journal of Hydrogen Energy*, 2016, v.41, iss.5, pp. 3591-3599. **doi: 10.1016/j.ijhydene.2015.12.186**.

22. José J. de-Troya, Álvarez C., Fernández-Garrido C., Carral L. Analysing the possibilities of using fuel cells in ships. *International Journal of Hydrogen Energy*, 2016, v.41, iss.4, pp. 2853-2866. **doi: 10.1016/j.ijhydene.2015.11.145**.

23. Nelson D.B., Nehrir M.H., Wang C. Unit sizing and cost analysis of stand-alone hybrid wind/PV/fuel cell power generation systems. *Renewable Energy*, 2006, v.31, iss.10, pp. 1641-1656. **doi: 10.1016/j.renene.2005.08.031**.

24. Ramli M., Hiendro A., Twaha S. Economic analysis of PV/diesel hybrid system with flywheel energy storage. *Renewable Energy*, 2015, v.78, pp. 398-405. **doi: 10.1016/j.renene.2015.01.026**.

25. Rezzouk H., Mellit A. Feasibility study and sensitivity analysis of a stand-alone photovoltaic-diesel-battery hybrid energy system in the north of Algeria. *Renewable and Sustainable Energy Reviews*, 2015, v.43, pp. 1134-1150. **doi: 10.1016/j.rser.2014.11.103**.

26. Vetter M., Lux S. Rechargeable Batteries with Special Reference to Lithium-Ion Batteries. *Storing Energy*, 2016, pp. 205-225. **doi: 10.1016/B978-0-12-803440-8.00011-7**.

27. Zahedi B., Norum L.E., Ludvigsen K.B. Optimized efficiency of all-electric ships by DC hybrid power systems. *Journal of Power Sources*, 2014, v.255, pp. 341-354. **doi: 10.1016/j.jpowsour.2014.01.031**.

28. Wang L., Lee D.J., Lee W.J., Chen Z. Analysis of a novel autonomous marine hybrid power generation/energy storage system with a high-voltage direct current link. *Journal of Power Sources*, 2008, v.185, iss.2, pp. 1284-1292. **doi: 10.1016/j.jpowsour.2008.08.037**.

29. Ovrum E., Bergh T.F. Modelling lithium-ion battery hybrid ship crane operation. *Applied Energy*, 2015, v.152, pp. 162-172. **doi: 10.1016/j.apenergy.2015.01.066.**

30. Haseltalab A., Negenborn R.R., Lodewijks G. Multi-Level Predictive Control for Energy Management of Hybrid Ships in the Presence of Uncertainty and Environmental Disturbances. *IFAC-Papers On Line*, 2016, v.49, iss.3, pp. 90-95. **doi: 10.1016/j.ifacol.2016.07.016**.

31. Lashway C.R., Elsayed A.T., Mohammed O.A. Hybrid energy storage management in ship power systems with multiple pulsed loads. *Electric Power Systems Research*, 2016, v.141, pp. 50-62. **doi: 10.1016/j.epsr.2016.06.031**.

32. Giannoutsos S.V., Manias S.N. Energy management and D/G fuel consumption optimization in the power system of marine vessels through VFD-based process flow control. *IEEE 15th International Conference on Environment and Electrical Engineering (EEEIC)*, 2015, pp. 842-850. **doi: 10.1109/EEEIC.2015.7165274**.

33. Zhao F., Yang W., Tan W.W., Yu W., Yang J., Chou S.K. Power management of vessel propulsion system for thrust efficiency and emissions mitigation. *Applied Energy*, 2016, v.161, pp. 124-132. **doi: 10.1016/j.apenergy.2015.10.022**.

34. Papalambrou G., Karlis E., Kyrtatos N. Robust Control of Manifold Air Injection in a Marine Diesel Engine. *IFAC-Papers On Line*, 2015, v.48, iss.14, pp. 438-443. **doi: 10.1016/j.ifacol.2015.09.496**.

35. Papalambrou G., Kyrtatos N. Controlled Injection of Compressed Air in Marine Diesel Engine Intake for Improved Load Acceptance. *IFAC Proceedings Volumes*, 2009, v.42, iss.26, pp. 140-147. **doi: 10.3182/20091130-3-FR-4008.00019**.

36. Shih N.-C., Weng B.-J., Lee J.-Y., Hsiao Y.-C. Development of a 20kW generic hybrid fuel cell power system for small ships and underwater vehicles. *International Journal of Hydrogen Energy*, 2014, v.39, iss.25, pp. 13894-13901. **doi: 10.1016/j.ijhydene.2014.01.113**.

37. Zhang S., Xiong R., Sun F. Model predictive control for power management in a plug-in hybrid electric vehicle with a hybrid energy storage system. *Applied Energy*, 2017, v.185, pp. 1654-1662. **doi: 10.1016/j.apenergy.2015.12.035**.

38. Butcher M., Maltby R., Parvin P.S. Compact DC power and propulsion systems – the definitive solution? *IEEE Electric Ship Technologies Symposium*, 2009, pp. 521-528. **doi: 10.1109/ESTS.2009.4906561**.

39. Hodge C.G., Mattick D.J. The electric warship then, now and later. *Proceedings of the 9th international naval engineering conference*, 2008, pp. 556-565.
40. Indragandhi V., Subramaniyaswamy V., Logesh R. Resources, configurations, and soft computing techniques for power management and control of PV/wind hybrid system. *Renewable and Sustainable Energy Reviews*, 2017, v.69, pp. 129-143. **doi: 10.1016/j.rser.2016.11.209**.
41. Budashko V., Nikolskyi V., Onishchenko O., Khniunin S. Physical model of degradation effect by interaction azimuthal flow with hull of ship. *Proceeding Book of International Conference on Engine Room Simulators (ICERS12)*. Istanbul: Istanbul Technical University, Maritime Faculty, 2015. pp. 49-53. ISBN 978-605-01-0782-1.
42. Nikolskyi V., Budashko V., Khniunin S. The monitoring system of the Coanda effect for the tension-leg platform's. *Proceeding Book of International Conference on Engine Room Simulators (ICERS12)*. Istanbul: Istanbul Technical University, Maritime Faculty, 2015. pp. 45-49. ISBN 978-605-01-0782-1.
43. Budashko V.V., Onishchenko O.A. Improving management system combined thruster propulsion systems. *Bulletin of NTU «KhPI»*, 2014, no.38(1081), pp. 45-51. (Ukr).
44. Budashko V.V. Implementation approaches during simulation of energy processes for a dynamically positioned ship. *Electrical Engineering & Electromechanics*, 2015, no.6, pp. 14-19. **doi: 10.20998/2074-272X.2015.6.02**. (Rus).
45. Budashko V.V., Onischenko O.A., Yushkov E.A. Physical modeling of multi-propulsion complex. *Collection of scientific works of the Military Academy (Odessa City)*, 2014, no.2, pp. 88-92. (Rus).
46. Budashko V.V., Nikolskyi V.V., Khniunin S.H. *Sudova systema monitorynhu dlya poperedzhennya effektu Koanda* [Ship monitoring system for the prevention of Coanda effect]. Patent UA, no.100819, 2015. (Ukr).
47. Budashko V.V., Yushkov E.A. *Systema impul'sno-fazovoho upravlinnya elektropryvodom sudnovoyi hvynto-kermovoyi ustanovky* [The pulse-phase control system of electric ship propeller-steering plant]. Patent UA, no.108074, 2016. (Ukr).
48. Khniunin S.H., Budashko V.V., Nikolskyi V.V. *Sudova systema monitorynhu dlya poperedzhennya effektu Koanda* [Ship system for monitoring for preventing the Coanda effect]. Patent UA, no.107006, 2016. (Ukr).
49. Budashko V., Nikolskyi V., Onishchenko O., Khniunin S. Decision support system's concept for design of combined propulsion complexes. Eastern-European Journal of Enterprise Technologies, 2016, v.3, no.8(81), pp. 10-21. **doi: 10.15587/1729-4061.2016.72543**.

Received 24.03.2017

V.V. Budashko, Candidate of Technical Science, Associate Professor,
Odessa National Maritime Academy,
8, Didrikhson Str., Odessa, 65029,
phone +380 48 7332367,
e-mail: bvv@te.net.ua

How to cite this article:
Budashko V.V. Design of the three-level multicriterial strategy of hybrid marine power plant control for a combined propulsion complex. *Electrical engineering & electromechanics*, 2017, no.2, pp. 62-72. **doi: 10.20998/2074-272X.2017.2.10.**